THERMOMECHANICAL RESPONSE OF FUCNCTIONALLY GRADED MATERIALS

by
ARJUN SINGH

DEPARTMENT OF MECHANICAL ENGINEERING
INDIAN INSTITUTE OF TECHNOLOGY KANPUR

February, 2000

THERMOMECHANICAL RESPONSE OF FUCNCTIONALLY GRADED MATERIALS

A Thesis Submitted
in Partial Fulfillment of the Requirements
for the Degree of

MASTER OF TECHNOLOGY

February, 2000

by

ARJUN SINGH

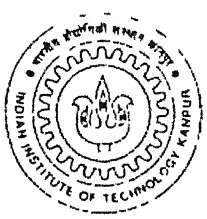

DEPARTMENT OF MECHANICAL ENGINEERING
INDIAN INSTITUTE OF TECHNOLOGY
KANPUR – 208016 (INDIA)

CERTIFICATE

It is certified that the work contained in the thesis entitled, "THERMOMECHANICAL RESPONSE OF FUNCTIONALLY GRADED MATERIALS" by *Mr. Arjun Singh* has been carried out under my supervision and that this work has not been submitted elsewhere for a degree

Om Prakash

Dr. Om Prakash

(Assistant Professor)

Department of Mechanical Engineering,

Indian Institute of Technology,

February, 2000

Kanpur

ACKOWLEDGEMENTS

I wish to express my deep sense of gratitude and indebtedness towards Dr. Om Prakash for his inspiring guidance, invaluable suggestions and constructive criticism. He was always a constant source of encouragement throughout my thesis work .

I heartily appreciate the help provided by Mr Amod, Mr. Sandeep Gupta and Mr. Sameer Agrawal during my work

I can not forget Mr Anupam Chandra, Mr Sharad Dwivedi, Mr. Sandeep Gupta, Mr Sameer Agrawal, Mr Vimal K Jaiswal, Mr. Himanshu, Ms. Meena Singh and all Design masters of 1998 batch, with whom I had spend the best days of my life at I I T Kanpur

I thank to all those who have contributed directly or indirectly to my thesis.

ARJUN SINGH

ABSTRACT

This work deals with the thermomechanical response of functionally graded materials A plate like structure subjected to sharp temperature gradient in the thickness direction is considered Theoretical models and numerical results for temperature field, heat flux, thermal residual stress, and thermal stress are presented both for functionally graded and equivalent bi-layered materials Significant trends and design guidelines to select appropriate composition profile for specific material pairs are presented. The role of microstructure, especially in regard to percolation phenomenon in transport properties and its significance for functionally graded materials is discussed and a novel approach to incorporate such effects in design calculations is presented.

Contents

List of Figures

CHAPTER 1.

Introduction

1.1 Need for Functional gradient material (FGM).

In recent years the environments in which materials are used have become more demanding. Conventional materials cannot withstand the severe environments confronting modern technologies. Further developments in science and technology rely heavily upon the development of new materials that can withstand the conditions that are created by advancing technology

In the development of these new materials there are two approaches. One is to develop new material that differs completely from any present materials The other option is to develop new function for existing materials The development of composites satisfies both of the above approaches. Many new types of composite have already been fabricated in accordance with the material properties demanded by today's technology.

A general requirement for industrial materials is uniformity in material properties That is, for industrial applications, it is essential that every part of the material in use exhibit uniform properties. The requirements for conventional composites are no exception. Most effort in the development of composites in the past has been put into determining how to uniformly mix the dispersoid within the matrix. As a result, from macroscopic viewpoint, even composites were regarded as homogeneous because in these materials the mechanical properties and other material characteristics prove to be homogeneous

In contrast, studies are also being conducted to design materials that have two different functions within the given material These materials

are inhomogeneous composites that are characterized by having different material characteristics on separate surfaces or in separate parts An example of a composite having different functions in its different parts is a coated or joined material designed to improve a material's surface characteristics However, these inhomogeneous composites possess sharp boundaries The boundary often exhibits various undesirable properties caused by the existence of discontinuities in the material's mechanical, physical, and chemical characteristics at the boundary An example is a separation at the boundary due to thermal stress

For this reason a proposal to design a new material aimed at eliminating the macroscopic boundary in laminated-type material is being examined That is, the approach is to synthesize inhomogeneous composites in which, the material's mechanical, physical and chemical property changes continuously, and which have no discontinuities within the material These materials are called Functional Gradient Materials (An alternative name is FGM). Fig 1.1 shows schematically the concept of a Functionally Graded Material

1.2 Definition of FGM and their importance.

FGM are those materials, which exhibit a progressive change in composition, structure, and properties as a function of position within the material See Fig 1 2

FGM are designed to take advantage of the attractive features of each of its constituents For example, one constituent may be a ceramic, which offers good high temperature behavior but is mechanically brittle. Another may be a metal which exhibits better mechanical and heat transfer properties but cannot withstand exposure to high temperature A structural component exposed to regions of both high and low temperature could thus be predominantly ceramic within the hotter region and metal within the cooler region. See Fig 1.3.

The design of an FGM is thus centered on the optimization of its structure in order to maximize (or minimize) some property associated with its in-service performance, while simultaneously maintaining other properties within acceptable limits.

Another aspect lies in predicting the characteristics of an FGM, for a given composition profile, during fabrication and under in service condition Use of theoretical models to aid in FGM design and to predict FGM fabrication and in-service behavior is of crucial importance.

The fact that the composition of an FGM can vary over such a wide range means that a variety of fundamentally different microstructures can exist across the graded direction This, in turn, means that the thermo-physical properties, which are generally strongly dependent on the microstructure, will also vary with position within the material A realistic model must appropriately account for this fact

1.3 Approaches to obtain FGM.

These are two approaches to obtaining FGMs, as shown in Fig 1.1. The first method is to eliminate the boundary of laminated-type composites [from (c) to (b)], thereby eliminating discontinuities in the properties at the boundary The second method is to make nonuniform distribution of dispersoids in homogeneous composites [from (a) to (b).], thus creating multiple functions within the material The gradient can be assigned not only in the direction of material's thickness but in the direction of its width as well

In normal FGMs, the concentration of the dispersoid changes gradually within the composite, but another type of FGM can be designed by continuously changing the morphology of the dispersoid, state, crystal structure and distribution pattern (Hirai, 1996).

1.3.1 Continuously changing the morphology of the dispersoids.

Spherical and fiber like dispersoids are distributed over surface X and Y. The shapes of these dispersoids are gradually varied (Fig 1 3a). Within a material, the dispersoid will be changed from spherical to fiber-like In this way a high Young's modulus and a high toughness value can be obtained on surface X while also achieving a high strength on surface Y. If surface Y is changed to a composite with a flake-like dispersoid it will be a material that is rich in lubricity. Plant systems observed in trees and bamboo often have this type of structure(MRS Bulletin, 1995)

1.3.2 Continuously changing the state.

With dense materials on surface X, introducing small voids into that surface can create a porous surface Y. Bioactive materials are an example of this type of composite The advantages are that surface X has sufficient strength to be used as a structural material, while surface

Y has good compatibility necessary for a biomaterial These voids also exhibit superior thermal stress relaxation This characteristic can be used to design unique and intriguing FGMs (Hirari, 1996)

When controlling the level of sintering from the front surface to back surface continuously changes the void distribution, the result is a simultaneous continuous change in the Young's modulus from the front to back This phenomenon is used to assign gradients in the piezoelectric properties within the material in order to generate a flexural vibration mode (Kawasaki and Watanabe, 1990)

This technique of continuously changing the state [Fig 1 3b] has some interesting applications in polymeric materials For example, by gradually lowering the degree of polymerization of a rod-like polymeric material, starting at the outer perimeter and continuing toward the center, it is possible to control the damping characteristics or vary the optical properties of the final material (Hirari, 1996).

1.3.3 Continuously changing the crystal structure.

In as amorphous material, high mechanical strength can be obtained by crystallization If a surface X is crystallized while the opposite surface, Y, is maintained in the amorphous state, surface X will have high mechanical strength while surface Y will have a good corrosion resistance, a gradient of these two properties will develop between the two surfaces [Fig 1 3c]. For metallic materials, an improvement in the surface properties is obtained by introducing ions to the surface, thereby making it amorphous These are examples of crystalline/amorphous FGMs If a crystallographic axis on surface X is oriented in one direction, and no specific orientation is given for surface Y, then it is possible to effectively utilize these anisotropic properties in order to influence the material's properties (Hirari, 1996).

By continuously changing the crystal structure in the thickness direction of a film from f c.c (surface X) to h.c.p (surface Y), an attempt has been made to prepare a high density perpendicular magnetic recording medium (Osaka et al , 1990).

By observing the change from paramagnetic to ferromagnetic that results from the martensite transformation, a magnetic FGM that has a gradual change in its saturation magnetization can be designed. This is achieved by continuously changing the transformation level from surface X to surface Y using the material to control deformation (Watanabe et al , 1993).

1.3.4 Continuously changing the distribution pattern.

High strength can be obtained by uniformly distributing the dispersoids on surface X High electrical conductivity can be obtained by distributing the dispersoids in the form of a network pattern on surface Y [Fig 1 3d]

1.3.5 Continuously changing the grain boundary characteristics.

By maintaining a nearly perfect grain boundary on surface X while introducing voids or faults into the boundary regions on surface Y, it is possible to control the diffusion of the atoms or molecules and thus obtain specialized characteristics suitable for a variety of sensor application, or for use as a catalyst

1.4. Applications of FGM.

Some important applications of FGMs are given below.

1. Joining Media

Since they have a potential for reducing thermal stress, FGMs have been investigated for joining metals to ceramic (Metal/FGM/Ceramic) and both metals and ceramic to FGMs (Metal/FGM, ceramic/FGM)

An FGM filler of Ni-MgO was used to join Ni to MgO, forming Ni/Ni-MgO(FGM)/MgO. The fracture strength (three-point flexural test) of the joints formed using the FGM Ni-NiO (72-128 Mpa) and FGM Ni-MgO (110 Mpa) was higher than when Ni was directly joined to MgO (30-60 Mpa). Iron was also successfully joined to AlN via an FGM of Al-AlN by containing the aluminum surface of the FGM with the iron and heating at 650^0C for 48 hours in flowing argon. The micro-hardness of the Al-rich zone in the FGM was greater than pure aluminum.
[Atarashiya, 1992]

2. Shuttle Thermal Insulation.

A shuttle protection FGM type tile developed for the space shuttle is more efficient and less costly than tiles currently being used. This tile, is known as Toughened Uni-Piece Fibrous Insulation (TUFI), is a low-

density composite thermal insulation It is the first FGM composite where the density of the material varies from high at the outer surfaces to low in the interior insulation

The current tiles are a rigid glass-fiber composite and are about 93% air, with a thin glass coating on top The Reaction-Cured Glass (RCG) coating is physically much like window glass and is only about 0 03 mm thick. Because of the coating gets little support from the underlying tile, it cracks or chips easily Unlike RCG, TUFI permeates the pores nearer the surface of the insulation material This supports and reinforces the outer surface, which makes the surface material less subject to impact damage (Aerospace Engr , 1994)

3. Surface Wave Devices.

Tani and Liu (1993) studied a piezoelectric FGM plate having continuously changing material properties in the direction of the plate thickness by wave propagation analysis The wave frequency spectrum, the energy propagation speed, the electromechanical coupling constants, and the mode shapes were determined by these analyses The results showed that the gradient properties can significantly improve the effectiveness of surface wave devices

4. Optical Fibers.

Kamaswami and Nishizawa (1965) proposed an optical fiber with a continuously changing refractive index in order to increase its transmission capacity. It has a higher refractive index at the core, while its sheath has a lower refractive index This type of optical fiber is called a graded index-type optical fiber (GI-type). The GI-type fiber has been shown to be capable of carrying more than 10 times the information compared to the step index-type optical fiber. Historically, GI-type fibers are the first example of a successful application of the graded property concept

5. Implant materials.

In order that man-made materials can coexist inside the human body, it is highly desirable on organically joining the material, that the boundary region between the human body and the material has a functional graded structure.

The Ti-Al-V alloy is known to be very compatible with the human body and is widely used for artificial bones and joints, nevertheless bonding them to human bone is still a problem However, a new type of implant material composed of a Ti-Al-V-type substrate has been made. This material is coated with Ti-Al-V beads to make it porous The material is further coated with the bioactive hydroxy-apatite (HAP) by plasma spraying Easier infiltration of the bone tissue thus occurs with time, creating a graded structure between the bone and implant material. The result is a better bonding between the human body and the inorganic material [Oonishi et al , 1994]

The bending strength of HAP/Ti is 150 Mpa, which is very close to that of a human bone This result suggests that the FGM is effective as an implant material [Watari, 1994].

6. Fire Retardant Material.

A phosphoric acid and amide mixture can be impregnated into wood by a high pressure technique When the phosphorus content is graded from the surface to the inner structure by phosphorylation, it becomes an excellent fire retardant material [Ishihara et al., 1992].

7. Building Material.

Takahashi et al.(1993) has successfully developed FGM with moisture absorption and release functions made by step wise or continuously changing the composition of two components-a zeolite or ligneous material-based humidity conditioning material, capable of absorbing and releasing moisture, and calcium silicate-based concrete. This FGM can absorb a maximum of approximately 2 5 times more moisture, and is particularly good in its initial response to humidity increase or decrease.

In addition this new material hardly changes its dimensions by expansion or contraction due to humidity, and it is strong, fire proof, frost damage resistant, and quite amenable to shape forming from flat board to curved corner material. As a building material, this material with a gradient moisture conditioning property from its outer wall to inner wall, could eliminate construction steps for faster completion of a project.

8. Future Shuttle and Aerospace Planes

Several study programs are underway to establish material design technology for creating complex-shaped FGMs and introducing FGM designs into the fuselage and engines of a reusable shuttle plane and other supersonic planes

In the development of large FGM test samples, a number of basic shapes have been adopted to promote the use of FGMs in the space plane fuselage and engines These shapes include a semi spherical shape that is required to create FGMs for use in the planes nose cone section, a hollow cylinder to make FGMs for application in the front edges of the wings and engines, and a squre plate to manufacture FGMs for use in other sections (MRS Bulletin, 1995).

9. Magnetic Recording Medium.

Osaka et al (1990) prepared a CoNiReP FGM film by electroless plating In this film the structure changes from a randomly oriented f.c.c structure to an oriented h c p structure in the thickness direction. They reported that by changing the composition and the structure of the film, a high density magnetic recording medium can be obtained A magnetic FGM was prepared by applying a gradual inhomogeneous deformation to SS304 austenite stainless steel (Fe-18Cr-8Ni) A magnetic FGM can be used as a position measuring device by combining it with a magnetic sensor For examples, it can be used as a device that determines the focal point in an automatic focussing camera [Watanabe et al., 1993].

1.5. Present Work.

The preceding sections have given a brief overview of the various form of FGM and a range of current and potential application of FGM.

The present work is concerned with FGM comprising of two materials with a composition gradient along a specified direction in a plate-like structure. Typically, such structures are used for intense thermal shielding and are subjected to sharp temperature gradients. Accordingly, metal/ceramic composites with a composition gradient are prime candidates for such applications. Their mechanical integrity under such service conditions is of great interest and the emphasis is on specifying concentration profile for a given material pair to minimize thermal stresses set up in the composite Current approaches to prediction of temperature distribution, thermal stress, thermal residual stress and

structure optimization, generally make use of FEM techniques and, are reviewed in chapter 2

The current work describes a simpler analytical/numerical approach for determination of temperature field and thermal stress in a FGM and these have been described in chapter 3 and chapter 4 respectively

In chapter 3, major emphasis is given to derive an expression for temperature distribution and heat flow rate in FGM, subjected to temperature difference across its thickness. Some attention is also paid to determine heat flow rate in bimetallic plate, having the same volume of each constituent as in FGM Finally, heat flow rate in FGM are compared with Bimetallic plate, having same volume of each constituent as in FGM, subjected to same temperature difference across their width

In chapter 4, an expression is derived for determination of thermal stress, which develops during in-service condition of FGM, due to temperature difference across the thickness of FGM Further, thermal residual stresses were determined in FGM, subjected to a temperature drop of 100^0C from a stress free state Thermal stresses are also calculated for bimetallic plate, having equal volume of each constituent as in FGM

Determination of temperature field and thermal stresses requires models for variation of various physical and mechanical properties with composition and suitable rules of mixture have been assumed as per general practice. However, the microstructure of a composite material may have an important bearing on its transport properties. Accordingly, a short discussion on the fabrication methods is also included in chapter 2 to better appreciate the effect of microstructure on the thermomechanical response of FGM. The related issues are discussed and a novel approach for incorporating such effects is proposed in chapter 5. Major conclusions and suggestions for future work are presented in chapter 6

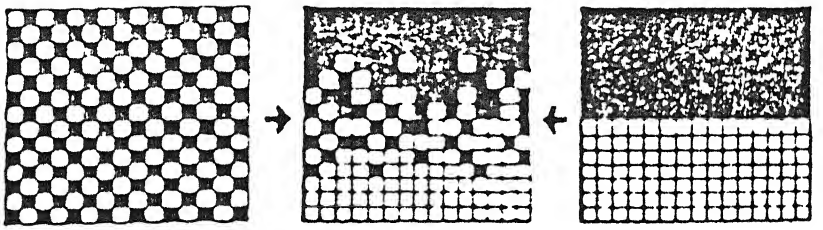

Fig 1.1 Conventional composites and a functional gradient material (a) homogeneous composite, (b) functional gradient material, and (c) coated or joined-type composite.

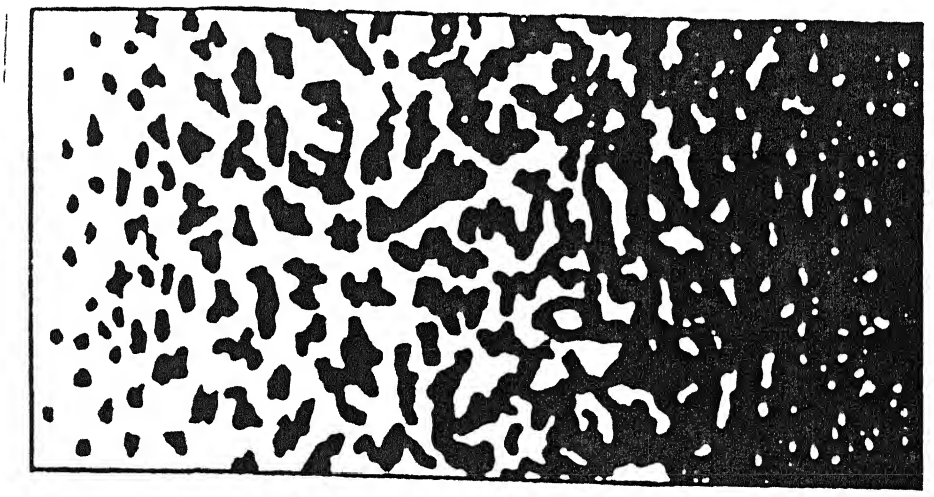

Fig 1.2 Schematic illustration o the microstructure of a two-component FGM, for which the composition gradually varies from entirely the one component to entirely the other

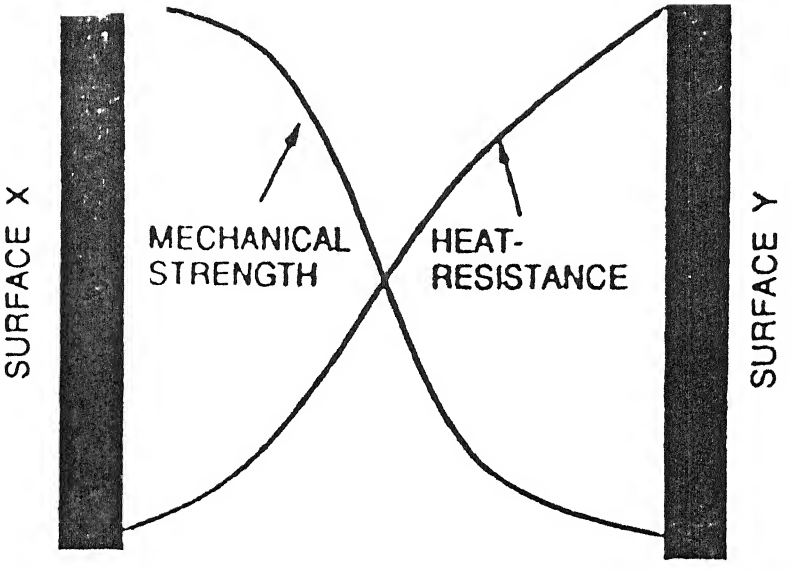

Fig 1 3 Schematic illustration of variation of variation of properties in FGM

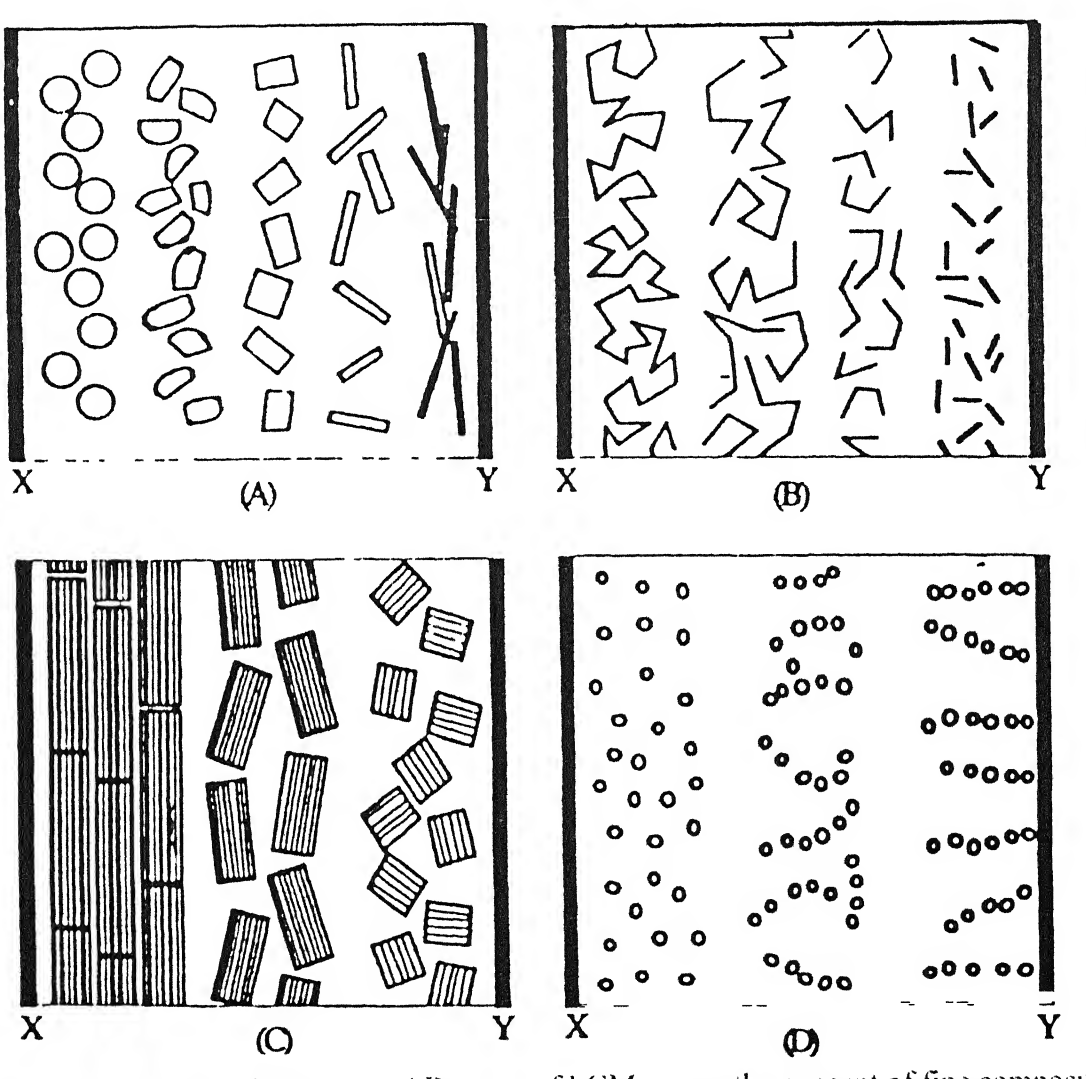

Fig 1 4 Schematic illustration of Designs of FGMs using the concept of fine composites. (A) continuously changing the morphology of the dispersoid, (B) continuously changing the state, (C) continuously changing the crystal structure, (D) continuously changing the distribution pattern

CHAPTER 2

Literature Review.

2.1 Methods of Manufacturing Functionally Gradient Materials

The most important objective in the preparation of an FGM is to achieve a well-controlled (according to the design) distribution of composition, texture, structure, and other necessary elements. That is, the preparation method for an FGM must be able to accommodate an arbitrary number *n* of the compositional distribution function On continuously changing the composition or structural elements within the material, the change can occur in two directions, in the thickness and width directions Most of the recent studies on FGM synthesis have been concentrated on change in thickness direction Therefore, in this section the methods used in the preparation of an FGM that has continuous change in the thickness direction will be discussed. The discussion also includes the method to produce an FGM having a step-wise change, as well as a continuous change Laminated-type FGMs, which are prepared by first producing sheets of film and then layering the films, will also be discussed.
There are several methods for the preparation of an FGM. However, for convenience they will be categorized according to the source material's state during fabrication of the FGM. They are: gas phase, liquid phase, and solid phase approaches

2.1.1 Vapor Phase Methods

(a) Chemical Vapor Deposition (CVD)

The CVD method yields a material deposit with source gases as the feed stock. This deposit is caused by the application of various form of energy

(heat, light, plasma, etc) onto the source gases after they are introduced into a reactor. Hydride, bromide and chloride are generally used for source materials When the source material is in liquid or solid form it is vaporized. In recent years, organometallic compounds have often been used as source materials By continuously changing the mixture ratio of source gases or by controlling the CVD conditions, such as deposition temperature or gas pressures the CVD method permits relatively east syntheses of various type of FGMs

SiC/C FGM coatings were prepared by changing the ratio of $SiCl_4/CH_4$ stepwise or continuously in a temperature range of 1300-1500^{0}C and a pressure range of 1 3-13 kPa on graphite plate, carbon fibers, and a cylindrical graphite tube (Uemura et al , 1990). Using the similar conditions, an SiC/C FGM of 120 μm thickness was coated on a model combustor with a cylindrical diameter of 30 mm made of three-dimensional C-C composite (Suemitsu et al , 1993).

In an effort to improve the oxidation resistance of C-C composites, C-fiber-reinforced SiC sintered bodies, a TiC/SiC FGM layer was coated on these substrates. In these cases, in order to minimize the difference between the expansion coefficients of the SiC coating and various composites materials, first a layer of TiC is produced on the surface of the composite material, followed by a layer of TiC/SiC FGM coating, whose composition changed gradually from TiC to SiC This CVD work was performed using the $TiCl_4$-CH_4-H_2 source gas system at 1350^{0}C and 8 kPa By changing the gas flow rates of $TiCl_4$ and $SiCl_4$ during the deposition process, an FGM coating of thickness 150 μm was obtained (Kawai et al., 1990).

(b) Chemical Vapor Infiltration (CVI)

The chemical vapor infiltration process, which evolved from the chemical vapor deposition for surface coatings, uses porous materials such as ceramic bodies and ceramic cloths which contain many residual pores. These materials are first placed inside a CVD furnace as a substrate. By decomposition or by chemical reaction of the source gases, a coating is deposited on the surface of the open-pore or the space inside of the porous substrate.

Agullo et al. (1993) pre-coated SiC-Nicalon fiber with C/SiC FGM (thickness; about 100 mm) by using continuous changes in the gas phase composition of tetraethylsilane ($SiEt_4$) and cumene ($iPrC_6H_5$) at 770^{0}C and 0.8 kPa. Agullo called it a compositional gradient layer (CGL). This CGL's composition changes continuously from C at the fiber side to SiC at the

surface side CVI is used to densify the FGM pre-coated, SiC-Nicalon plain weave fabrics above 1000^0C

(c) Physical Vapor Deposition (PVD) Methods

In the PVD method, a solid source material is energized using different kinds of energy source to obtain vaporized particles, which deposit on a substrate to form a film There is also a technique to accomplish chemical reaction of the vaporized particles in a gas phase The deposition speed of the PVD is rather slow Therefore only a thin film can be produced using this method However, since this technique does not require high temperature heating of the substrate, this method is preferred for the preparation of the FGM films used in electronics

Partially stabilized zirconia (PSZ) with a gradient density of 4.2 –5 g/cm^3 (70-84% theoretical) from the surface to the metal/ceramic interface has been prepared on a super-alloy substrate by an electron-beam PVD technique (Fritscher and Bunk, 1990)

2.1.2 Liquid Phase Methods

(a) Plasma Spraying Methods

In the plasma spraying method, the spraying source power is transported to the plasma jet by a torch nozzle. The molten source material is then sprayed on to the substrate to form a coating There are mainly two types of plasma sprayed FGM coatings, that is, the porosity-graded coating and the composition graded coating Use of plasma spraying in the preparation of FGM coatings requires the cleaver design of an apparatus that provides a continuously changing mixture ratio of the source power to the torch nozzle.

The MgO-ZrO_2/NiCrAl laminated (7 layers) FGM coating was prepared on a steel substrate by a plasma spraying technique using MgO (24 wt.%)-ZrO_2 and NiCr-Al (6 wt.%) powers. The spraying took place in the air using a single-torch plasma spray reactor (Eroglu et al., 1993).

Fukushima et al. (1990) developed a twin torch for use in FGM preparation. In this method two plasma torches are placed so that the centerline of each torch is aligned to the point of spray deposition on the substrate. Two different source materials are sprayed from each nozzle simultaneously onto the same spot on the substrate to obtain a coating of composite. Since each torch can be independently controlled for the required spray conditions, this method can easily use two source materials having

widely different melting points, such as metal and ceramic, to form an FGM coating Using this technique, an eleven-layered FGM coating of thickness 0 3-0 4 mm has been prepared using an Ni-based alloy (NiCrAlY) and YSZ. By using a smaller spray angle the amount of pores in the coating is increased This contributes to improved thermal barrier characteristics.

(b) *Copolymerization Method*

Koike et al (1989) have prepared graded index-type polymer optical fiber using the copolymerization method. The source materials for copolymerization are methylmethaacrylate (MMA) with a refractive index of 1.492, and benzyl methacrylate (BMA) with a refractive index of 1.562. First a polymer tube is prepared using poly-MMA A monomer mixture, of MMA and BMA is then added to this tube and circumferentially heated (60-80 ^{0}C) to obtain polymerization The inner wall of the polymer tube swells, interacting with the monomer mixture, and eventually a thin gel phase forms on the surface of the wall Then the copolymerization proceeds towards the center of the tube When polymerization the polymerization is completed, a polymer solid is obtained that has a radially varied mixture ratio of two kinds of polymers from the center to the outer perimeter The resulting solid has a radial distribution of refractive indices (Koike, 1991). This graded index polymer rod can be heat-drawn at 190-280^{0}C into an optical fiber with a graded index

2.1.3 Solid Phase Methods

(a) Sintering Methods

Normal Sintering and High Pressure Sintering Techniques

On preparing FGM by sintering cracks can often appear on the sintered body due to differences in the sintering characteristics and the mixture ratio of the two source powders Watanbe et al. (1991) controlled the shrinkage of the powder mixture by blending fine and course particle sizes.

Rabin and Heaps (1993) prepared six-layered Al_2O_3/Ni FGM using the power processing method. Graded compacts were produced by sequentially layering the power mixture in the die followed by CIP at 140 Mpa. The sintering was carried out at 1400^{0}C for 3 h in Ar, or by HP at about 1300^{0}C for 1 h at a pressure less than 10 Mpa, or by HIP at about

1350^{0}C and 100 Mpa They concluded that for the best quality FGM, careful selection and control of the powder particle size ratio and the preparation of a proper compositional distribution profile are necessary

Temperature Gradient Sintering Technique

In preparing FGM using source powder having a wide difference in their sintering temperature (for example metal/ceramic system), one sintering temperature cannot be used to obtain a good quality sintered body due to the difference in shrinkage characteristics of each source powder To overcome this problem, the portion containing more of the higher sintering temperature source is sintered at a higher temperature and the portion which contains more of the lower sintering temperature source must be sintered at a low temperature That is, the sintering must be accomplished under a prescribed temperature gradient One way to achieve this temperature gradient is to apply additional heat by use of a laser beam or infrared beam onto one side of the sample while it is in the sintering furnace.

It is also possible to assign a gradient to the density by use of temperature gradient sintering Kawasaki and Watanabe (1990) sintered a cylindrical PZT power compact in air for 1 h They heated one side of the sample by an infrared lamp, and created a temperature gradient of 150^{0}C within a depth of 5 mm from the sample surface The resulting sintered body was of higher density in the upper portion, while the lower portion was of low density. Such a density difference gives a continuous change in the piezoelectric characteristics within the material.

Plasma Activated Sintering Technique·

In plasma activated sintering an instantaneous pulsed electric current is applied to the subject powder to initiate current discharges in the voids between the powder particles Successful sintering can be accomplished by use of the heat generated by these discharges. Due to this current discharge, the powder surface is purified and activated. This method requires a relatively short time for sintering, and thus it is easier to control the grain growth. This method is also suitable for sintering materials with lower melting points (Bennett et al., 1968)

Using this technique a laminated-type (8-layers) FGM of the YSZ/SS410 system, which has a wide difference in sintering temperature between the two sources, was produced In this process the YSZ side was heated to 1200^{0}C, while the SS side was heated to 1000^{0}C using a specially shaped

graphite resistance heater, in order to obtain a temperature gradient (Omori et al , 1994)

(b) *Self-Propagating High-Temperature Synthesis (SHS) Methods*

This technique uses an exothermic reaction at temperatures exceeding 2000-3000 ^{0}C to obtain reaction products at a relatively high speed Because of its high-speed reaction the diffusion of atoms is prevented and thus it is possible to obtain a graded composition When pressure (water pressure, gas pressure etc) is applied during the SHS process the synthesis of dense composites can be achieved

Gas Reaction Sintering Technique.

Ni powder and Al fine powder (0.42 μm in diameter) are sintered in N_2 using the exothermic reaction of Al-N_2 to obtain AlN/Ni FGM. Using a similar technique, AlN/Al FGM can also be produced (Atarashiya et al., 1993).

Hydrostatic Compression SHS Technique

TiB_2, Ti, B and Cu powders are used as the source for the preparation of TiB_2/Cu FGM by this technique (Sata, 1993) Using the automatic powder spraying and stacking device, these powders were sprayed onto a Cu substrate The stacked compact was then ignited at room temperature under a high hydrostatic pressure of 58 Mpa TiB_2/Cu FGM with diameter 30 mm and thickness 1 mm was obtained on the Cu substrate.

(c) *Martensite Transformation Technique*

Watanabe et al. (1993) have attempted to prepare an FGM using crystallographic transformation. The paramagnetic phase in austenite stainless steel (Fe-18 Cr-8 Ni) transforms into the ferromagnetic martensite phase by plastic deformation The amount of martensite increases with increasing deformation. Thus the saturation magnetization of the deformed austenite stainless steel increases with increasing deformation (strain). Using this phenomenon a magnetic gradient function can be assigned by inhomogeneously deforming the stainless steel.

2.2 Models for thermophysical properties.

The problem of calculating effective thermophysical properties of heterogeneous materials is an old one However with new application for such materials continuing to emerge, interest and activity in this subject continues to the present day New approaches are sometimes developed with specific applications in mind (e g electrical, magnetic, superconducting, mechanical, or thermal properties), and, consequently, are not readily accessible to all that might be interested This is unfortunate, because their applicability may extend well beyond their immediately intended use Some particularly comprehensive reviews, related to this general subject, have been published within the past several decades

Models for specific thermophysical properties of a hetrogeneous material are based on some kind of microstructure-dependent "mixture rule". Wakishima et al , used a rule of mixture which is discussed here in some detail because of its application to the modeling of FGMs. They considered a material having two components, denoted by A and B. Let P_A and P_B be the values of some particular property for pure A and pure B, respectively, and let their respective volume fractions be c and c_1, where $c_1 = 1 - c$ if the material is 100% dense. For an FGM, these volume fractions are dependent upon position along the graded direction. The well-known Voigt-type estimate for the effective value, P, of this property is

$$P = P_A c + P_B c_1 \tag{2.1}$$

Which is simply an arithmetic mean On the other hand, the likewise well-known Reuss-type estimate is given by

$$\frac{1}{P} = \frac{c}{P_A} + \frac{c_1}{P_B} \tag{2 2}$$

which is a harmonic mean. As the authors pointed out, these expressions have only limited validity. They discussed the use of a more general expression

$$P = cP_A + c_1 P_B + cc_1 Q_{AB} \tag{2.3}$$

Where Q_{AB} is a function that depends on P_A, P_B, c and c_1, as well as on microstructure-dependent quantities.

A question that must also be addressed is that of how much information regarding microstructure must be included in order to describe adequately material properties and behavior Becker and Richmond treated this particular issue, as it relates to effects of grains, pores, and second-phase particles in numerical simulations of the mechanical response of ductile materials. Their models were limited to two dimensions, although the need for inclusion of micro-structural features, in order to be physically realistic, was demonstrated

Additional consideration of mixture rules for thermophysical properties were given by Hirano et al (1988), who related the pertinent rule for various properties to the nature of microstructure The specific microstructures they included were laminates, fiber composites with fiber aligned transversely and longitudinally to the graded direction, thin-layered composites, and composites in which the second phases are either flake-like or spherical inclusions.

Another way to estimate properties of heterogeneous media is to use statistical information on the microstructure to compute rigorous bounds on property values. Torquato (1991) reviewed these methods and showed that these bounds can often be used to provide good estimate of properties despite having incomplete statistical information on the microstructure. In some cases, these methods can result in improved predictions over bounds computed solely from the volume fraction occupied by the constituent phases and from individual phase properties

Still another approach to describing transport properties in heterogeneous media is that developed by Ben-Amoz (1976), in which the concept of heat transfer, as a whole, is redeveloped starting with an analysis of "micro- (or local) conduction" within a "micro-medium". The collection of all these micro-media makes up the entire medium. The macroscopic heat conduction equations, and the pertinent boundary conditions, are obtained using variation formalism. This approach was extended Baker-Jarvis and Inguva (1985) using green function technique.

Argyris (1994) described Analytical and numerical models for mechanical and thermal properties of plasma-sprayed ceramic coatings as a function of microstructure. Although these studies were not directed specifically toward FGMs, they are nevertheless relevant from the standpoint that plasma-spray is one method for ceramic fabrication of FGMs.

2.3 Models for Functionally Graded Materials.

In this section, we review approaches that have been used for modeling FGM design, processing, and performance Since processing and performance of such materials are generally integrally connected, features of both are incorporated into various models We look first at models foe the spatial variation of composition, then at system-type models for design and performance, and finally at models developed for a variety of aspects of FGM behavior

2.3.1 Models for spatial Variation of composition.

FGM models generally require an assumption regarding the spatial distribution of their constituent phases Consider, for example, an FGM that has two constituents, which we denote as 1 and 2. Assume the geometry is one-dimensional, with the x-direction being the direction of the microstructural gradient We first treat the local volume of phase 1, c, as a continuous function (the volume fraction of phase 2 being $1-c$ if the material is fully dense). These functions can be quite simple, the ability to exhibit curvature, both "concave upward" and "concave downward", being desirable.
Wakashima et al (1990), used the following expression for c.

$$c = \left[\frac{x_2 - x}{x_2 - x_1}\right]^n \qquad (2\,4)$$

Where x_1 and x_2 border regions of pure phase 1 and phase 2, respectively, and n is a variable parameter, the magnitude of which determines the curvature of c. The curvature can be made concave upward and concave downward, to a greater or lesser degree, by proper choice of n.

Markworth and Saunders (1995) used a quadratic function i e.

$$c = a_0 + a_1 x + a_2 x^2 \qquad (2.5)$$

Where the $a_i (i = 0,1,2)$ are variable parameters whose values are determined by imposing constraints and by optimization process itself.

These simple functions still offer considerable flexibility of choice relative to the "shape" of the c function

Markworth et al (1995) plotted the equation 2 4 for various values of n and eq 2 5 for the case $c(0)=0$ and $c(X)=1$, where X is the thickness of FGM along the graded direction These two condition were used to eliminate a_0 and a_1 from equation 2 5, leaving a_2 as the sole variable parameter. They observed that equation 2 4 offers a greater range of composition profiles than does equation 2 5, although the latter equation can be shown to be simpler to deal with, from an analytical point of view, than the former.

2.3.2 Systems approach to FGM modeling.

A useful approach to the overall modeling of FGM processing is based on a system-analysis strategy that has been employed by various investigators. Hirano et al (1988), have developed an "inverse design procedure" which is illustrated by the flow chart shown in Fig 2.3 Here, the structure and boundary conditions are specified initially. Then, several combinations of materials are assumed along with different assumptions for the spatially dependent mixture ratio. The temperature and thermal stress distributions are calculated for these various combinations, and the calculations are repeated until "optimum" conditions are obtained Attention is paid to the use of appropriate microstructure-dependent material-property models.

Another systems-type approach to the optimization process was used by Tanaka et al (1993), and consists of the following sequence of steps.

1. Choose an initial composition profile.
2 Carry out a preliminary analysis of non-stationary heat conduction and thermal stress.
3. At each time step, examine the design criteria
4. If the design criteria are violated, calculate a quantity known as " thermal stress sensitivity increment".
5. Find the optimum composition profile that satisfied the design criteria.
6. Repeat the analysis of non-stationary heat conduction and thermal stress with the composition profile determined
7 If the design criteria are violated at another time step, return to step 4.

These systems-type approaches to FGM design are just ordered sequences of steps, carried out to ensure that the resultant material will perform adequately in its intended application However, it is important to note that the term "optimum conditions" used above may not necessarily

have a unique definition, but may instead involve a set of compromises among various quantities (e g material types, heat flow rate, FGM thickness, maximum thermal stress, etc) in order that the desired application is achieved over an acceptably long in-service lifetime

2.3.3 Studies of Thermomechanical Response of FGM behavior.

Next, we turn our attention to some modeling studies that were directed toward a variety of aspects of FGM behavior. These may vary in degree of sophistication, but they share, together with the studies already described, the common goal of maintaining both the performance characteristics of the FGM and its structural integrity

An early version of an FGM was studied by Stewart et al (1986) for intended use as a thermal protection system for spacecraft re-entry. The anticipated need was high-temperature capability at one end and good mechanical behavior at the other end Two different materials were bonded together to serve this purpose Computation of thermal response agreed well with experiment

Markworth and Saunders used their model (1995) to maximize or minimize, as desired, the heat flux traversing the graded direction In so doing, they found some unusual behavior, as follows they assumed that thermal conductivity, modulus of elasticity and thermal expansion coefficient were all given by Voigt-type estimates, for a FGM that was pure ceramic at one end and pure metal at the other end (x=0 and x=X, respectively). The ceramic end was taken to be at a higher temperature than the metal end. Then for certain values of thermal conductivity, modulus of elasticity and thermal expansion coefficient for the pure metal and pure ceramic, and for conditions corresponding to the extreme cases of maximum and minimum rates of heat flow across the graded direction, the thermal stress distributions are as shown in Fig 2.4. Clearly, the stress distribution for maximum heat flow has a maximum value that lies inside the FGM, a fact that would have to be accounted for in material design. Another result (one that was expected) was that the optimum design for minimum heat flux across the FGM contained minimal metal in the structure, subject to imposed design constraints, and vice versa for maximum heat flux.

Result of finite-element calculations of axial, radial, circumferential, and shear stresses in disc-shaped FGMs, were reported by Watanabe and Kawasaki (1990). They pointed out two considerations that are relative to such calculations. One is to minimize the thermal stress caused by cooling

from the sintering temperature. The other is to minimize the stress generated during performance, e g as a thermal barrier.

Another numerical study of thermal stresses in FGMs, associated with both processing and performance, was conducted by Matsuzaki et al. (1991). They concluded that one of the important factors affecting these stresses is the compositional distribution In addition, they found that the key issue for this particular FGM ($MoSi_2$-SiC/TiAl) is the high thermal stress generated during processing, a problem that requires furthers attention

A finite element model, developed by Miller et al (1993) was intended to be a guide in both the design and fabrication of a NiAl-Al_2O_3 FGM The model was used to estimate residual stress as a function of structure of the material It also included effects of thermal cycling. Elastoplastic analyses were conducted by Giannakopoulos et al. (1994) of cyclic thermal response in multi-layered materials These layers consisted of a metal, a ceramic, and an FGM between the metal and the ceramic. Analytical and finite element methods were both used It was found that the smooth gradation of composition between metal and ceramic resulted, under thermal cycling conditions, in a reduction of (a) thermal residual stress, (b) accumulation of plastic strain, and (c) stress concentrations at free edges. Parametric information was also obtained relative to effects of the FGM or thermal response of the layered material occurring during processing

Kawasaki and Watanabe (1987) carried out a finite element analysis of thermal stresses in metal/ceramic FGMs with a 1400°C-temperature difference assumed to exist across the material. A linear dependence of material properties on composition was assumed. The variables studied were the interlayer width, fineness of the compositional gradation, and the compositional profile. They found, for example, that the maximum axial thermal stress decreased strongly with increasing interlayer width They also calculated this stress as a function of n [see eq 2.4] and found that a value of this parameter exists where the stress is a minimum

Matsuzaki et al. (1992) carried out an analytical design of a ZrO_2/TiAl FGM intended to insulate the cooling structure of Scramjet engines. Use of an FGM having optimized thermal resistance parameters was found to reduce the required mass of coolant to just 35% of that needed for a cooling structure without an FGM.

The thermal shock response to heating abruptly an isotropic metal/ceramic FGM was modeled by Zhang et al. (`1994), who found that thermomechanical coupling exerted a strong effect on this response. One can thus conclude that the neglect of such coupling effects under conditions of non-uniform exposure and sudden, intense heating needs to be questioned.

Transient thermal stresses in an FGM plate were studied by Taraki et al. using an elastic-plastic formalism. A micro-mechanical approach was used, based on the assumption that local microstructures can be described in terms of spherical ceramic (metal) particles embedded within a metal (ceramic) host phase at volume fractions that vary in a quasi-continuous manner Transient thermal stresses were calculated for a zirconia/stainless steel FGM plate, subjected to cycling thermal load, for both elastic and elastoplastic conditions A possible thermal ratcheting effect was observed.

Jin and Noda (1994) who modeled a crack in a semi-infinite plate of a FGM carried out a study of transient thermal stress intensity factors This involves a reduction of the thermal and mechanical problems to two systems of singular integral equations It was found that substantial lowering of stress intensity factors could be obtained by appropriate selection of thermophysical properties

A non-destructive method for detecting and evaluating the distribution of elastic parameters along the graded direction of an FGM has been developed by Kuwahara et al (1992) The method that was used was "reflective impulse response", which includes determination of the acoustic impedance profile (Acoustic impedance is the product of density times speed of sound) The composition profile that was assumed is that given by eq 2 4.

Levit et al (1996) determined the residual stresses in Plasma-sprayed ZrO_2-$7Y_2O_3$ thermal barrier coatings deposited on Ni-base superalloy substrates which were kept at different temperatures. The stress measurements were carried out on as-sprayed specimens with X-ray diffraction equipment using the "$\sin^2\psi$" technique. It was found that the residual stresses in ceramic layer changes from tensile to compressive with increasing substrate temperature during deposition from 75 ^{0}C to 500 ^{0}C. From microstructural observations and residual; stress analysis it followed that the high tensile stresses are responsible for the "segmented structure" formed within the ceramic layer, while high compressive stresses lead to the development of microcracks parallel to the coating-substrate interface. A mathematical model was developed for predicting stress distribution in as-sprayed coating-substrate composites. The experimental data showed good agreement with predicted result

Erdogan and Ozturk (1995) considered the antiplane elasticity problem for a functionally graded coating bonded to a homogeneous half space. The coating is assumed to contain periodic cracks perpendicular to the surface. The problem is formulated in terms of an integral equation with strongly singular kernels Three dimensionless parameters representing the

crack depth, the material nonhomogeneity and the crack periodicity are identified In addition to the mode 3 stress intensity factor calculated by varying these three parameters, the results presented include a qualitative discussion of the question of fracture instability, the effect of periodic cracking on the relaxation of stresses on the coating surface, and the comparison of the total strain energy released as a result of surface cracking with that assumed in a simple stress relaxation model

Ostoja-Starzewski et al (1996) considered a unidirectional fiber-reinforced composite with an interphase between the fiber and matrix taken as a graded zone of two randomly interpenetrating phases of these materials. In particular, they take this interphase as a functionally graded material The objective was to present a micromechanics based method to treat FGM and to calculate the effective macroscopic properties (transverse conductivity, or, equivalently, axial shear modulus) of such a composite material. This problem requires the treatment of several length scales the fine interphase microstructure, its mesocontinuum representation, the fiber size, and the macroscale level (of many fibers) at which the effective properties are defined. It is shown through an example that a convergent hierarchy of bounds on the effective response is obtained with systematically mesoscale resolutions.

Finot et al. (1996) studied experimentally and numericallly the elastoplastic deformation characteristics of a plasma-sprayed, tri-layered composite plate subjected to thermal cycling from 20^0C upto 800^0C. The tri-layered solid comprised polycrystralline Ni and Al_2O_3 outer layers and a 2.2 mm thick compositionally graded Ni-Al_2O_3 composite interlayer (FGM) wherein the composition varied approximately linearly along the layer thickness The experiment involved in situ and ex situ measurements, employing a scanning laser technique, of the changes in the overall curvature of the unconstrained plate arising from the thermal mismatch between the constituent phases. The variations of curvature, accumulated plastic strains and thermal stresses at different locations in the layered solid were also assessed numerically with the aid of available continuum formulations, and the numerical predictions were compared with experiments, wherever appropriate. It was shown that when only small plastic strains exist in the Ni layer or in the Ni-rich end of the FGM layer, known formulations are capable of providing approximate predictions of the cyclic variation in curvature, the onset of plasticity and some features of the initiation of cracking (and its location). They also examined possible sources of error in the experimental measurements of curvature and in the

interpretation of thermally induced deformation due to some processing conditions

Taya et al (1996) proposed a new dislocation punching model for a functionally graded material subjected to a temperature change, using Eshelby's model. FGM, consisting of several layer, is deposited on aceramic substrate Two types of microstructure were examined for a layer: one consists of a metal matrix and ceramic particles and the other of a ceramic matrix and metal particles. An elastic energy was evaluated when plastic strain, in addition to thermal mismatch strain, is introduced in the metal phase. The work dissipated by the plastic deformation was also calculated From the condition that the reduction in the elastic energy is larger than the work dissipated, a critical thermal mismatch strain to induce stress relaxation was determined The magnitude of the plastic strain was also determined, when the relaxation occurs. The theory was applied to a model FGM consisting of mixtures of Pd and Al_2O_3 on an Al_2O_3 substrate.

Weissenbek et al (1997) analyzed the elasto-plastic deformation due to thermal and mechanical loading of layered metal-ceramic composites with compositionally graded interface using detailed finite element models. The madel material considered was a Ni-Al_2O_3 layered system with a compositionally graded interface. The analyses considered planer geometries with perfectly periodic arrangements of the constituent phase, by recourse to new classes of square-packing and hexagonal-packing unit cell formulations for the graded material. They also considered graded graded phase arrangements within which large numbers of microstructural units of the two phases are randomly placed within the unit cell. It was found that square-packing arrangements provide the best possible bounds for the thermal strains and coefficient of thermal expansion of the graded multi-layer, among the different unit cell models examined, however, no unique bounds could be identified for mechanical loading The numerical predictions of thermal and mechanical response were compared with those provided by the mean-field approach involving an incremental Mori-Tanaka analysis and by the simple rule of mixture approximations. The former method provides a stiffer mechanical response than the finite-element unit cell models. The finite element prediction of bending coefficient thermal expansion due to thermal excursions match the overall trends observed experimentally for the Ni-Al_2O_3 graded system, and further provide a quantitative prediction of the temperature for the onset of plastic flow in the graded material.

Kesler et al. (1997) proposed an experimental method, which enables the determination of processing –induced intrinsic stresses, elastic modulus, and the coefficients of thermal expansion of surface coatings of homogeneous

and graded compositions. In this method, a number of identical substrate specimens are coated simultaneously with surface layers of fixed and graded compositions, and the specimens with different layer thickness were periodically removed from the deposition chamber. It was shown that the following result could be obtained from knowledge of the strain or curvature and thermal history of the coated specimens, in conjunction with simple four-point bend tests and thermal loading/cycling at different temperature:

1 the magnitude of the processing-induced intrinsic stresses through the thickness of the coatings,
2 the in-plane Young's modulus, E, as a function of the coating thickness,
3. the coefficient of thermal expansion, α, as a function of coating thickness,
4 the variation of E and α as a function of temperature at any thickness location within the coatings, and
5 the separation of internal stresses arising from the deposition process (so called "intrinsic" or "quench" stresses)

The thermo-mechanical analyses underlying this method were discussed in detail, and its significance and limitations were addressed The proposed method was used to determine the evolution of processing-induced stresses during the successive build-up of plasma-sprayed Ni-Al_2O_3 coatings of homogeneous and graded compositions.

Suresh et al. (1997) presented computational and experimental results on the evolution of stresses and deformation fields due to indentation from a rigid spherical indentor on a graded substrate. The analyses addressed the variation of Young's modulus, E, of the substrate as a function of depth, z, beneath the indented surface for an exponential law, $E = E_0 e^{\alpha z}$, where E_0 is the Young's modulus at the surface and $1/\alpha$ is a length parameter. The theoretically predicted force-indenter penetration (P-h) curves were also compared with direct experimental measurements made on compositionally graded Ni-Al_2O_3 and TiAl-Y_2O_3-stabilized TZP composites of known composition gradients. A new method was proposed for the estimation of Young's modulus variations through a compositionally graded layer by recourse to spherical indentation

Dao et al. (1997) developed a physically based computation micromechanics model to study random and discrete microstructures in FGMs. The influences of discrete microstructures on residual stress distributions at grain size level were examined with respect to material gradient and FGM volume percentage (within a ceramic-FGM-metal three-layer structure). Both thermoelastic and thermoplastic deformation were considered, and the plastic behavior of metal grains was modeled at the

single crystal level using crystal plasticity theory. The results were compared with those obtained using a continuous model, which does not consider the microstructural randomness and discreteness. yIn an averaged sense both the micromechanics model and the continuous model give practically the same macroscopic stresses, whereas the discrete micromechanics model predicts fairly high residual stress concentration at grain size level with only a 300^0C temperature drop in a Ni-Al_2O_3 FGM system. Statistical analysis showed that the residual stress concentrations are insensitive to material gradient and FGM volume percentage The results obtained provide some insights for improving the reliability of FGMs against fracture and de-lamination.

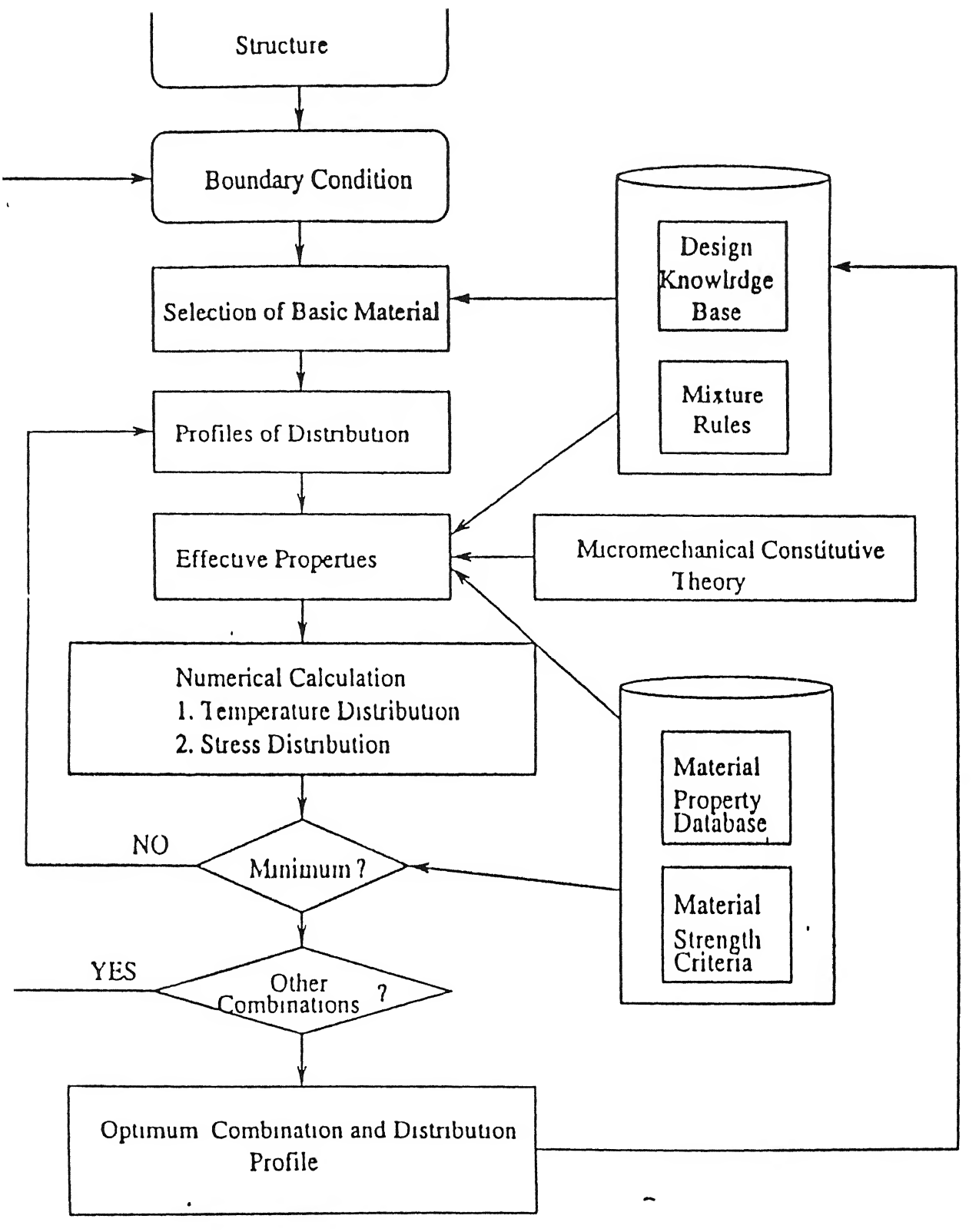

Fig 2.1 Flow chart for the "inverse design procedure" used for FGM design

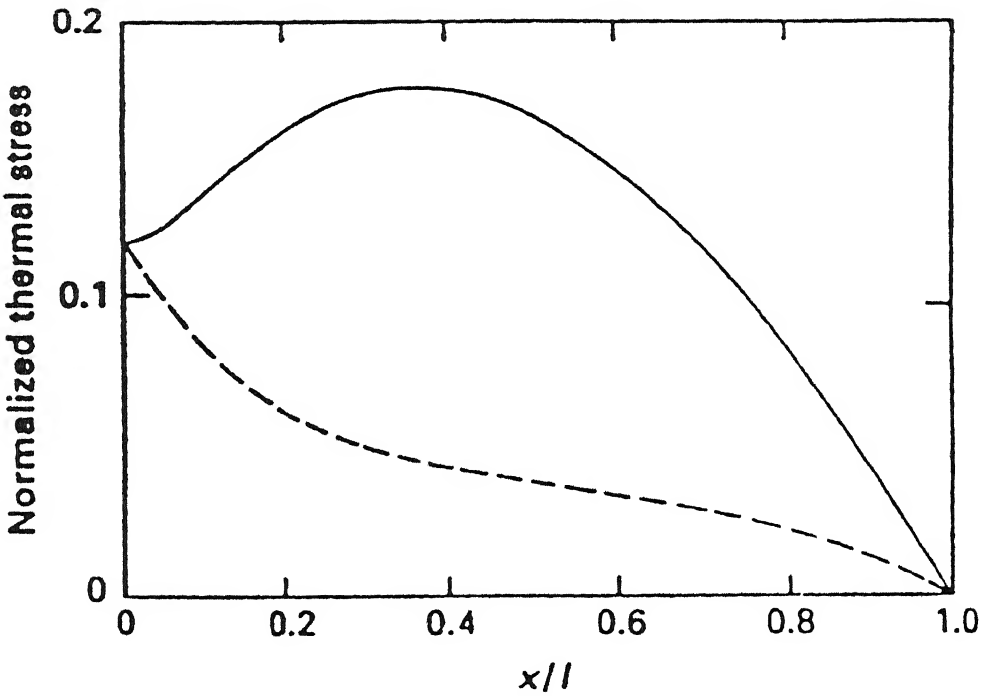

Fig 2 2 Thermal stress distribution across a metal-ceramic FGM designed for maximum heat flow (-) and minimum heat flow (---) across the graded direction The stress is normalized with respect to the maximum thermal stress in an all metal layer

CHAPTER 3

Temperature Distribution and Heat flow rate.

The present study is concerned with thermomechanical response of a FGM plate subjected to temperature variation across its two surfaces. In this chapter we look at the steady-state temperature distribution across the plate as a function of various material parameters such as thermal conductivity and composition profile. In some applications FGM is used as insulator i.e to minimize heat flow through structure, in other way one may like to maximize the heat flux. The basic equations are outlined in this chapter for heat flow rate and temperature distribution in FGM. Further an expression for heat flow rate in bimetallic plate having the same volume of individual constiuent as in FGM is also derived. As a specific example, results for a given material pair (Al_2O_3- Ni) are presented and some general observations are made.

3.1 Temperature Distribution in FGM

In this study a metal-ceramic FGM having a plate like structure is assumed. The size of plate is large compared to its thickness. Temperatures on ceramic and metal side are T_1 and T_2 respectively (Fig. 3.1). On the left hand side there is pure ceramic and on the right hand side there is pure metal The concentration of metal varies according to a power law from left-hand side to right hand side. The use of power-law expression covers a wide range of composition profile by adjusting the value of the exponent n as shown in Fig. 3.2. Temperature T_1 is greater than Temperature T_2. k_1 and k_2 are the thermal conductivities of ceramic and metal respectively. The

temperature at an arbitrary location x is given by T at steady state Similarly k_x is the thermal conductivity at an arbitrary location x.

Following assumptions are made

1. The y and z dimensions of FGM are large compared to the plate thickness that is X
2. Concentration of metal in FGM varies only in the x-direction and follows power law that is given by the following equation:

$$c = \left(\frac{x}{X}\right)^n \qquad \textbf{(3. 1)}$$

where n is an arbitrary index and c is the concentration of metal at location x.

3. Thermal conductivity of FGM at an arbitrary location is determined using Voigt-type estimate (Rule of mixtures)
4. The heat flow is essentially one-dimensional in nature.

Defining

$\eta = \frac{x}{X}$, as a non-dimensional distance, we obtain ·

$$c = \eta^n \qquad (3\ 2)$$

where η ranges between 0 and 1.

For 1-D steady state heat conduction [Holman, 1996], assuming unit area for heat flow:

$$q_x = -k_x \frac{dT}{dx} \qquad (3.3)$$

where, q_x is the heat flux, T is the temperature, and k_x is the thermal conductivity at an location x.

Using rule of mixture for k_x

$$k_x = k_1(1-c) + k_2 c$$
$$= k_1 + (k_2 - k_1)\eta^n \qquad (3.4)$$

Defining non-dimensional temperature as

$$\theta = \frac{T - T_2}{T_1 - T_2} \qquad (3.5)$$

Then, θ ranges between 0 and 1.

From equation 3.1 and 3.5, we obtain

$$\frac{dT}{dx} = \frac{T_1 - T_2}{X} \frac{d\theta}{d\eta} \qquad (3.6)$$

Substituting for k_x and $\frac{dT}{dx}$ in eq 3 3

$q_x = -\left[k_1 + (k_2 - k_1)\eta^n\right] \frac{T_1 - T_2}{X} \frac{d\theta}{d\eta}$, which gives

$$\frac{d\theta}{d\eta} = -\frac{q_x X}{(T_1 - T_2)} \frac{1}{k_1(1 + m\eta^n)} \tag{3.7}$$

Here

$$m = \frac{k_2 - k_1}{k_1} \tag{3.8}$$

On Integrating eq. 3 7 from $\eta = 0$ to 1

$$\int_{\theta_0}^{\theta_\eta} d\theta = -\int_0^{\eta} \frac{q_x X}{(T_1 - T_2)} \frac{1}{k_1(1 + m\eta^n)} d\eta + c_1$$

$$\theta_\eta - \theta_0 = -\frac{q_x X}{(T_1 - T_2)k_1} \int_0^{\beta_1} \frac{1}{1 + m\eta^n} d\eta + c_1 \tag{3.9}$$

where θ_η is the value of θ at η.

Imposing the boundary conditions

$\theta = 1$ at $\eta = 0$

$\theta = 0$ at $\eta = 1$

in eq. (3.9) we obtain:

$c_1 = 0$

and

$$q_x = \frac{(T_1 - T_2)k_1}{X} \frac{1}{\int_0^1 \frac{d\eta}{1 + m\eta^n}} \tag{3.10}$$

Substitute these values in eq (3 9)

$$\theta = 1 - \frac{\int_0^{\eta} \frac{d\eta}{1+m\eta^n}}{\int_0^{1} \frac{d\eta}{1+m\eta^n}} \qquad (3.11)$$

The actual temperatures are therefore obtained by

$$T = T_1 - (T_1 - T_2)\left(\frac{\int_0^{\eta} \frac{d\eta}{1+m\eta^n}}{\int_0^{1} \frac{d\eta}{1+m\eta^n}} \right) \qquad (3.12)$$

Equation (3.9) gives the value of temperature at any value of η $(0 \le \eta_1 \le 1)$.

3.2 Heat flow rate in FGM and Bimetallic plate, having equal volume of metal and ceramic

(A) Heat flow rate in FGM

Heat flow rate in FGM is given by eq. (3 10) for a given values of m and n

$$q_x = \frac{(T_1 - T_2)k_1}{X} \frac{1}{\int_0^{1} \frac{d\eta}{1+m\eta^n}}$$

This may be expressed as a non-dimensional parameter H given by

$$H = \frac{q_x X}{(T_1 - T_2)k_1} \qquad (3.13)$$

$$= \frac{1}{\int_0^{1} \frac{d\eta}{1+m\eta^n}} \qquad (3.14)$$

(B) Heat flow rate in a bimetallic plate, having equal volume of metal and ceramic as in a corresponding FGM.

Metallic volume fraction V_M in FGM for a given value of n is determined in the following manner:

$$V_M = \int_0^{1} \eta^n d\eta$$

$$= \frac{1}{n+1}$$

Since

$V_M + V_C = 1$

Therefore,

$$V_C = 1 - \frac{1}{n+1}$$

$$V_C = \frac{n}{n+1} \qquad (3.15)$$

where V_C is the volume fraction of ceramic in FGM for a given value of n

Now consider a bimetallic plate having volume fraction of metal and ceramic equal to V_M and V_C, the relative thickness of the layers will be $\frac{1}{n+1}$ and $\frac{n}{n+1}$ respectively.

The temperature at the interface of ceramic and metal will have an intermediate T_0 between T_1 and T_2.

The following assumptions are made

1. y and z dimensions of plate are large as compared to X.
2. Area of heat flow is taken unity
3 Nature of heat flow is one dimension steady state conduction flow.

For steady state heat flow

$$q_x = \frac{k_{eq}(T_1 - T_2)}{X} \qquad (3.16)$$

where k_{eq} is the equivalent thermal conductivity of the bimetallic composite. Since heat flux should be same through the metal and ceramic plates (in the absence of any heat source or sink).

$$q_x = \frac{k_1(T_1 - T_0)}{\frac{nX}{n+1}} = \frac{k_2(T_0 - T_2)}{\frac{X}{n+1}} \qquad (3.17)$$

Therefore we obtain:

$$T_0 = \frac{k_1 T_1 + n k_2 T_2}{n k_2 + k_1} \qquad (3.18)$$

From eq. (3 8)

$$m = \frac{k_2 - k_1}{k_1}$$

$$k_2 = (m+1)k_1$$

$$k_2 = rk_1$$

Where

$$r = m+1$$

Substituting $k_2 = rk_1$ in eq (3 18)

$$T_0 = \frac{T_1 + nrT_2}{nr+1} \qquad (3\ 19)$$

From eq (3 17) and (3 20), we obtain

$$q_x = \frac{k_1(n+1)(T_1 - T_2)r}{X(nr+1)} \qquad (3.20)$$

and substituting in eq. (3.16), we obtain

$$k_{eq} = \frac{k_1(n+1)r}{nr+1}$$

$$k_{eq} = k_1\left(1 + \frac{1}{n+1+\frac{1}{m}}\right) \qquad (3.21)$$

Substituting this value of k_{eq} into eq (3.16)

$$q_x = \frac{k_1(T_1 - T_2)}{X}\left(1 + \frac{1}{n+1+\frac{1}{m}}\right) \qquad (3\ 22)$$

In term of the non-dimensional parameter (H), defined in (3.13) we obtain:

$$H = \frac{q_x X}{k_1(T_1 - T_2)} = \left(1 + \frac{1}{n+1+\frac{1}{m}}\right) \qquad (3.23)$$

$$= \left(1 + \frac{1}{n+1+\frac{1}{m}}\right) \qquad (3.24)$$

Note that non-dimensional heat flux has the same definition as for the FGM.

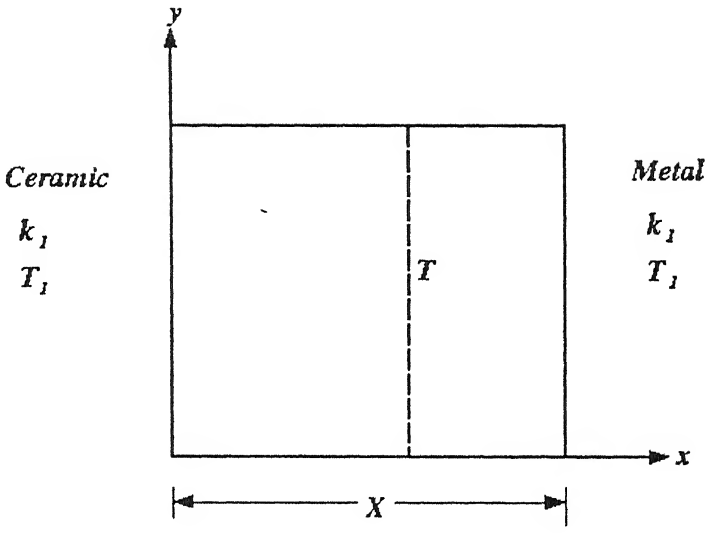

Figure 3 1 A metal-ceramic FGM in which concentration of metal varies in x-direction according to power law ($c = \beta_1^n$)

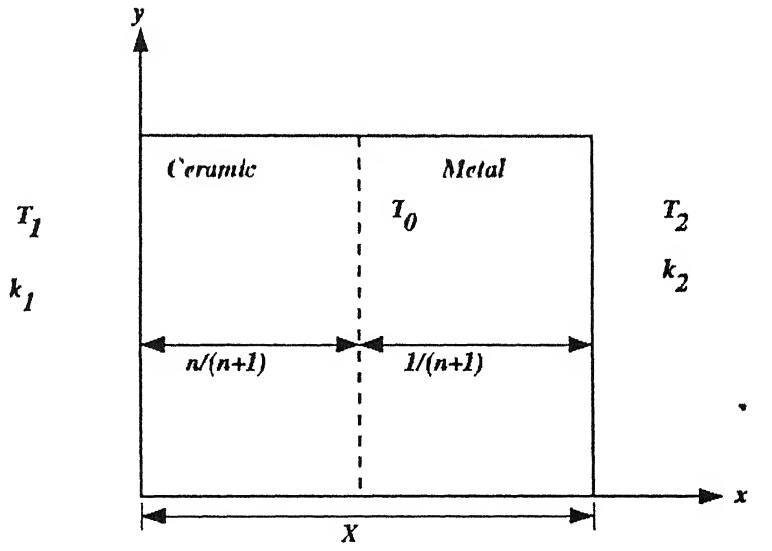

Figure 3 2 A metal-ceramic bimetallic plate, having equal volume fraction of metal and ceramic as in FGM for an arbitrary value of n

3.3 Results and Discussion

In this section results are presented based on the theory developed in preceding sections MATLAB Simulink is used to determine the temperature distribution and heat flow rate in FGM as well as in the corresponding bilayered plate having the same fraction of individual constitute as in FGM.

Figs. 3.3-3.6 show the variation of non-dimensional temperature θ in the plate thickness direction for various values of composition profiles (n= 25-3.0). The value of $m\left(m=\frac{k_2-k_1}{k_1}\right)$ ranges from 1- 4.

In each of these cases, there is a smooth change in slope of θ verses η curve unlike the case of a equivalent bi-layered plate where there is a sudden change in slope across the interface This has an important bearing on the stress field in the material, as described inn chapter 4.

The variation of non-dimensional heat flux with composition profile and its comparison with corresponding heat flux in equivalent layered material is shown in Figs 3 7 – 3.12

For small values of n, FGM is better than the corresponding bi-layered material in maximizing/removing heat. However, there is a cross over point (n_{cr}) , beyond which the bi-layered material will be more effective If the intended application is thermal insulation, the FGM is better for values of n greater than n_{cr} . The position of cross over point is dependent on the ration of the thermal conductivity of the two materials as shown in Figs 3.7-3.12.

The variation of n_{cr} with thermal conductivity ratio has been obtained through a parametric study and is shown in Figs 3 13.

From fabrication point of view, it would generally be difficult to make materials with n>10 or so, therefore a detailed view of Fig. 3.13 in the range n=.1- 10 is given in Fig. 3.14.

This information serves as useful design guideline in selecting the constituent materials and specifying the appropriate composition profile to maximize the performance of the structure.

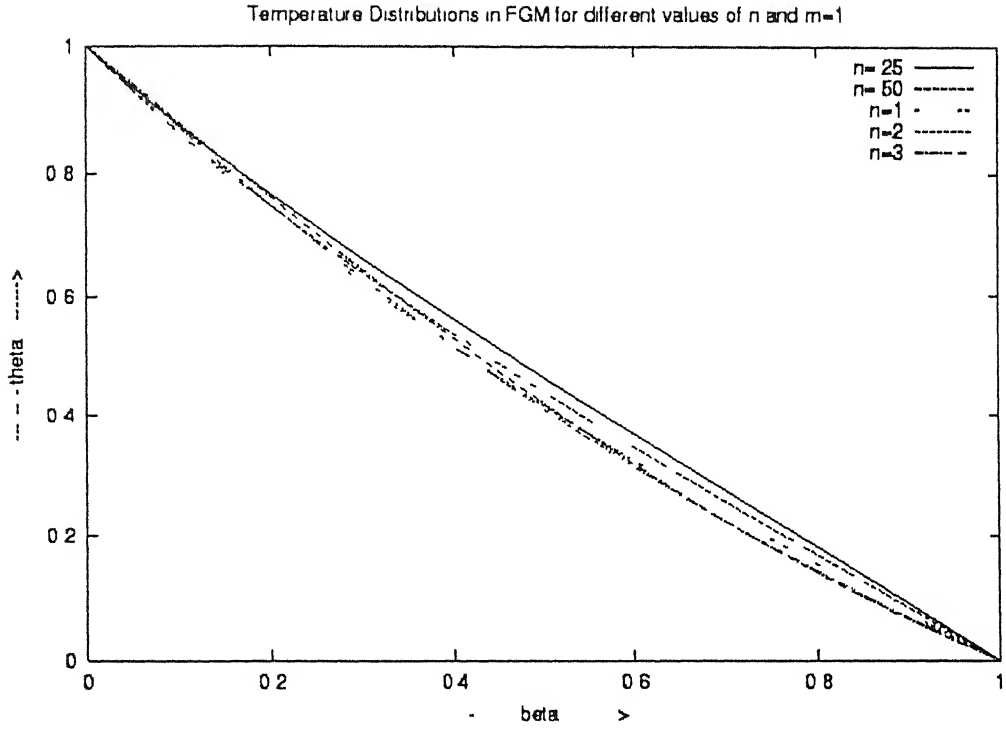

Fig 3 3 Temperature distributions in metal-ceramic FGM for different values of n and $k_2 = 2k_1$

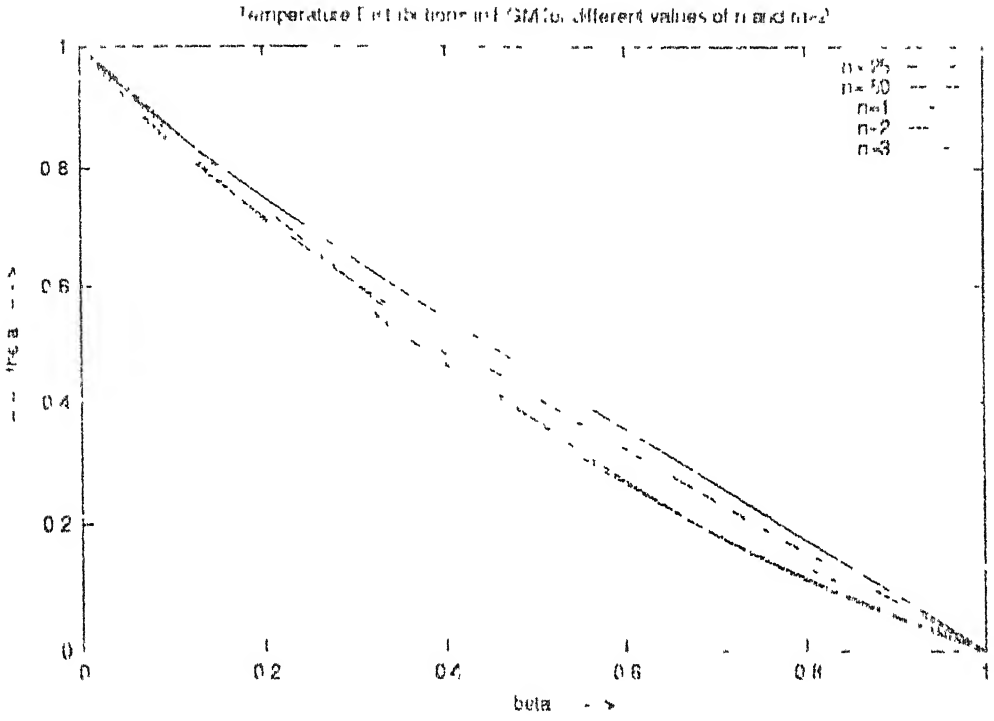

Fig 3.4 Temperature distributions in metal-ceramic FGM for different values of n and $k_2 = 3k_1$

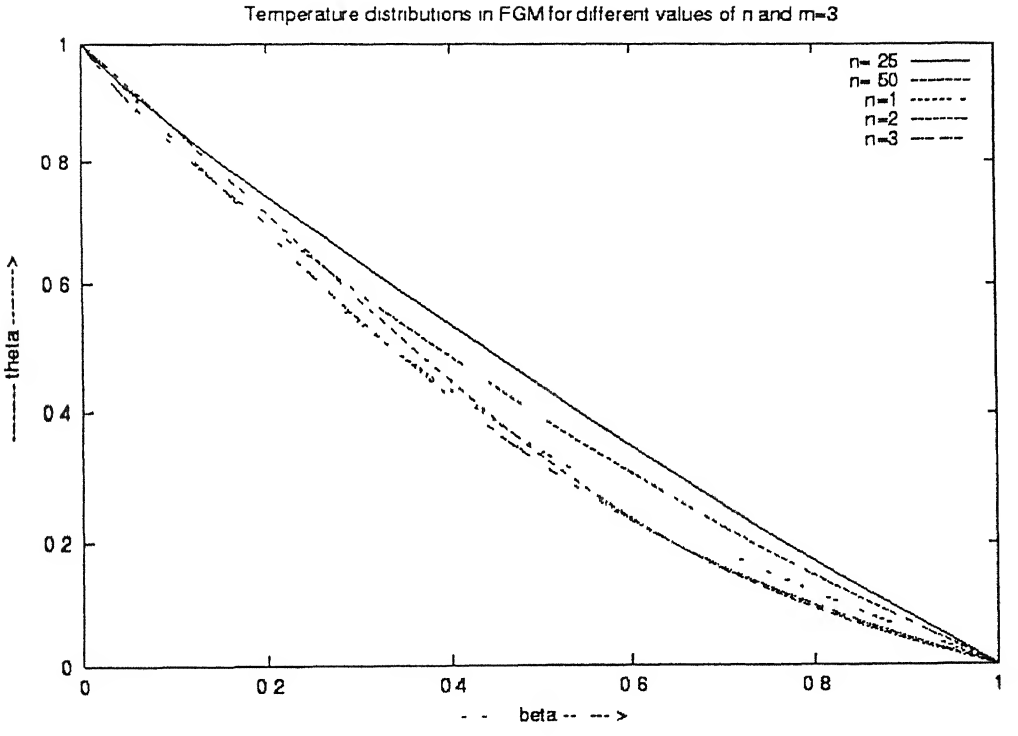

Fig 3 5 Temperature distributions in metal-ceramic FGM for different values of n and $k_2 = 4k_1$

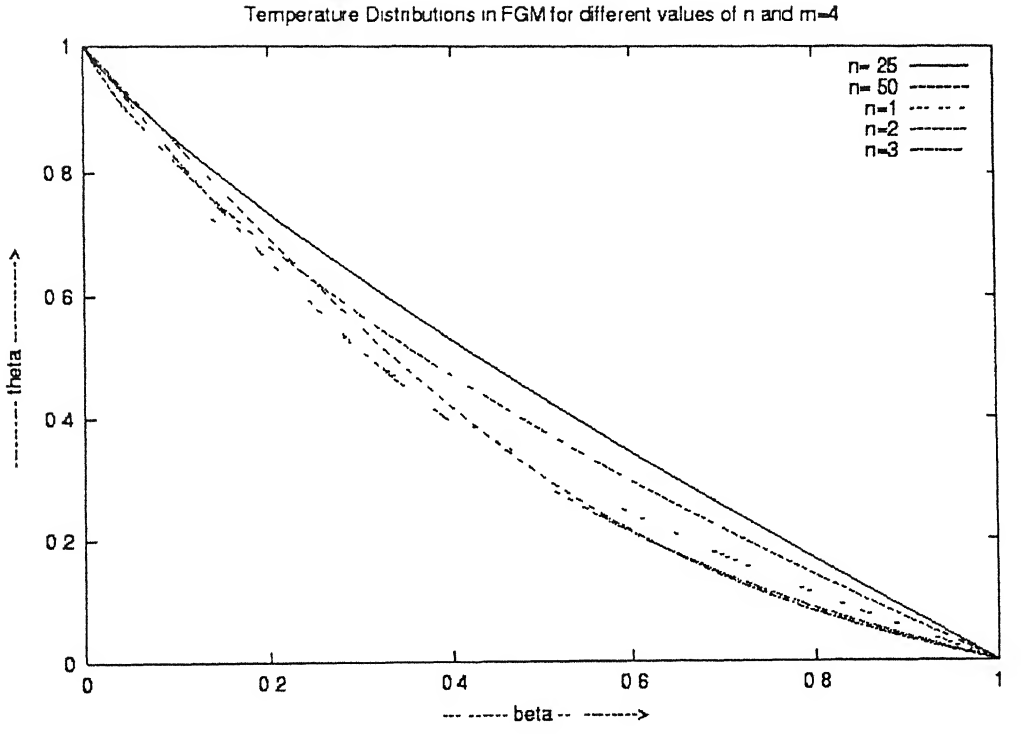

Fig 3 6 Temperature distributions in metal-ceramic FGM for different values of n and $k_2 = 5k_1$

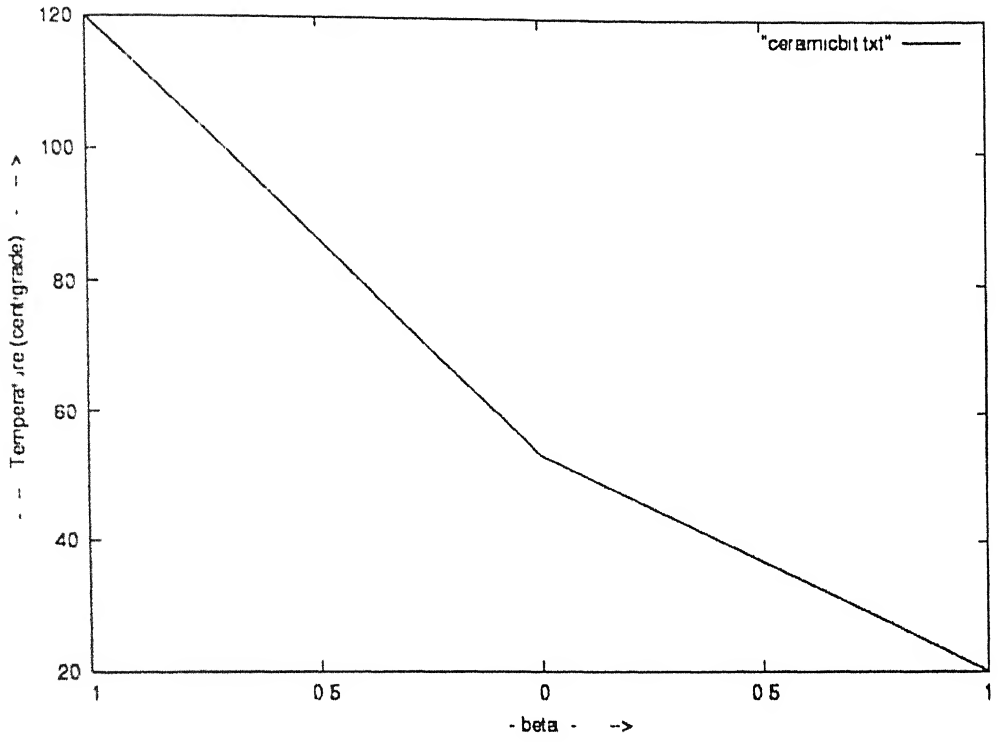

Fig 3 6 1 Temperature distribution in Bi-layered structure, which corresponds to a FGM, having the value of n as 1 (n=1)

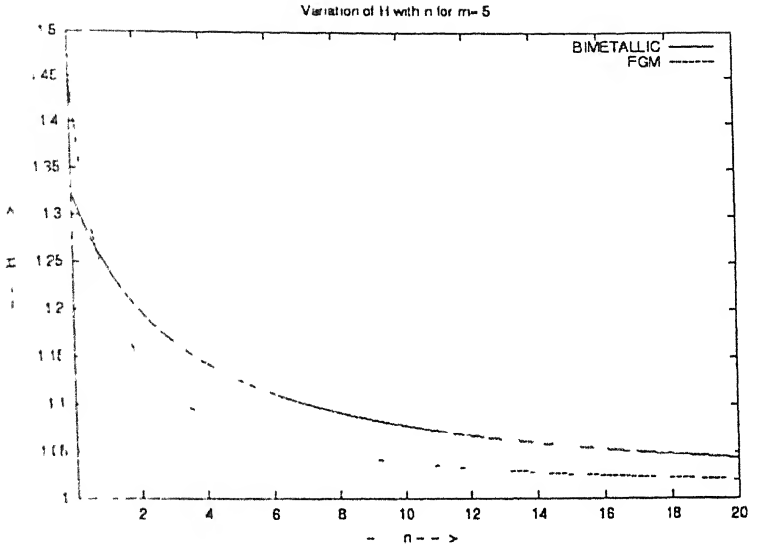

Fig 3 7 Variation of heat flow rate in terms of H (non-dimensional parameter) in FGM and bimetallic plate for $k_2 = 1.5k_1$

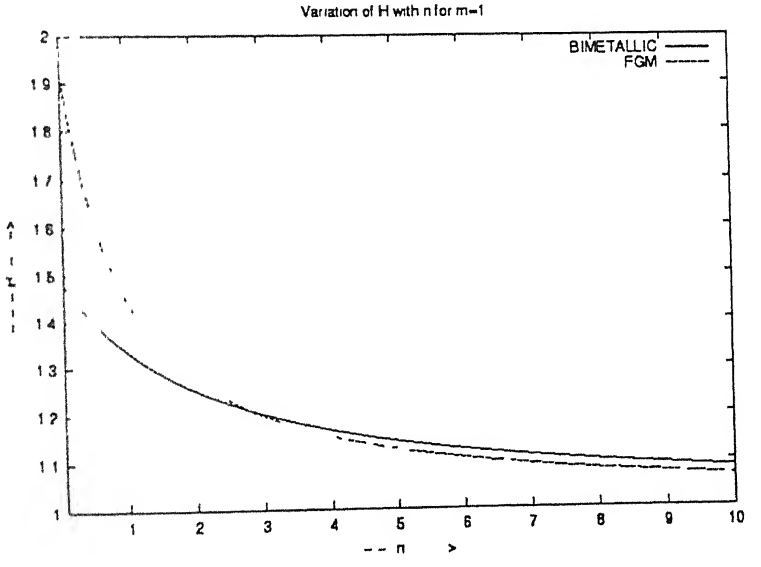

Fig 3 8 Variation of heat flow rate in terms of H (non-dimensional parameter) in FGM and bimetallic plate for $k_2 = 2k_1$

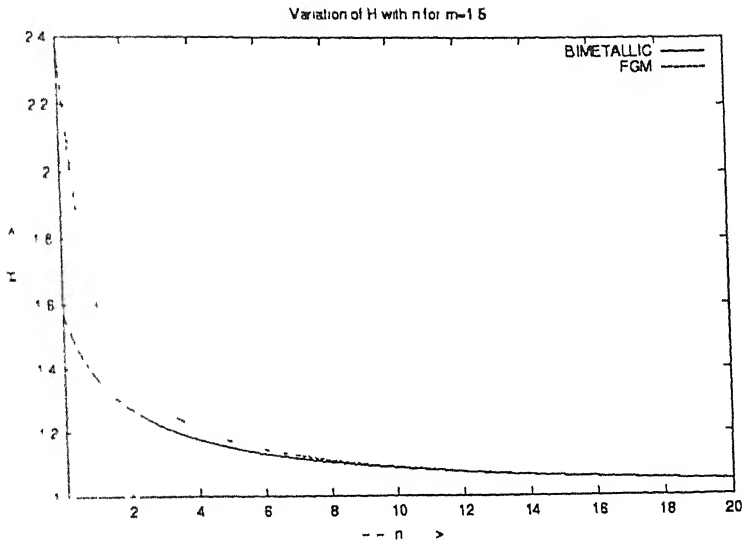

Fig 3.9 Variation of heat flow rate in terms of H (non-dimensional parameter) in FGM and bimetallic plate for $k_2 = 2.5k_1$

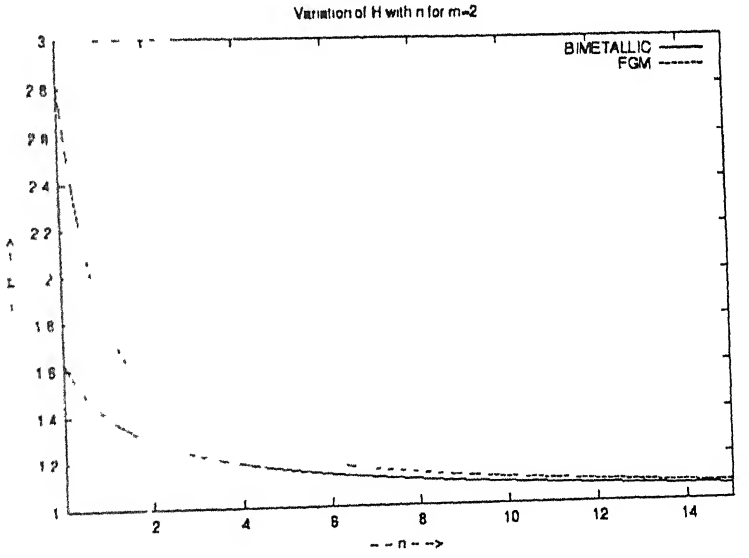

Fig 3.10 Variation of heat flow rate in terms of H (non-dimensional parameter) in FGM and bimetallic plate for $k_2 = 3k_1$.

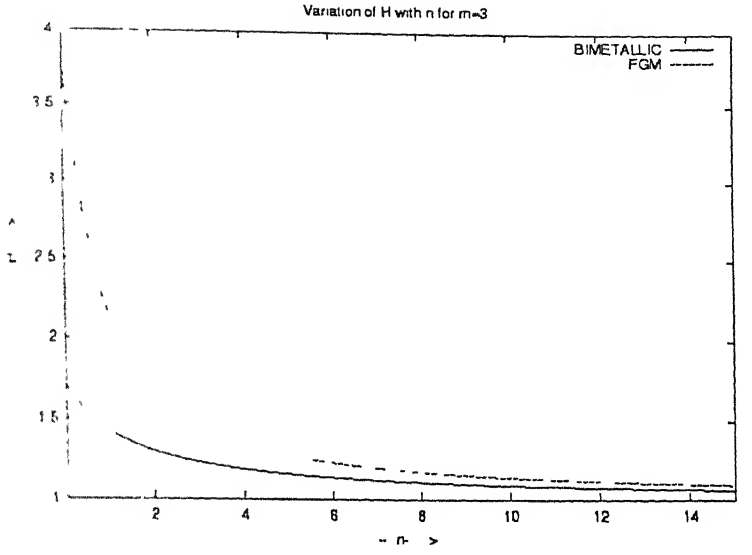

Fig 3 11 Variation of heat flow rate in terms of H (non-dimensional parameter) in FGM and bimetallic plate for $k_2 = 4k_1$

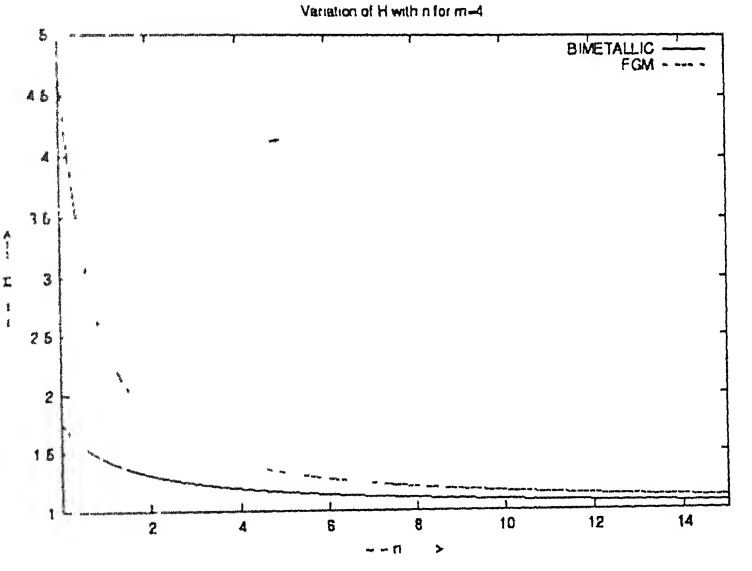

Fig 3 12 Variation of heat flow rate in terms of H (non-dimensional parameter) in FGM and bimetallic plate for $k_2 = 5k_1$

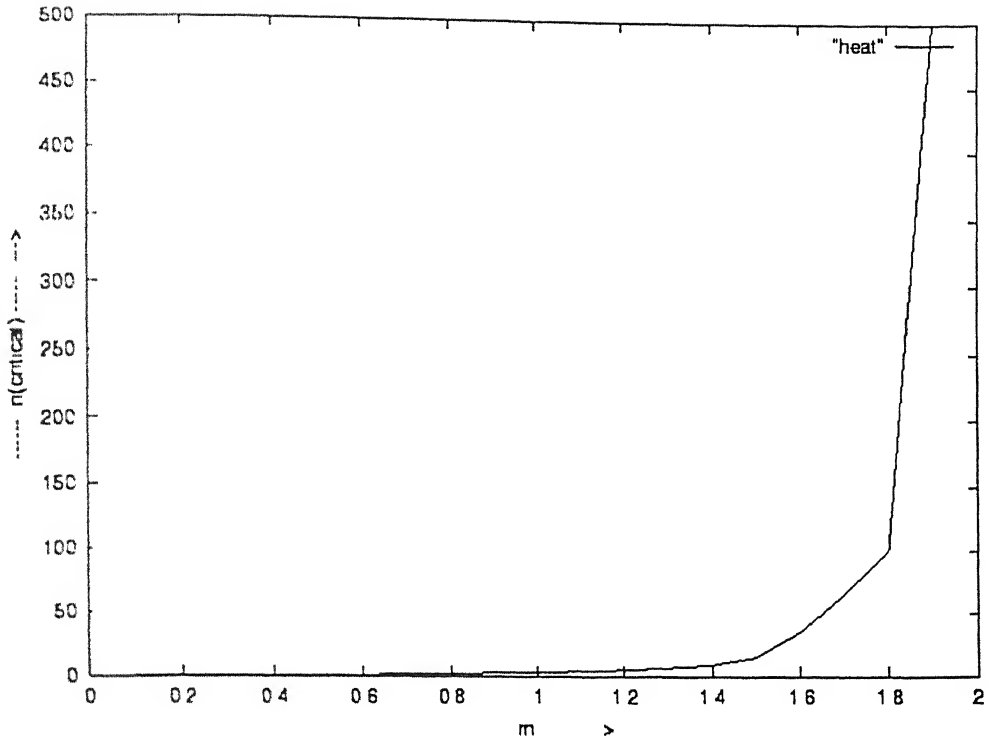

Fig. 3.13 Variation of n_{cr} with $m\left(m=\frac{k_2-k_1}{k_1}\right)$ for a FGM/bilayered material

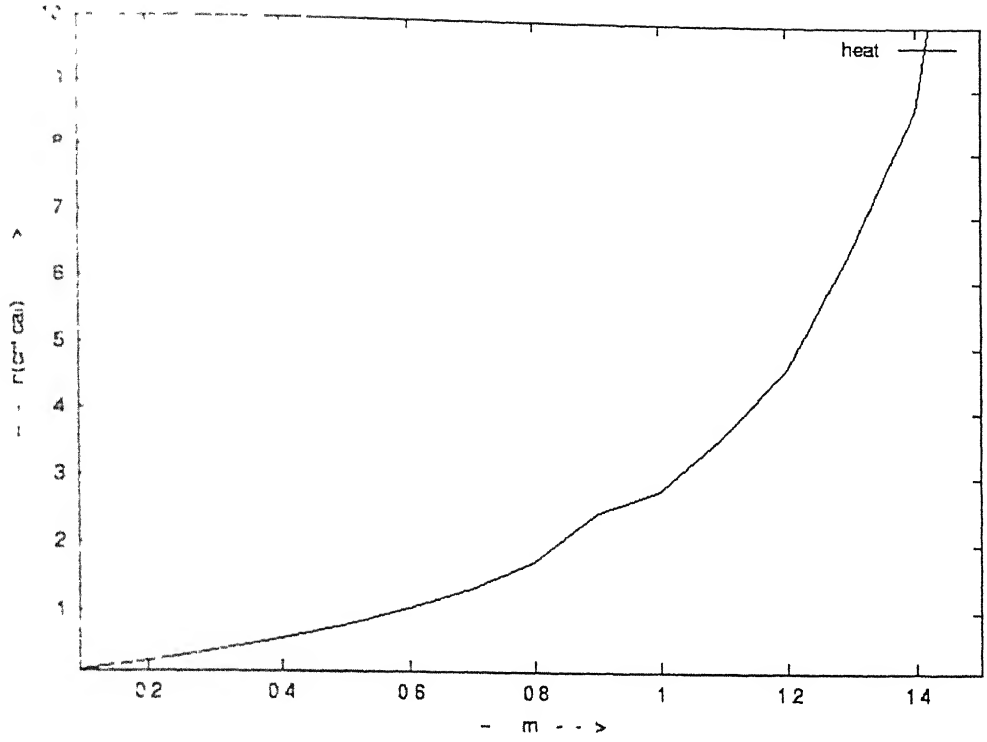

Fig 3 14 Detailed view of Fig 3 13 highlighting the range n= 0 1- 10

CHAPTER 4

Thermal stresses

This chapter deals with thermal stresses in a FGM plate as a function of various material parameters and composition profile when the plate is subjected to temperature gradients. The temperature distribution required for such calculations has already been described in the preceding chapter.

Attention is paid to determination of thermal residual stresses developed during fabrication of FGM. A trilayered ceramic-FGM-metal structure is considered & subjected to $100^{\circ}C$ temperature drop Such structure is often employed for metal-ceramic joints and is of great practical significance.

4.1 Determination of thermal stresses in FGM

We consider classic beam and plate theory analysis of stresses and curvature, which develop in the layered solid during temperature change[Boley and Weiner, 1960] The resulting kinematics does not resort to the beam/plate approximations but are exact within the context of small strain analyses. The model system investigated is ceramic-metal FGM, in which composition changes gradually and continuously according to power law, from pure ceramic to pure metal For this continuum approach to be valid, the thickness of FGM must be significantly larger than the characteristics microstructural dimensions (e g. grain size). Creep of constituent materials is neglected. The FGM is assumed to be initially stress free.

The geometry of the FGM considered here is such that the problem can be reduced to one dimension. Fig. 4.1 schematically illustrates the geometry of the FGM. The total length, width and height of FGM are l, w and 2h, respectively. When l,w>>h, the geometry modeled represents plane stress conditions. Here, the variables of interest in the study of thermomechanical response depend only on the vertical position x(along the thickness direction).

It is also assumed that thermomechanical and physical properties follow voigt type estimate . Only elastic response is considered

Composition of metal vary according to power law(eq 3 1b), that is

$$c = \eta^n \tag{4 1}$$

here

$$\eta = \frac{x}{2h} = \frac{x}{X} \tag{4 2}$$

Define

$$\beta = \frac{x}{h} \tag{4. 3}$$

Now relationship between η and β is determined using coordinate transformation relationship.

$$x = x + h$$

$$\frac{x}{2h} = \frac{1}{2}\left(\frac{x}{h} + 1\right)$$

$$\eta = \frac{1}{2}(1 + \beta) \tag{4. 4}$$

Substituting this value in eq (4. 1)

$$c = \left[\frac{1}{2}(1 + \beta)\right]^n \tag{4. 5}$$

E_1 and E_2 are the elastic modulus of ceramic and metal respectively. Similarly α_1 and α_2 are the thermal expansion coefficient of ceramic and metal respectively.

Now, using rule of mixtures (voigt type estimate) for above properties

$$E = E_1(1 - c) + E_2 c$$

$$E = E_1 + (E_2 - E_1)c \tag{4.6}$$

$$\alpha = \alpha_1(1 - c) + \alpha_2 c$$

$$\alpha = \alpha_1 + (\alpha_2 - \alpha_1)c \tag{4.7}$$

In general, the components of any three dimensional strain field are subjected to six conditions of compatibility [Srinath, 1996] But if the strain is allowed to be a function of x only, that is in the present study, then four of these conditions are satisfied identically and the remaining two condition both reduce to

$$\frac{d^2}{dx^2}(\varepsilon_{xx}) = 0$$

$$\varepsilon(x) = \varepsilon_{xx} = a + bx \qquad (4\ 6)$$

Here a is the strain at $x = 0$ and b is the curvature of the beam in its plane. In plane stress condition, the only non-zero stress component is $\sigma(x) = \sigma_{xx}$.

Therefore

$$\sigma(x) = E(x)[\varepsilon(x) - \alpha(x)\Delta T(x)]$$

$$\sigma(x) = E(x)[a + bx - \alpha(x)\Delta T(x)]$$

$$\sigma(x) = aE(x) + bxE(x) - E(x)\alpha(x)\Delta T(x) \qquad (4.7)$$

ΔT represents the change in temperature from initial stress free state

The resultant force and the resultant moment of the stress distribution $\sigma(x)$ along the height, x, must be equal to zero as there is no external applied force and moment.

Using force balance:

$$\int_{-h}^{h} \sigma(x)dx = 0$$

Put the value of $\sigma(x)$ from eq (4 9)

$$a\int_{-h}^{h} E(x)dx + b\int_{-h}^{h} xE(x)dx = \int_{-h}^{h} E(x)\alpha(x)\Delta T(x)dx$$

$$aA_1 + bA_2 = A_3 \qquad (4.8)$$

Using moment balance:

$$\int_{-h}^{h} \sigma(x)xdx = 0$$

Substitute the value of $\sigma(z)$ from eq (4. 9)

$$a\int_{h}^{h} zE(z)dz + b\int_{h}^{h} z^2E(z)dz = \int_{-h}^{h} zE(z)\alpha(z)\Delta T(z)dz$$

$$aA_2 + bA_4 = A \qquad (4.9)$$

On solving eq (4. 10) and (4 11), we get

$$a = \frac{A_3 A_4 - A_5 A_2}{A_1 A_4 - A_2^2} \qquad (4\ 12)$$

$$b = \frac{A_5 A_1 - A_3 A_2}{A_2^2 - A_1 A_4} \qquad (4\ 13)$$

Here

$$A_1 = \int_{-h}^{h} E(x)dx$$

$$A_2 = \int_{h}^{h} xE(x)dx$$

$$A_3 = \int_{-h}^{h} E(x)\alpha(x)\Delta T(x)dx$$

$$A_4 = \int_{-h}^{h} x^2 E(x)dx$$

$$A_5 = \int_{-h}^{h} xE(x)\alpha(x)\Delta T(x)dx$$

$$\beta = \frac{x}{h}$$

$$d\beta = \frac{dx}{h}$$

$$dx = hd\beta \qquad (4.\ 14)$$

Limits of β varies between -1 to 1,corresponding to limits of x which varies between $-h$ to h.

Put these limits and $dx = hd\beta$ in above expressions of A_1, A_2, A_3, A_4 and A_5.

$$A_1 = h\int_{-1}^{1} E(\beta)d\beta \qquad (4.\ 15)$$

$$A_2 = h^2 \int_{-1}^{1} \beta E(\beta)d\beta \qquad (4.\ 16)$$

$$A_3 = h\int_{-1}^{1} \beta E(\beta)\alpha(\beta)\Delta T(\beta)d\beta \qquad (4.\ 17)$$

$$A_4 = h^3 \int_{1}^{1} \beta^2 E(\beta)d\beta \qquad (4.\ 18)$$

$$A_5 = h^2 \int_{-1}^{1} \beta E(\beta)\alpha(\beta)\Delta T(\beta)d\beta \qquad (4.\ 19)$$

4.2 Condition for zero thermal stress on ceramic side

Thermal stress in FGM is given eq 4 9 which is as follow

$$\sigma(x) = aE(x) + bxE(x) - E(x)\alpha(x)\Delta T(x)$$

or

$$\sigma(\beta) = aE(\beta) + b\beta F(\beta) - E(\beta)\alpha(\beta)\Delta T(\beta)$$

For ceramic surface,

$\beta = -1, E(\beta) = E_1, \alpha(\beta) = \alpha_1$ and $\Delta T = (\Delta T)_{max}$

Substituting these values in above equation and equating it to zero, we get

$$\frac{a-b}{\alpha_1(\Delta T)_{max}} = 1 \qquad (4\ 20)$$

This expression is independent of α_1 and $(\Delta T)_{max}$, because a and b contain these term, hence these stands canceled out in the above eq 4.20 From the above condition we can find out the value of a and b, which will give zero stress on ceramic surface The value of a and b, depends on $\frac{E_2}{E_1}, \frac{\alpha_2}{\alpha_1}, \frac{k_2}{k_1}$ and n. So for given values $\frac{E_2}{E_1}, \frac{\alpha_2}{\alpha_1}, \frac{k_2}{k_1}$ we can find the composition profile n^* for which there is zero stress on ceramic surface.

4.3 Condition for zero thermal stress on metal surface in FGM

Similarly a condition has to be satisfied for having zero thermal stress on metal surface, which is as follow

$$a + b = 0 \qquad (4.\ 21)$$

Remaining argument remain same as in section 4.2

4.4 Determination of thermal residual stresses in FGM

The model system investigated here is a three-layered composite, where the two outer layers comprise a metal and ceramic; the in-between interlayer is compositionally graded wherein the composition changes gradually (and continuously) from pure ceramic to pure metal. In an attempt, to illustrate quantitatively the salient features of the result and to provide specific examples, we consider Ni and Al_2O_3 as the model metal and ceramic,

respectively The FGM layer is a composite of the Ni- Al_2O_3 mixture, with varying proportions of the two phases. Same assumptions regarding the size of the plate and material properties have been made here as in previous section 4 1

The FGM layer extends from x=-a to x = +a It is assumed in this study that a = 6h Only elastic response is considered

Formulation of the problem is same as in section 4 1 The only difference is this that, here, $\Delta T = -100^{0}C$ (drop)

Here composition of metal in FGM is assumed to vary as follow:

$$c = \left(\frac{x + a}{2a}\right)^{n} \quad \text{for} \quad -a \le x \le +a$$

$$c = \left[\frac{1}{2}\left(1 + \frac{x}{a}\right)\right]^{n} \tag{4. 27}$$

Define

$$\frac{x}{a} = \lambda \tag{4. 28}$$

Then

$$dx = a d\lambda \tag{4. 29}$$

Now

$$c = \left[\frac{1}{2}(1 + \lambda)\right]^{n} \tag{4. 30}$$

Using rule of mixtures for E and α.

$$E = E_1(1 - c) + E_2 c$$

$$E = E_1 + (E_2 - E_1)\left[\frac{1}{2}(1 + \lambda)\right]^{n} \tag{4.31}$$

$$\alpha = \alpha_1(1 - c) + \alpha_2 c$$

$$\alpha = \alpha_1 + (\alpha_2 - \alpha_1)\left[\frac{1}{2}(1 + \lambda)\right]^{n} \tag{4.32}$$

From section 4.1

$$A_1 = \int_{-h}^{h} E(x)dx$$

$$A_1 = \int_{h}^{-a} E_1 dx + \int_{a}^{a} E(x)dx + \int_{a}^{h} E_2 dx$$

$$A_1 = (h-a)(E_1 + E_2) + \int_a^a E(x)dx$$

Substitute

$dx = ad\lambda$

$$A_1 = (h-a)(E_1 + E_2) + a\int_1^1 E(\theta)d\theta \qquad (4.33)$$

$$A_2 = \int_{-h}^{h} xE(x)dx$$

$$A_2 = \int_h^a E_1 x dx + \int_a^a xT(x)dx + \int_a^h E_2 x dx$$

$$A_2 = E_1\left(\frac{a^2 - h^2}{2}\right) + E_2\left(\frac{h^2 - a^2}{2}\right) + \int_{-a}^{a} xE(x)dx$$

Substitute

$x = a\lambda$ and $dx = ad\lambda$

$$A_2 = (h^2 - a^2)\left(\frac{E_2 - E_1}{2}\right) + a^2\int_{-1}^{1}\lambda E(\lambda)d\lambda \qquad (4.34)$$

$$A_3 = \int_{-h}^{h}[\alpha(x)E(x)\Delta T(x)dx]$$

Here

$\Delta T(z) = \Delta T = -100^0 C$

$$A_3 = -100\left[\int_h^a \alpha_1 E_1 dx + \int_{-a}^{a}\alpha(x)E(x)dx + \int_a^h \alpha_2 E_2 dx\right]$$

$$A_3 = -100\left[(\alpha_1 E_1 + \alpha_2 E_2)(h-a) + \int_{-a}^{a}\alpha(x)E(x)dx\right]$$

Substitute

$x = a\lambda$ and $dx = ad\lambda$

$$A_3 = -100\left[(\alpha_1 E_1 + \alpha_2 E_2)(h-a) + a\int_{-1}^{1}\alpha(\lambda)E(\lambda)d\lambda\right] \qquad (4.35)$$

$$A_4 = \int_{-h}^{h} x^2 E(x)dx$$

$$A_4 = \int_{-h}^{-a} x^2 E_1 dx + \int_{-a}^{a} x^2 E(x)dx + \int_a^h x^2 E_2 dx$$

$$A_4 = F_1\left(\frac{h^3 - a^3}{3}\right) + E_2\left(\frac{h^3 - a^3}{3}\right) + \int_{-a}^{a} x^2 E(x)dx$$

Substitute

$x = a\lambda$ and $dx = ad\lambda$

$$A_4 = (h^3 - a^3)\left(\frac{E_1 + E_2}{3}\right) + a^3\int_{1}^{1}\lambda^2 E(\lambda)d\lambda \qquad (4.36)$$

$$A_5 = \int_{h}^{h} x\alpha(x)E(x)\Delta T(x)dx$$

Here

$\Delta T = -100^{\circ}C$

$$A_5 = -100\left[\int_{h}^{a} x\alpha_1 E_1 dx + \int_{a}^{a} x\alpha(x)E(x) + \int_{a}^{h} x\alpha_2 E_2 dx\right]$$

Substitute

$x = a\lambda$ and $dx = ad\lambda$

$$A_5 = -100\left[\left(\frac{h^2 - a^2}{2}\right)(\alpha_2 E_2 - \alpha_1 E_1) + \lambda^2\int_{-1}^{1}\lambda\alpha(\lambda)E(\lambda)d\lambda\right] \qquad (4.37)$$

From section 4.1

$\sigma(x) = aE(x) + bxE(x) - \alpha(x)E(x)\Delta T(x)$

Here

$\Delta T = -100^{0}C$

Hence

$\sigma(x) = aE(x) + bE(x)dx + 100\alpha(x)E(x)$

The values of $E(x)$ and $\alpha(x)$ are different in different layer. So the expression of $\sigma(x)$ will be different in different layer. The expressions are as follow:

$\sigma(x) = aE_1 + bxE_1 + 100\alpha_1 E_1$ for $-h \le x \le -a$ (4.38)

$\sigma(x) = aE(x) + bxE(x) + 100\alpha(x)E(x)$ for $-a \le x \le a$ (4.39)

$\sigma(x) = aE_2 + bxE_2 + 100\alpha_2 E_2$ for $a \le x \le h$ (4 40)

4.5 Thermal stresses in bimetallic plate, having equal volume of metal and ceramic as in FGM

For comparison of metal-ceramic FGM with bimetallic plate, having equal volume fraction of metal and ceramic, it become necessary to determine the thermal stress distribution in bimetallic plate using same assumption and conditions as were in FGM thermal stress study. For determination of thermal stresses in bimetallic plate, it is necessary to know the temperature distribution in bimetallic plate.

(A) Temperature distribution in bimetallic plate

From section 3.2, volume fraction of metal and ceramic in FGM is given by the following expressions

$$V_m = \frac{1}{n+1}$$

and

$$V_c = \frac{n}{n+1}$$

Now consider a bimetallic plate, which has volume fraction of metal and ceramic equals to V_m and V_c, respectively

From section 3.2

$$T_0 = \frac{T_1 + n(m+1)T_2}{n(m+1)+1}$$

Hence temperature at an arbitrary location η in ceramic part is given by the following expression

$$T_c = T_1 - w\eta \qquad 0 \le \eta \le \frac{n}{n+1} \qquad (4.34)$$

Where w is a constant.

At $\eta = \frac{n}{n+1}$, $T_c = T_0$

Putting this condition in equation (4. 34), we get

$$w = \frac{(n+1)(T_1 - T_0)}{n}$$

Put this value in eq. (4. 34)

$$T_c = T_1 - \frac{(n+1)(T_1 - T_0)}{n}\eta \qquad (4.35)$$

Similarly the temperature at an arbitrary location β in metallic part is given by the following expression:

$$T_m = T_2 + \nu(1-\eta) \qquad \frac{n}{n+1} \le \eta \le 1 \tag{4.36}$$

Where ν is a constant

At $\eta = \frac{n}{n+1}$, $T_m = T_0$

Putting this condition in eq (4.36), we get

$\nu = (T_0 - T_2)(n+1)$

Put this value of ν in eq (4.36)

$$T_m = T_2 + (T_0 - T_2)(n+1)(1-\eta) \tag{4.37}$$

(B) Thermal stresses in bi-layered plate

From section 4.2,

$\eta = \frac{1}{2}(1+\beta)$

Where

$\eta = \frac{x}{2h}$ and $\beta = \frac{x}{h}$

Now

$\eta = 0 \Rightarrow \beta = -1$,

$\eta = \frac{n}{n+1} \Rightarrow \beta = \frac{n-1}{n+1}$;

$\eta = 1 \Rightarrow \beta = 1$;

Hence

$$T_c = T_1 - \frac{(n+1)(T_1 - T_0)(1+\beta)}{2n} \tag{4.38}$$

$$T_m = T_2 + \frac{(n+1)(T_0 - T_2)(1-\beta)}{2} \tag{4.39}$$

Now from section 4.1

$$A_1 = h\int_{-1}^{1} E(\beta)\,d\beta$$

$$A_1 = h\left(\int_{-1}^{\frac{n-1}{n+1}} E_1 d\beta + \int_{\frac{n-1}{n+1}}^{1} E_2 d\beta\right)$$

$$A_1 = \frac{2h}{n+1}(nE_1 + E_2) \tag{4.40}$$

$$A_2 = h^2\int_{-1}^{1} \beta E(\beta)\,d\beta$$

$$A_2 = h^2\left(\int_{-1}^{\frac{n-1}{n+1}} \beta E_1 d\beta + \int_{\frac{n-1}{n+1}}^{1} \beta E_2 d\beta\right)$$

$$A_2 = \frac{2nh^2}{(n+1)^2}(E_2 - E_1) \qquad (4.41)$$

$$A_3 = h\int_{-1}^{1} \beta E(\beta)\alpha(\beta)\Delta T(\beta)d\beta$$

$$A_3 = h\left[\int_{-1}^{\frac{n-1}{n+1}} \alpha_1 E_1 (\Delta T)_c \, d\beta + \int_{\frac{n-1}{n+1}}^{1} \alpha_2 E_2 (\Delta T)_m d\beta\right]$$

Here

$(\Delta T)_c = T_c - T_2$

Where T_2 is assumed as room temperature.

$$(\Delta T)_c = (T_1 - T_2) - \frac{(n+1)(T_1 - T_0)(1+\beta)}{2n}$$

Similarly

$(\Delta T)_m = T_m - T_2$

$$(\Delta T)_m = \frac{(n+1)(T_0 - T_2)(1-\beta)}{2}$$

Hence

$$A_3 = h\left[\alpha_1 E_1 \int_{1}^{\frac{n-1}{n+1}} \left\{(T_1 - T_2) - \frac{(n+1)(T_1 - T_0)(1+\beta)}{2n}\right\} d\beta + \alpha_2 E_2 \int_{\frac{n-1}{n+1}}^{1} \frac{(n+1)(T_0 - T_2)(1-\beta)}{2} d\beta\right]$$

(4 42)

$$A_4 = h^3\int_{-1}^{1} \beta^2 E(\beta)d\beta$$

$$A_4 = h^3\left(\int_{-1}^{\frac{n-1}{n+1}} \beta^2 E_1 d\beta + \int_{\frac{n-1}{n+1}}^{1} \beta^2 E_2 d\beta\right)$$

$$A_4 = \frac{h^3}{3(n+1)^3}\left[E_1\left\{(n-1)^3 + (n+1)^3\right\} + E_2\left\{(n+1)^3 - (n-1)^3\right\}\right] \qquad (4.43)$$

$$A_5 = h^2\int_{-1}^{1} \beta E(\beta)\alpha(\beta)\Delta T(\beta)d\beta$$

$$A_5 = h^2\left[\int_{-1}^{\frac{n-1}{n+1}} \beta\alpha_1 E_1 (\Delta T)_c \, d\beta + \int_{\frac{n-1}{n+1}}^{1} \beta\alpha_2 E_2 (\Delta T)_m \, d\beta\right]$$

$$A_5 = h^2\left[\alpha_1 E_1 \int_{1}^{\frac{n-1}{n+1}} \beta\left\{(T_1 - T_2) - \frac{(n+1)(T_1 - T_0)(1+\beta)}{2n}\right\} d\beta + \alpha_2 E_2 \int_{\frac{n-1}{n+1}}^{1} \frac{\beta(n+1)(T_0 - T_2)(1-\beta)}{2} d\beta\right]$$

(4. 44)

Expressions for thermal stress will remain same as in previous section. Only values of a, b, and expression for ΔT will change.

4.5 Results and Discussion

Model system chosen for this study is a Ni-Al_2O_3 FGM The choice of this model system is predicated upon the following considerations:

1. The thermomechanical and physical properties of Ni and Al_2O_3 are well known as these materials have been widely studied
2. Compositionally graded microstructures based on Ni and Al_2O_3 have been produced using a variety of available techniques.
3. Ni-based alloys are extensively used is aircraft turbine engines where the thermal cycling response of the alloy bonded to ceramic coatings is a topic of considerable interest.
4. Ni, has a high melting point (1726 K), there exist many practically significant temperature regimes, well below the melting point, wherein the thermomechanical response can be studied without incorporating the complicating effect of creep, diffusion and chemical reactions

The numerical values of material parameters used are as follow:

$E_1 = 380$ Gpa

$E_2 = 214$ Gpa

$\alpha_1 = 7.4 \times 10^{-6} K^{-1}$

$\alpha_2 = 15.4 \times 10^{-6} K^{-1}$

Thermal stress are determined in FGM for $T_1 = 120^{\circ}C$ and $T_2 = 20^{\circ}C$ (room temperature) by using MATLAB simulink for different composition profile and $m\left(m - \frac{k_2}{k_1}\right)$.

Figs. 4.3.1 – 4.3.11 show the variation of stress along the plate thickness as a function of n where n ranges between 0.75 to 4 and m=1.

The main points to note are:

(a) The stress variation is continuous, unlike that for a bi-layered material where a discontinuity exists at the interface. Sudden changes in stress across a layer are potentially damaging for the material and must be avoided.

(b) The stresses on the ceramic side may be tensile or compressive depending on the value of n. Since ceramics are brittle in nature and fail through crack propagation, it is desirable to have compressive stresses, which inhibit fracture. Thus, the present analysis offers a valuable approach to enhance the reliability of a FGM through proper choice of composition profile (value of n).

Similarly results for $m = 2$ also have been obtained (Figs. 4.4.1- 4.4.11).

The variation of thermal residual stress with position for a tri-layered material where the intermediate layer is a FGM and the surface layers correspond to pure ceramic and pure metal respectively are presented in Figs. 4.5.1- 4.5.3. These results are obtained for a drop in temperature of 100 C.

The main observations are as follow.

(a) There is no sharp change in stress value at the two interfaces, although the stress variation is not continuous for $n=1$.

(b) The discontinuity in the stress variation at the interfaces can be removed through proper choice of composition profile. For example, for n=2 and 3, the stress changes continuously at the ceramic/FGM interface.

Similarly, the slope at the second interface may be adjusted. Although the FGM/metal interface is more forgiving

Depending on the intended application, it may be desirable to have zero stress on the ceramic or metal surface through proper choice of composition profile. This is shown in Fig. 4.6- 4.9.

In view of the brittle nature of ceramics, it is desirable to minimize the tensile stresses on the ceramic side. Accordingly a parametric study is carried out to determine the composition profile (n^*) which would give zero stresses on ceramic side as a function of $\delta\left(\delta=\frac{E_2}{E_1}\right)$, $\gamma\left(\gamma=\frac{\alpha_2}{\alpha_1}\right)$ and $\frac{k_2}{k_1}$.

These results are presented in Figs. 4.10 – 4.22.

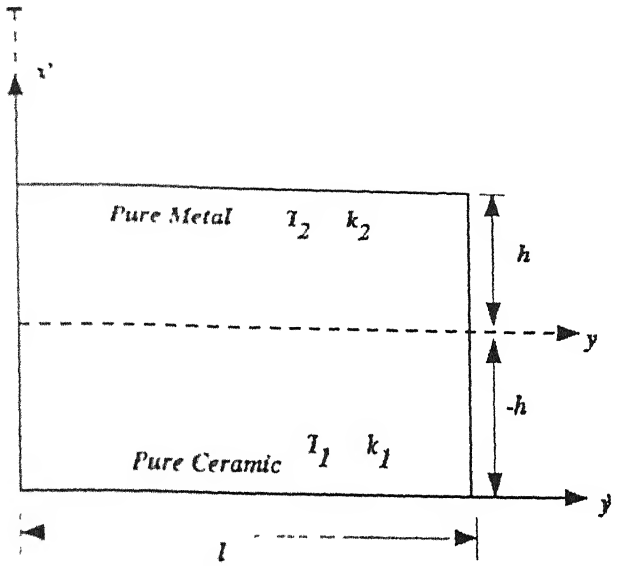

Fig 4.1 A metal-ceramic FGM, in which the concentration of metal varies according the power law

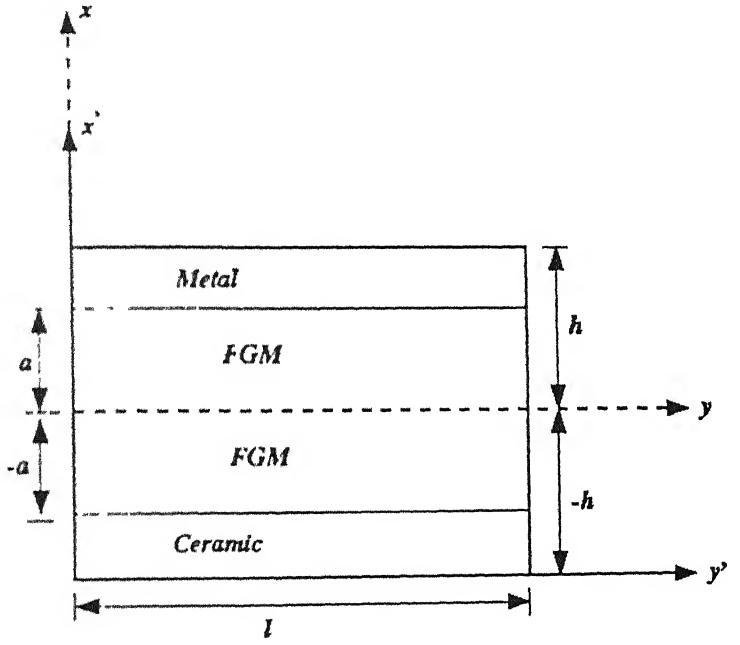

Fig 4.2: A schematic representation of ceramic-FGM-metal plane stress model (a=0.6h)

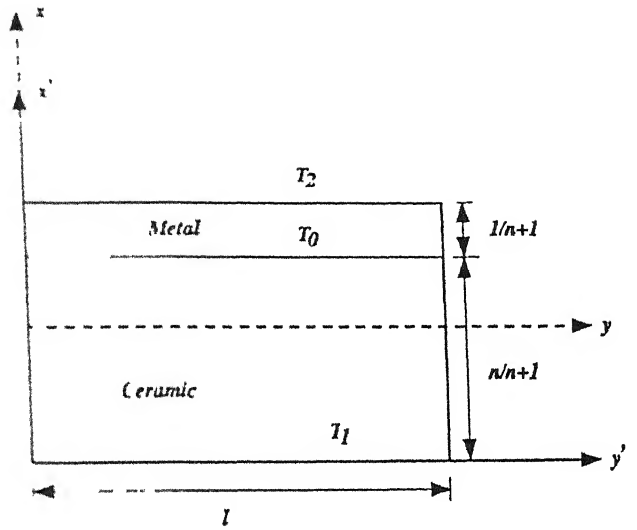

Fig 4 2 1 Schematic illustration of a bi-layered material, which have the same volume fraction of individual constituents as in FGM having the composition profile n

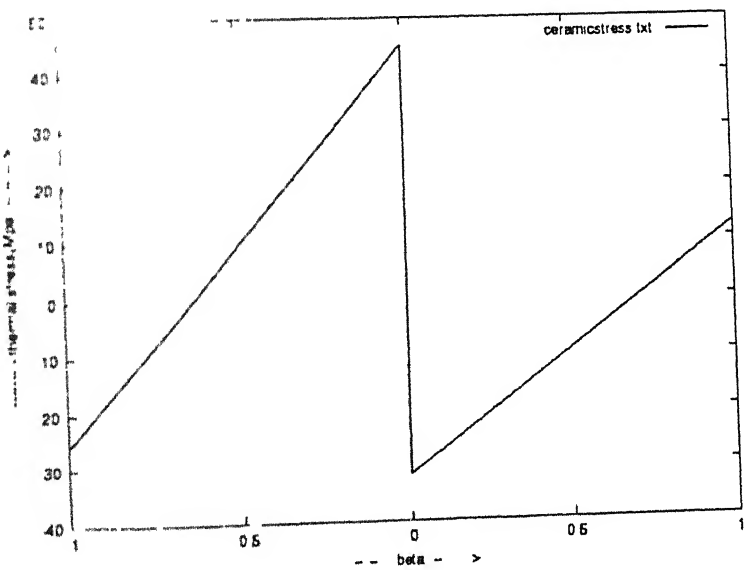

Fig4.2 2: Variation of thermal stress in bi-layered structure, which is equivalent to FGM having the value of n=1.

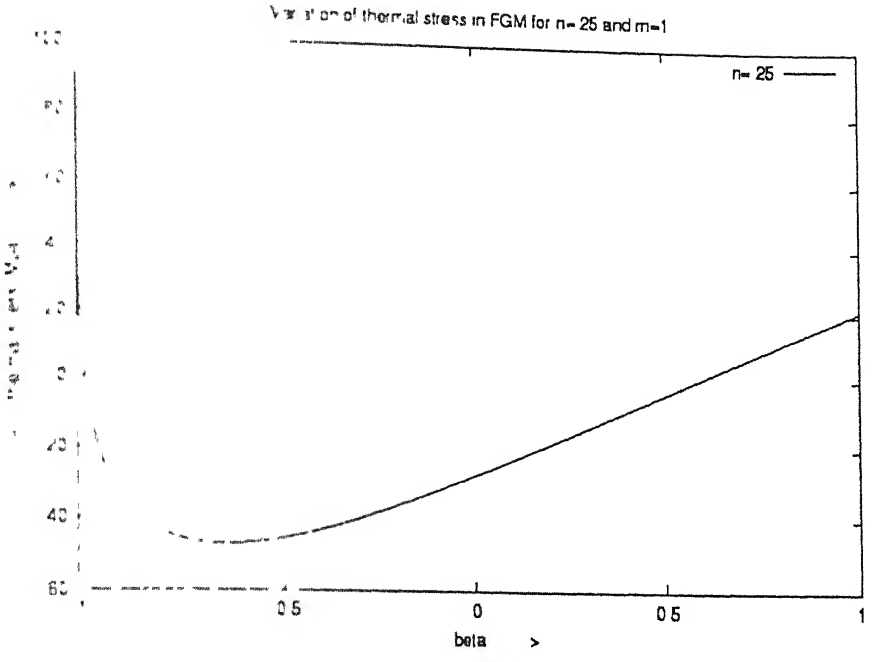

Fig 4.3 1 Prediction of variation of thermal stress in FGM for n= 25 and m=1

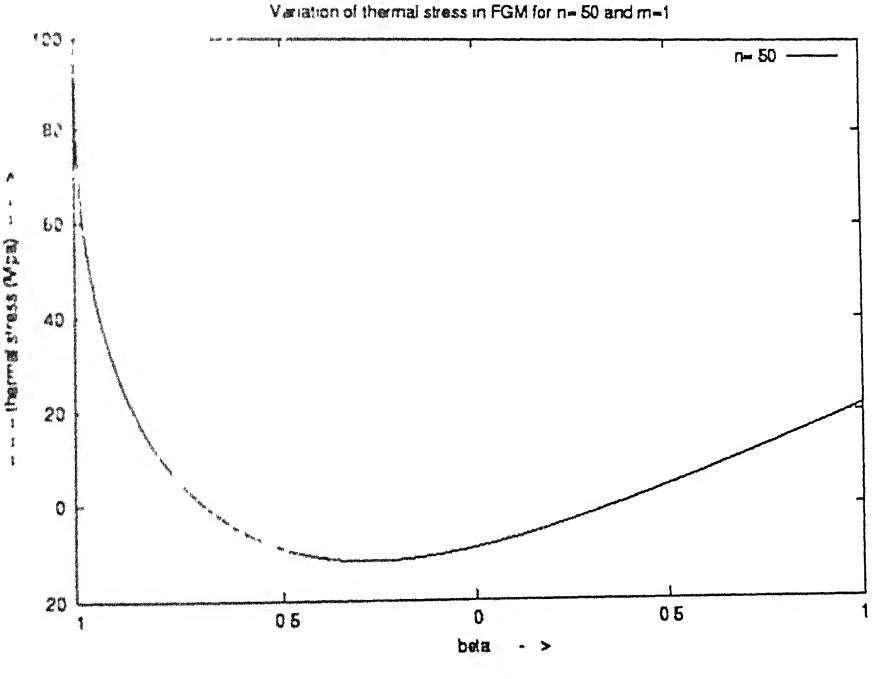

Fig 4 3 2· Prediction of variation of thermal stress in FGM for n=0.50

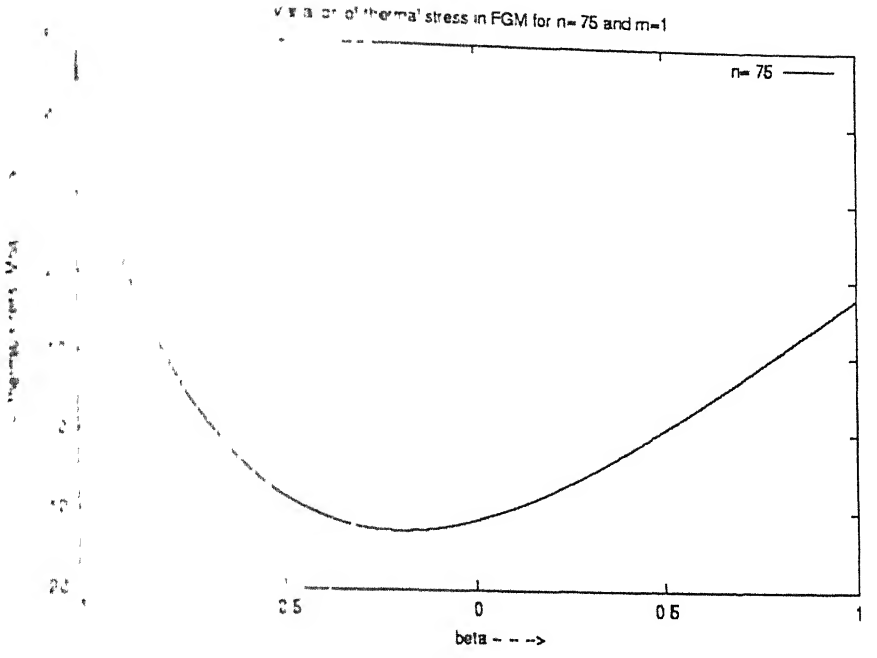

Fig 4.3 3 Prediction of variation of thermal stress in FGM for n=0 75 and m=1

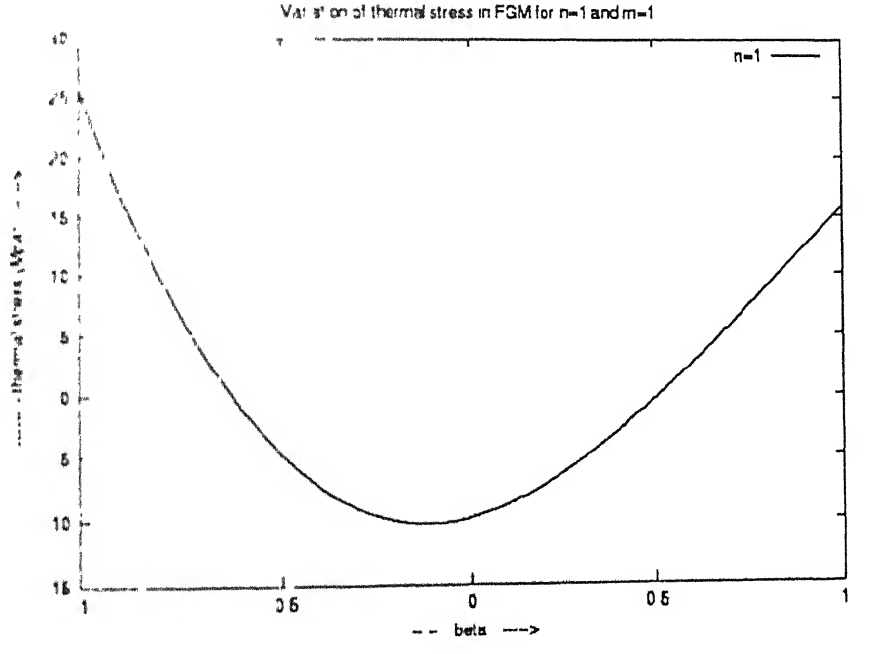

Fig 4 3.4: Prediction of variation of thermal stress in FGM for n=1 and m=1

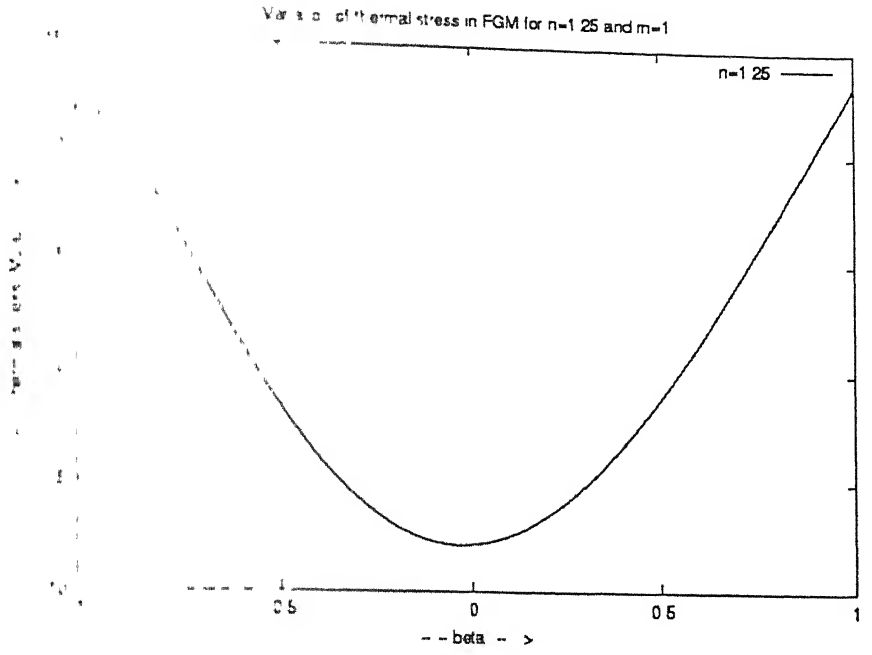

Fig 4 3 5 Prediction of variation of thermal stress in FGM for n=1 25 and m=1

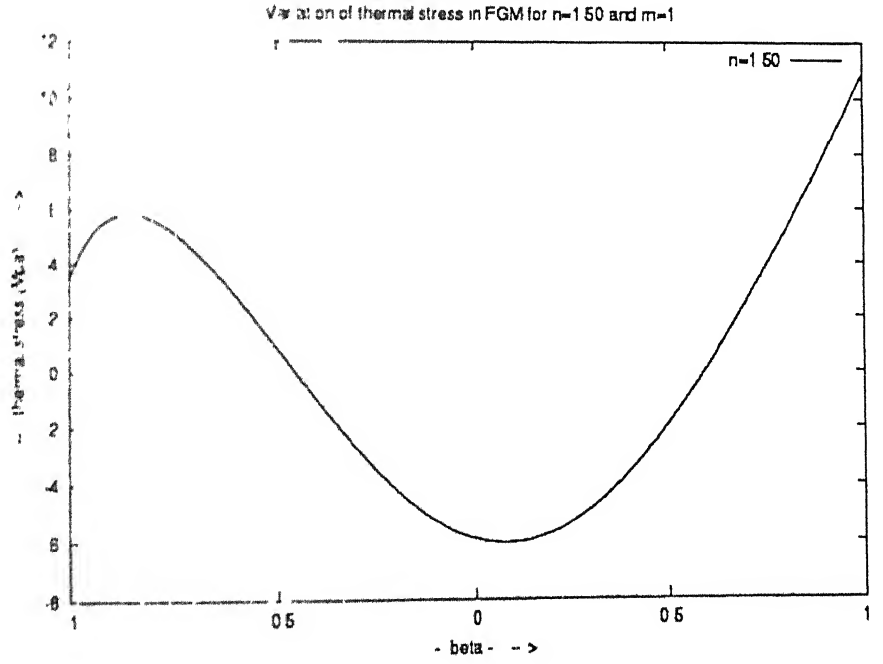

Fig 4.3 6· Prediction of variation of thermal stress in FGM for n=1 50 and m=1

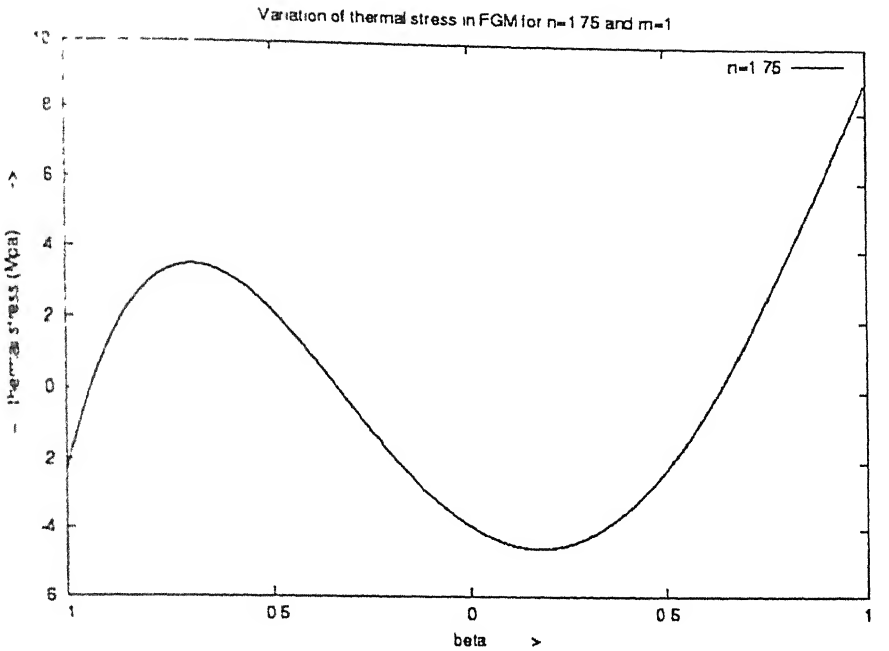

Fig 4 3 7: Prediction of variation of thermal stress in FGM for n=1.75 and m=1.

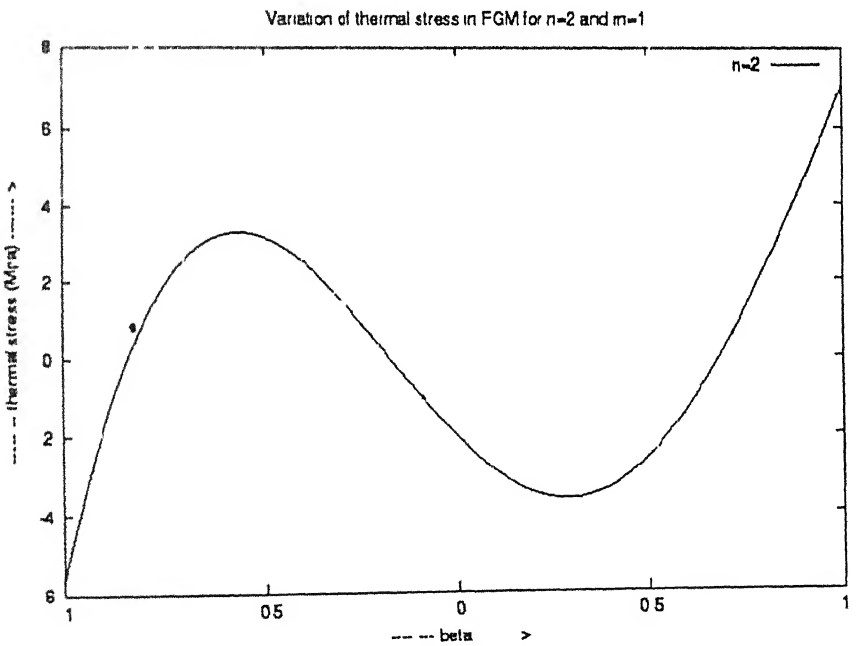

Fig 4 3 8 Prediction of variation of thermal stress in FGM for n=2 and m=1.

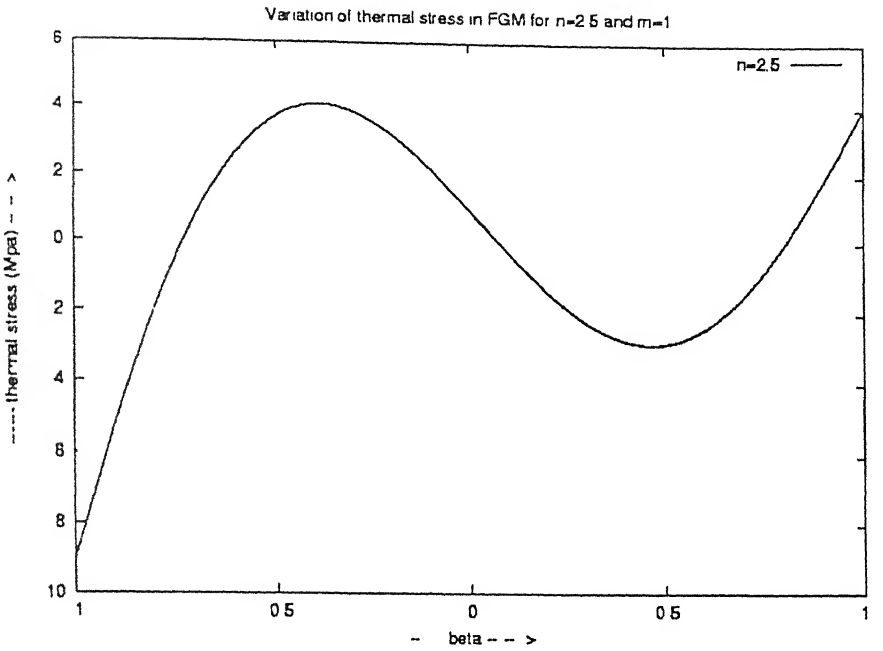

Fig 4 3 9 Prediction of variation of thermal stress in FGM for n=2 50 and m=1

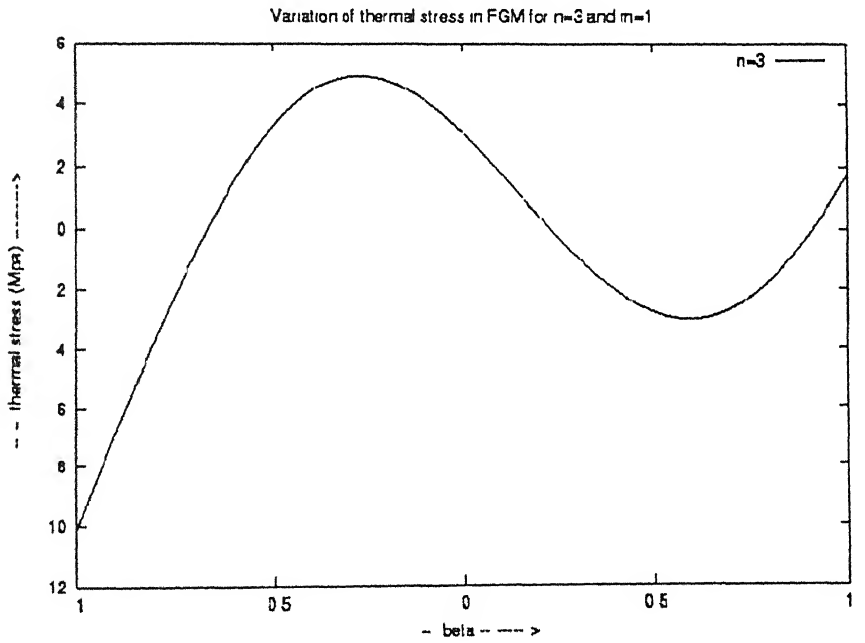

Fig 4 3 10 Prediction of variation of thermal stress in FGM for n=3 and m=1

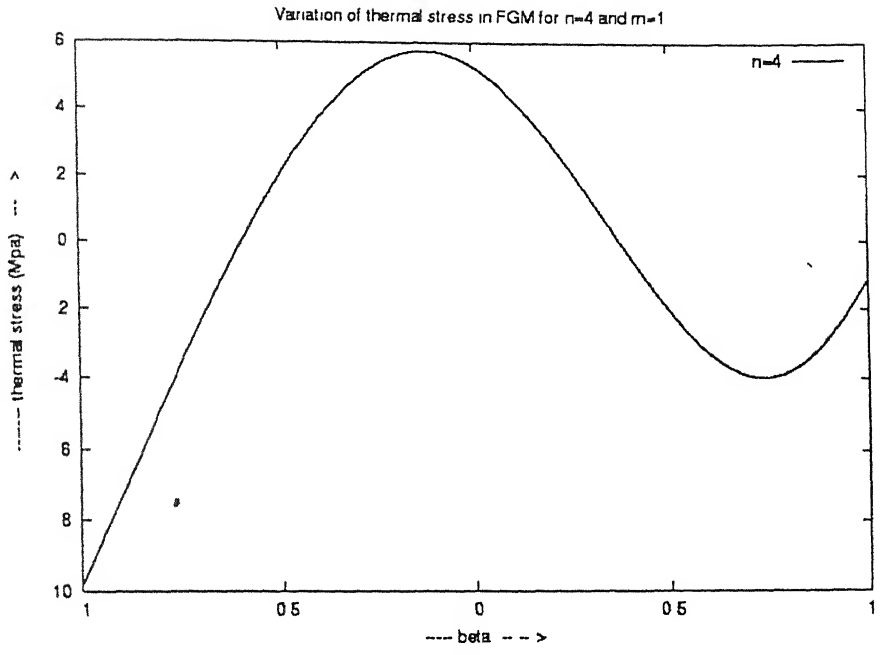

Fig 4 3 11 Prediction of variation of thermal stress in FGM for n=4 and m=1

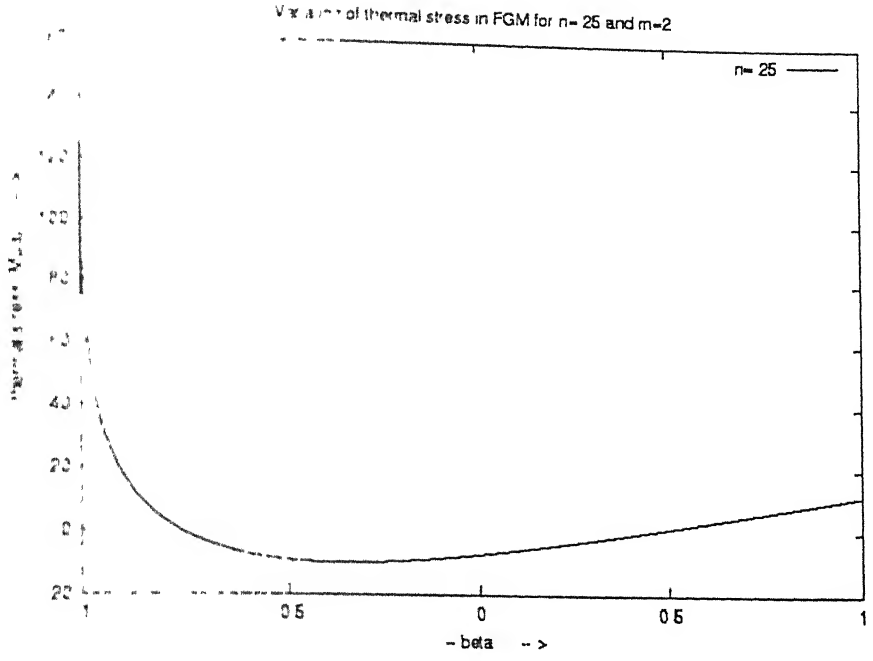

Fig 4.4.1 Prediction of variation of thermal stress in FGM for n=0.25 and m=2

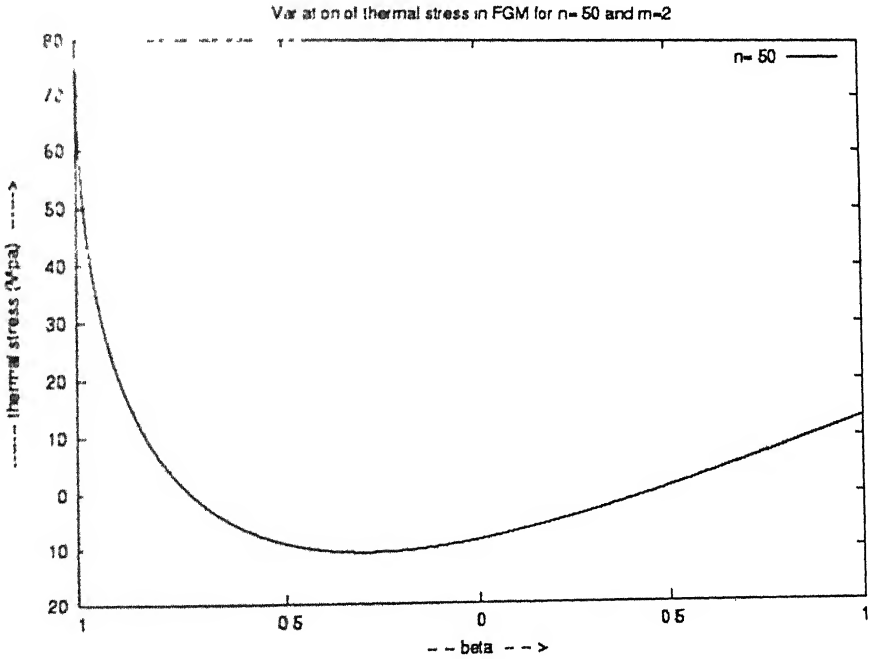

Fig 4.4.2. Prediction of variation of thermal stress in FGM for n=0.50 and m=2

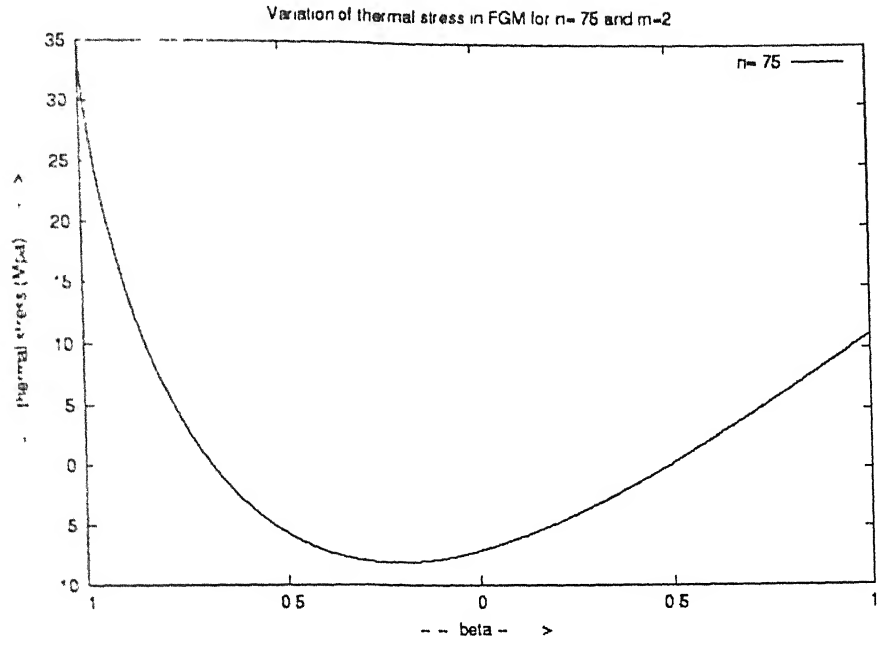

Fig 4 4 3 Prediction of variation of thermal stress in FGM for n=0 75 and m=2

Fig 4 4 4: Prediction of variation of thermal stress in FGM for n=1 and m=2

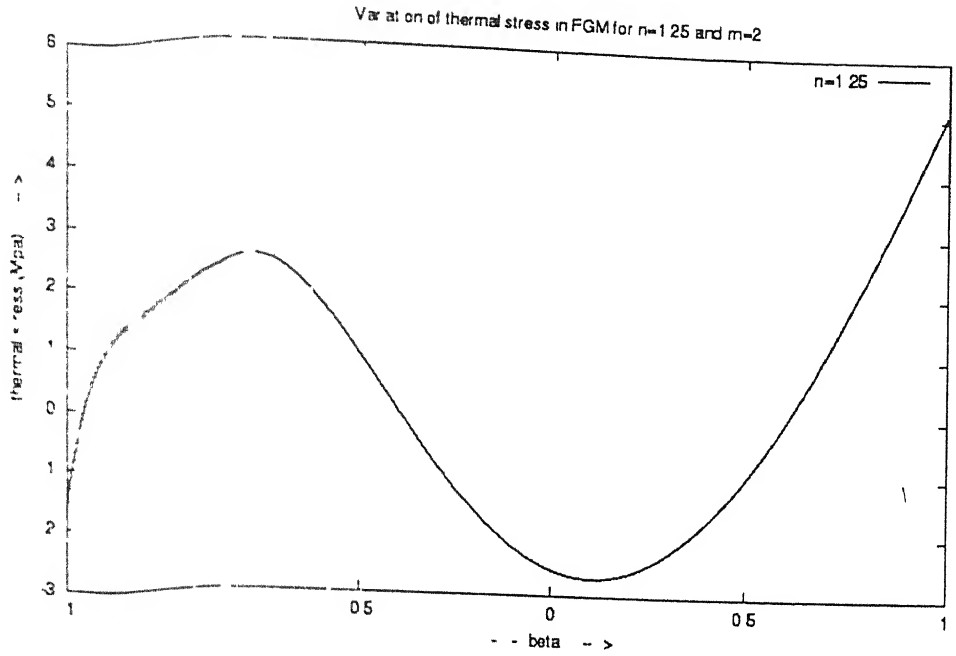

Fig 4 4 5 Prediction of variation of thermal stress in FGM for n=1 25 and m=2

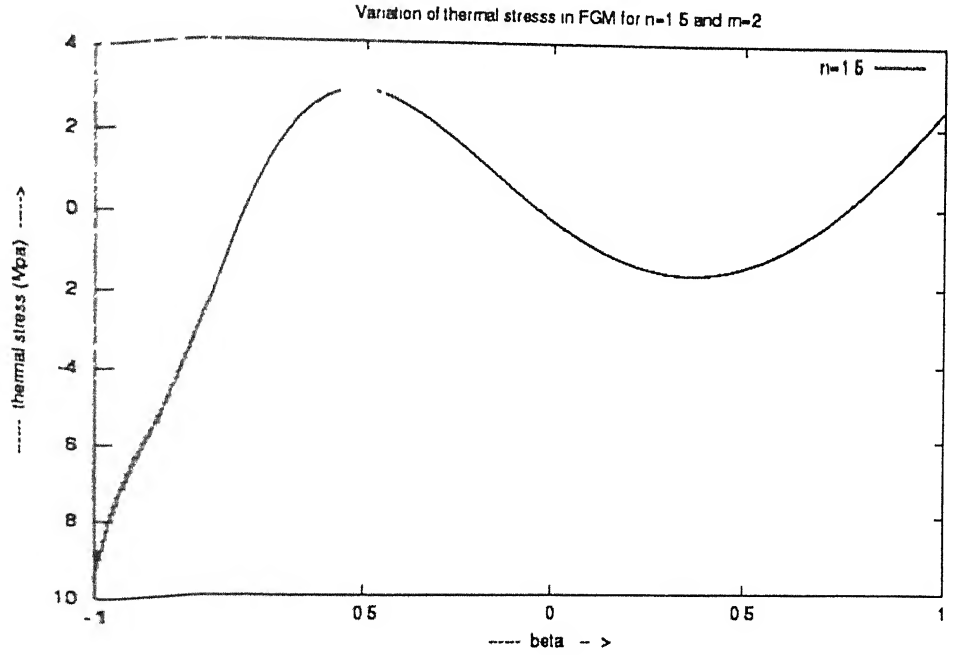

Fig 4.4.6. Prediction of variation of thermal stress in FGM for n=1 50 and m=2.

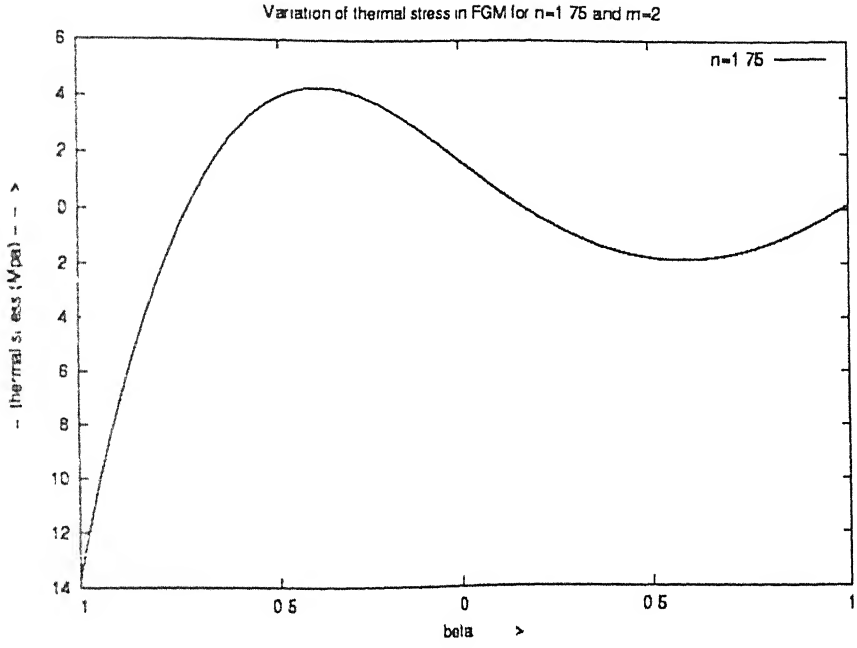

Fig 4 4 7 Prediction of variation of thermal stress in FGM for n=1 75 and m=2

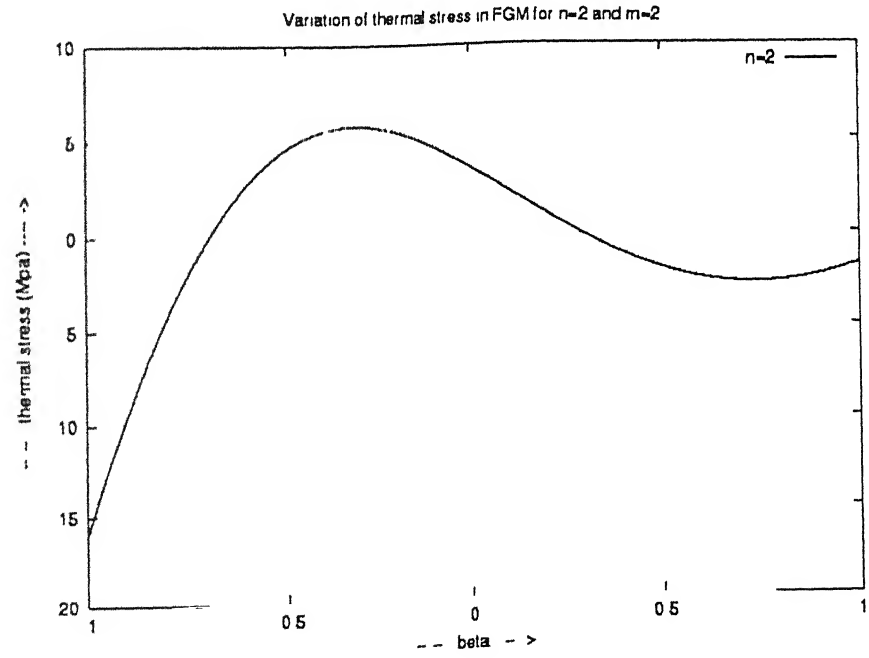

Fig 4 4.8: Prediction of variation of thermal stress in FGM for n=2 and m=2

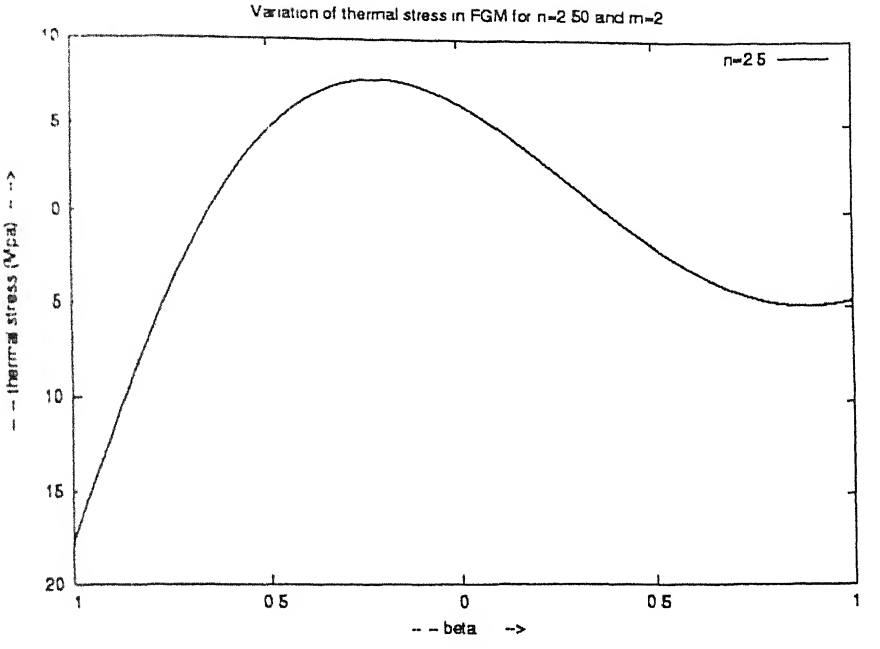

Fig 4 4 9 Prediction of variation of thermal stress in FGM for n=2 50 and m=2

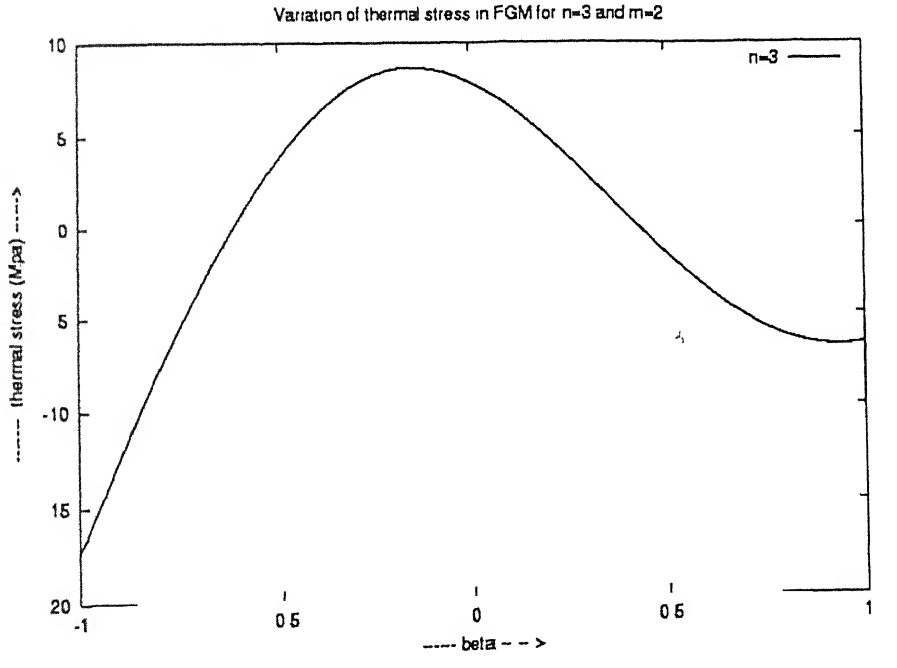

Fig 4.4 10 Prediction of variation of thermal stress in FGM for n=3 and m=2

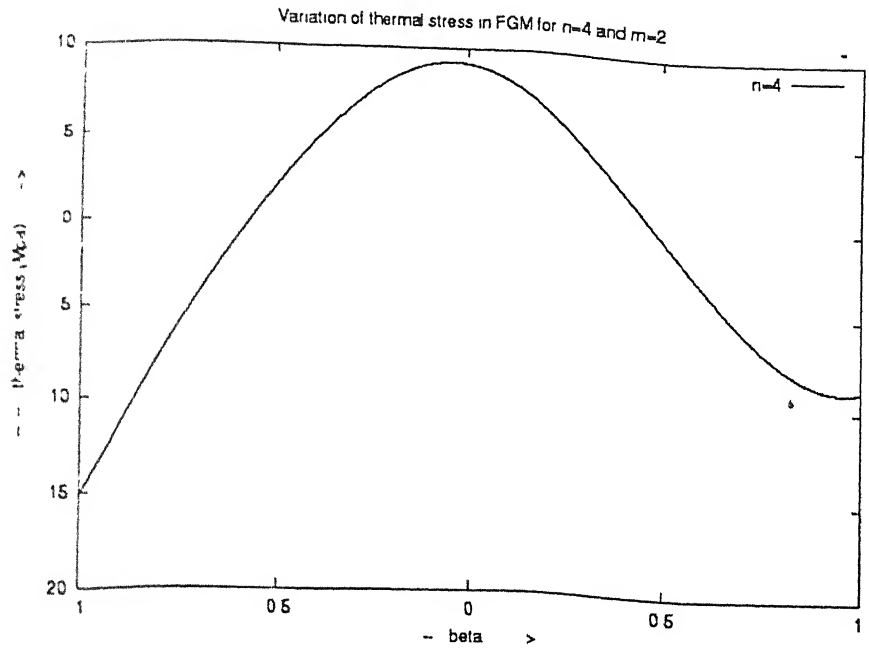

Fig 4.4.11 Prediction of variation of thermal stress in FGM for n=4 and m=2

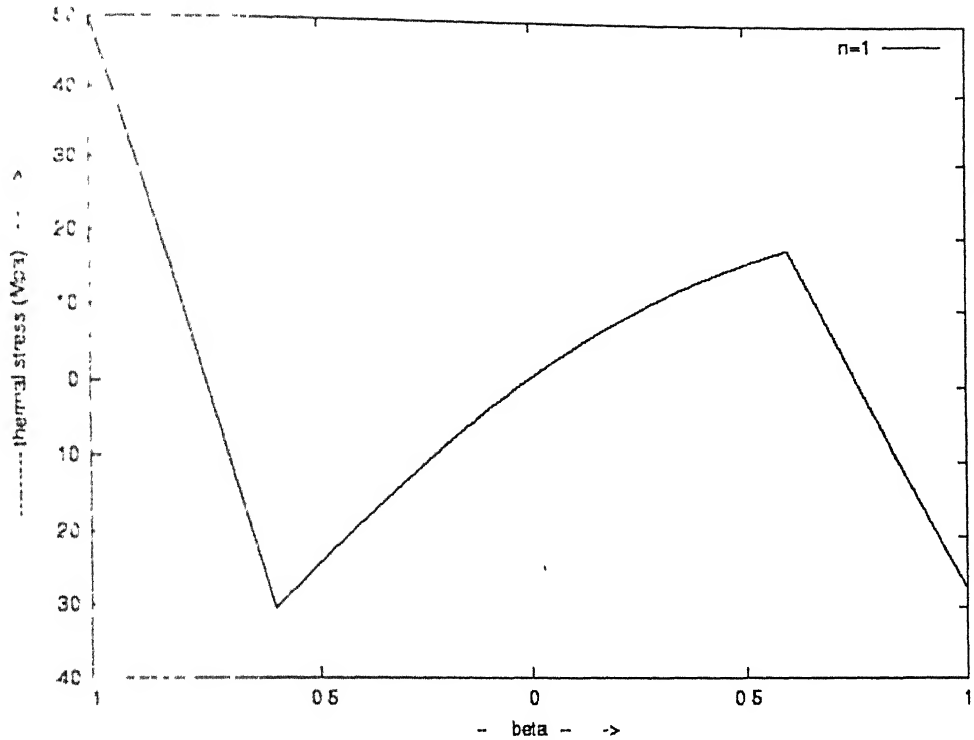

Fig 4 5.1 Prediction of the thermal residual stress distribution in ceramic-FGM-metal tri-layered material for $\Delta T = -100^0 C$ and n=1

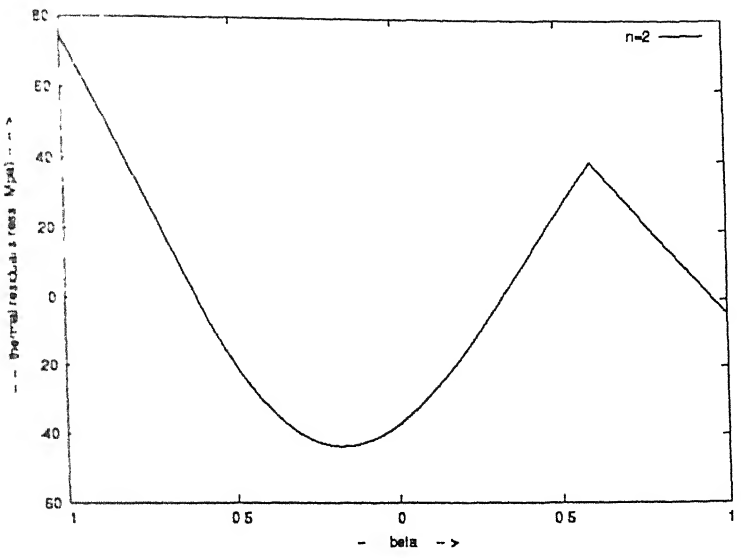

Fig 4 5 2 Prediction of the thermal residual stress distribution in ceramic-FGM-metal trilayered material for $\Delta T = -100^0 C$ and n=2

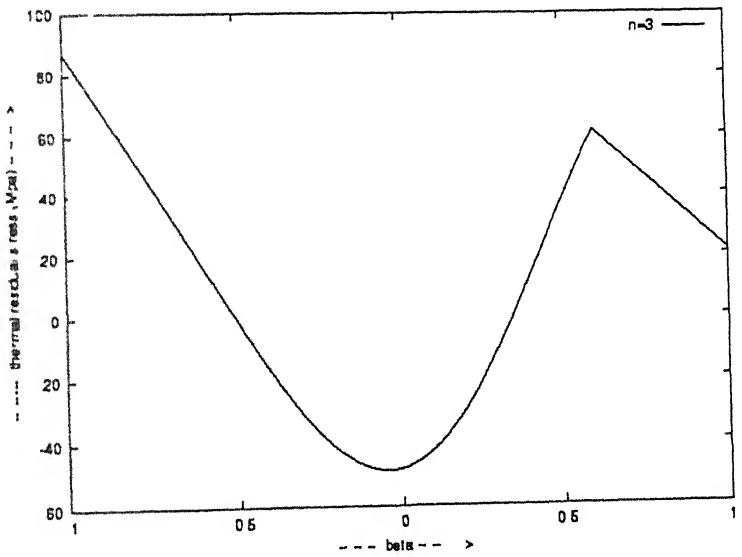

Fig 4.5.3 Prediction of the thermal residual stress distribution in ceramic-FGM-metal trilayered material for $\Delta T = -100^0 C$ and n=3

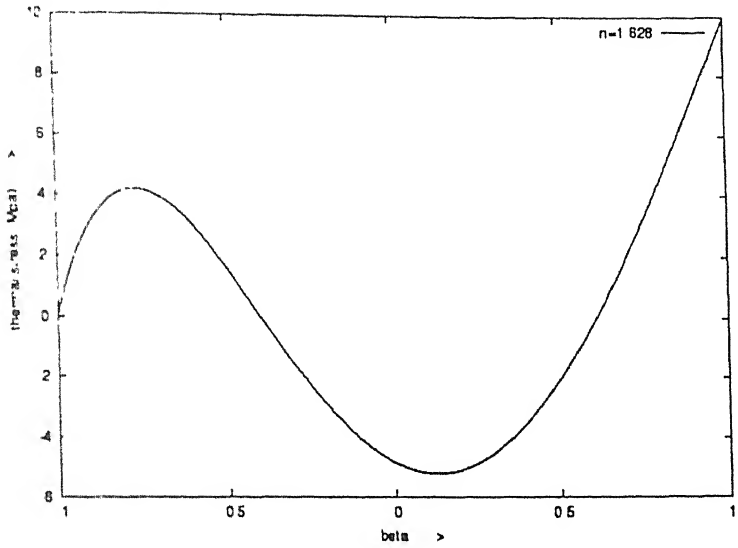

Fig 4 6 Illustration of zero thermal stress on ceramic surface for m=1 Corresponding value of n is 1 628

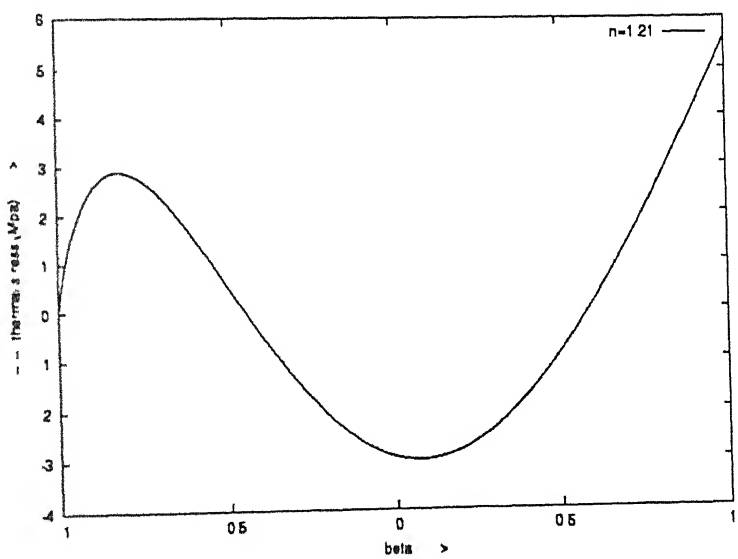

Fig. 4.7· Illustration of zero thermal stress on ceramic surface for m=2. Corresponding value of n is 1 21

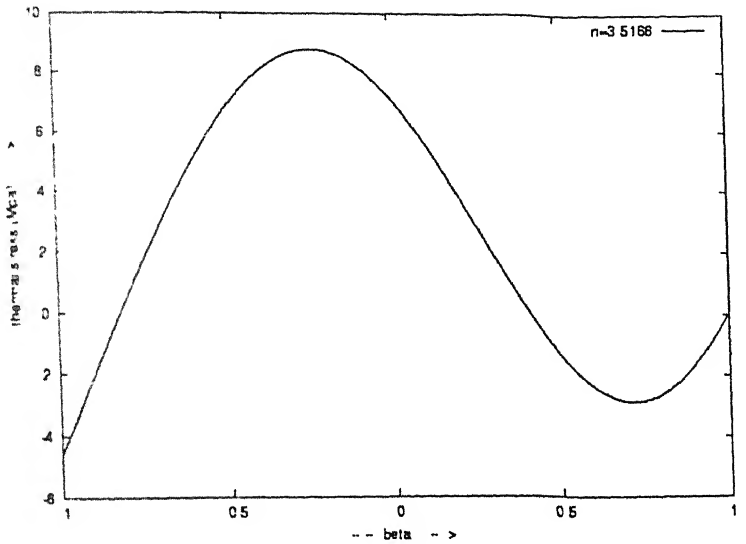

Fig 4 8 Illustration of zero thermal stress on metal surface for m=1 The corresponding value of n is 3 5166

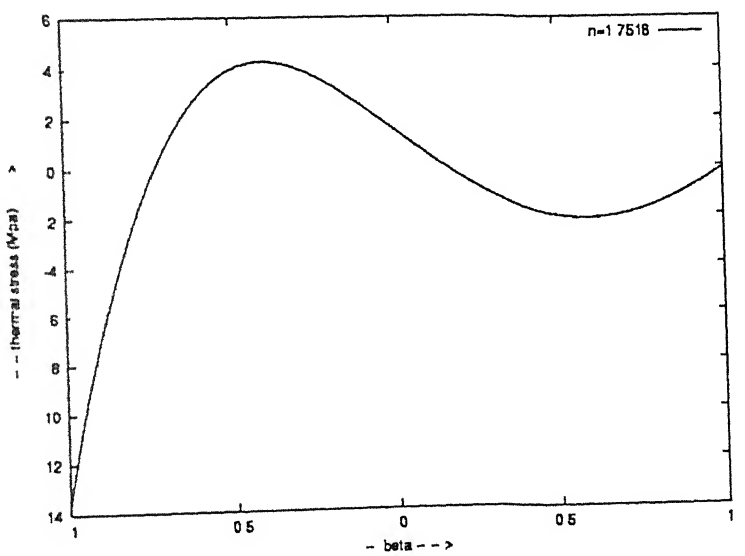

Fig. 4 9 Illustration of zero thermal stress on metal surface for m=2. The value of n is1.7516.

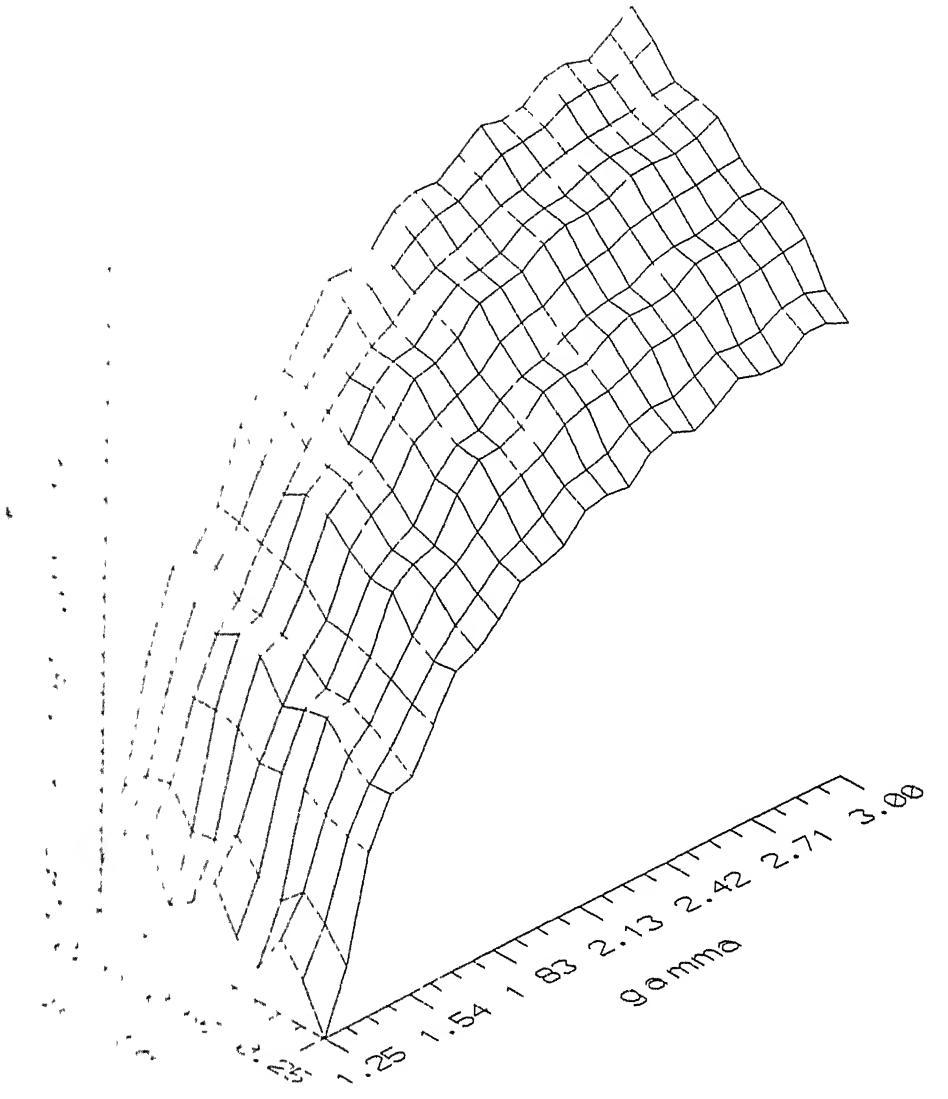

Fig 4.10: Surface view of variation of n^* as a function of $\gamma\left(\gamma=\frac{\alpha_2}{\alpha_1}\right)$ and $\delta\left(\delta=\frac{E_2}{E_1}\right)$ for $\frac{k_2}{k_1}$=1 25

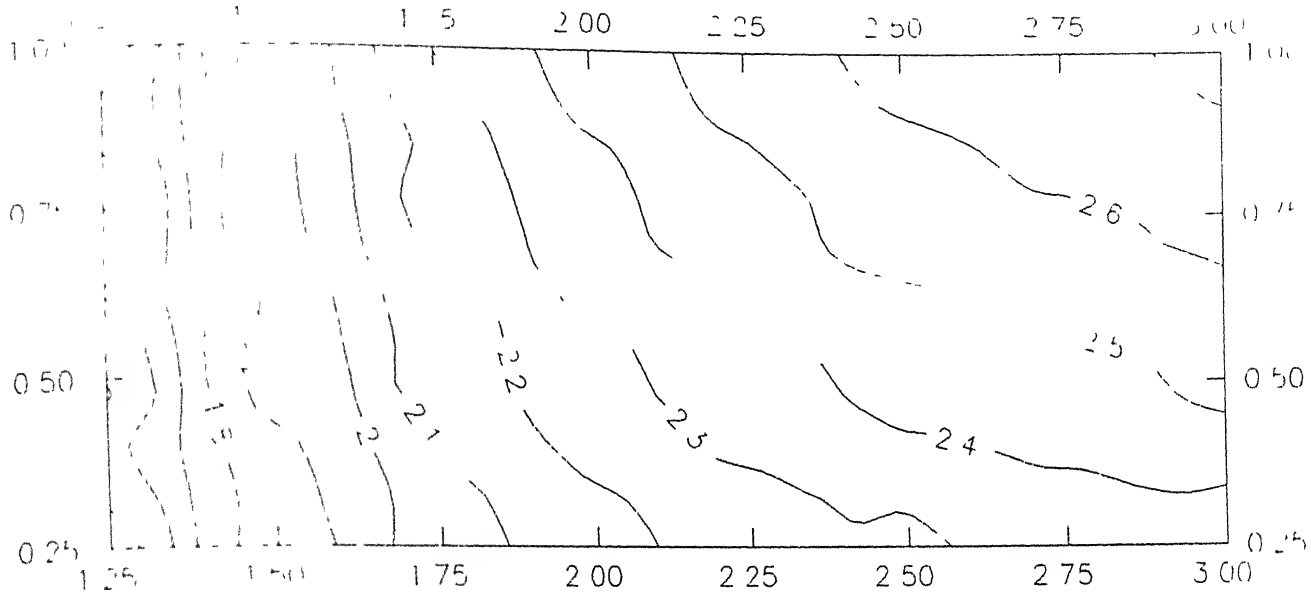

Fig 4 11 Surface view of variation of n* as a function of $\gamma\left(\gamma=\frac{\alpha_2}{\alpha_1}\right)$ and $\delta\left(\delta=\frac{E_2}{E_1}\right)$ for

$\frac{k_2}{k_1}$=1 25

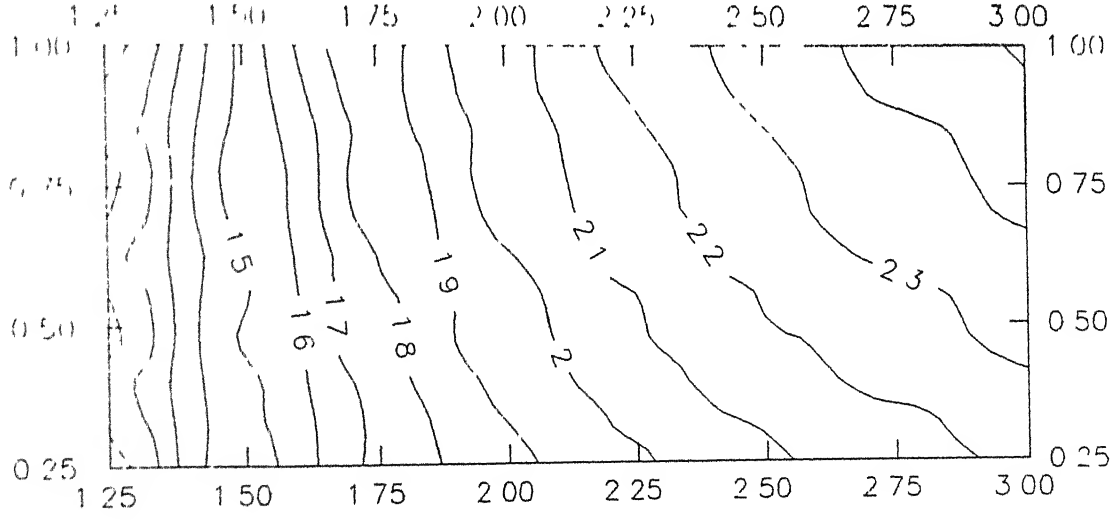

Fig 4 12 Surface view of variation of n* as a function of $\gamma\left(\gamma=\frac{\alpha_2}{\alpha_1}\right)$ and $\delta\left(\delta=\frac{E_2}{E_1}\right)$ for

$\frac{k_2}{k_1}$=1 50

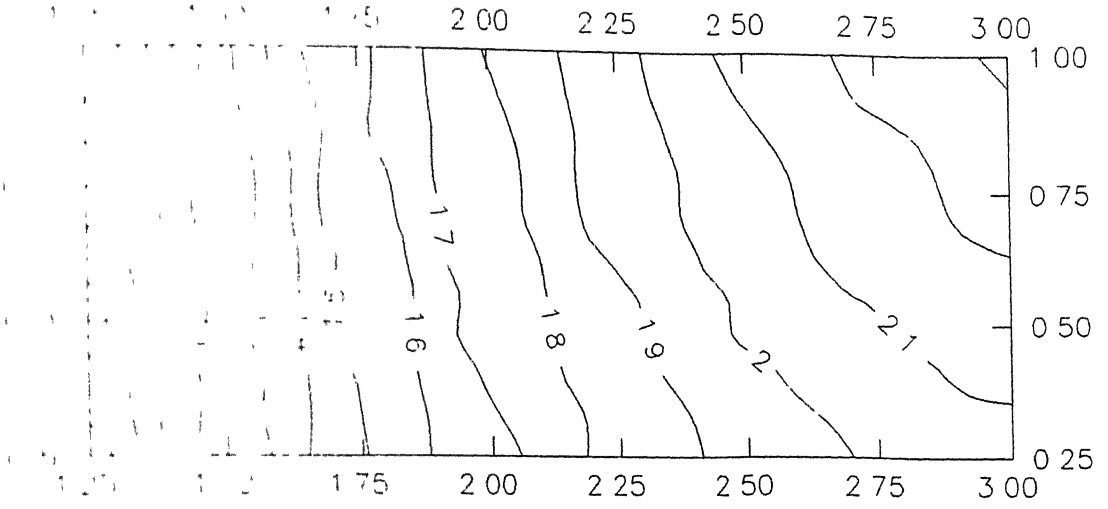

Fig 4 13 Surface view of variation of n^* as a function of $\gamma\left(\gamma=\frac{\alpha_2}{\alpha_1}\right)$ and $\delta\left(\delta=\frac{E_2}{E_1}\right)$ for $\frac{k_2}{k_1}$=1.75.

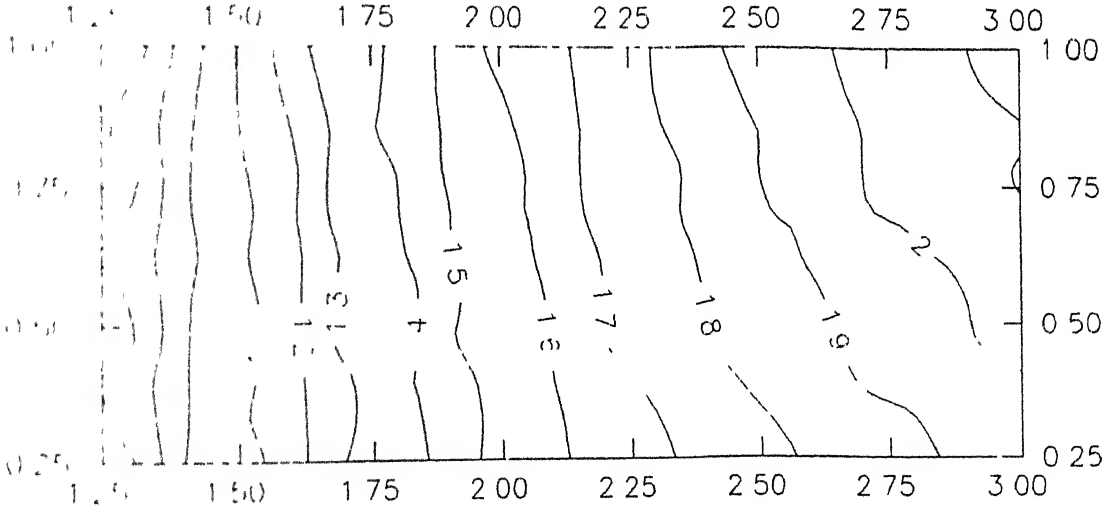

Fig 4.14. Surface view of variation of n^* as a function of $\gamma\left(\gamma=\frac{\alpha_2}{\alpha_1}\right)$ and $\delta\left(\delta=\frac{E_2}{E_1}\right)$ for $\frac{k_2}{k_1}$=2.00.

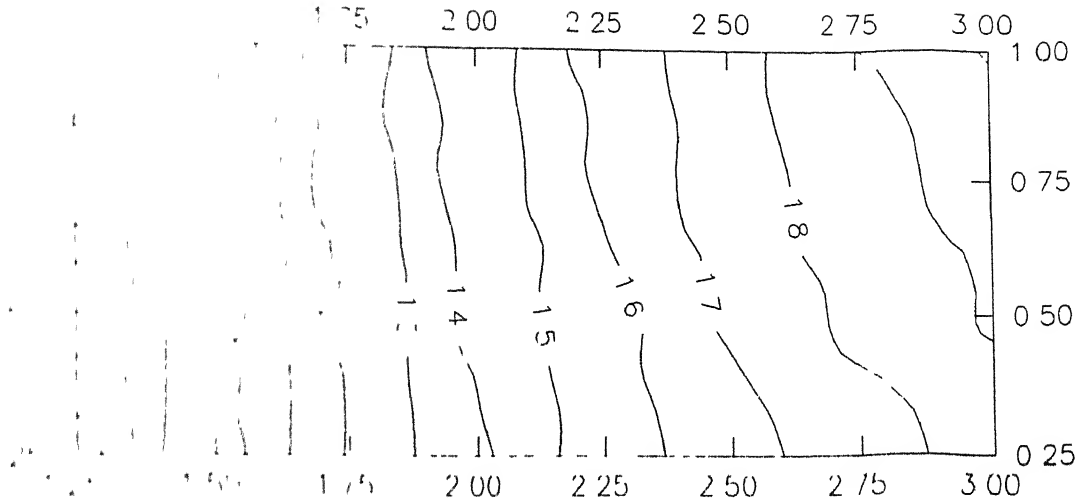

Fig 4 15 Surface view of variation of n^* as a function of $\gamma\left(\gamma=\frac{\alpha_2}{\alpha_1}\right)$ and $\delta\left(\delta=\frac{E_2}{E_1}\right)$ for $\frac{k_2}{k_1}$=2 25

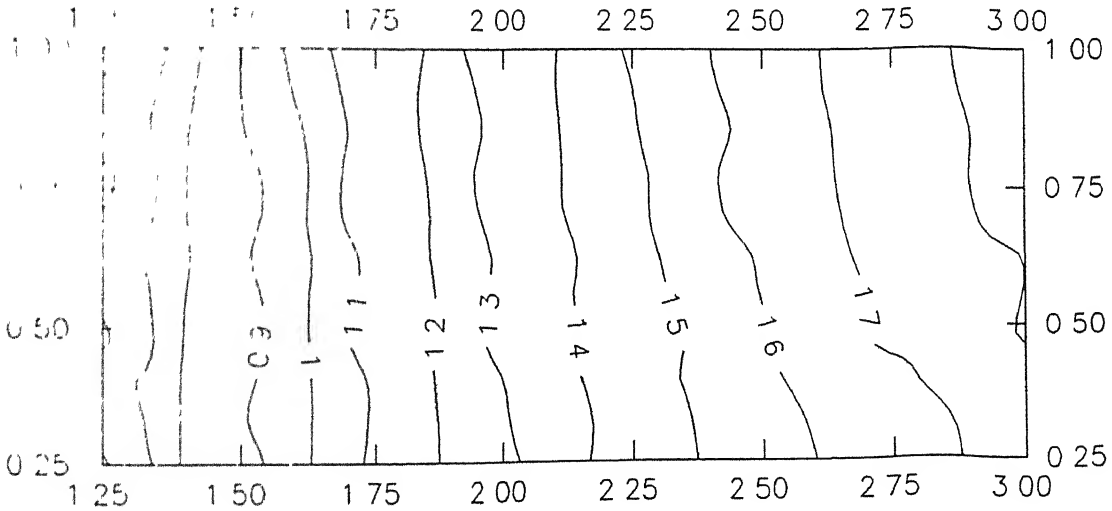

Fig. 4.16: Surface view of variation of n^* as a function of $\gamma\left(\gamma=\frac{\alpha_2}{\alpha_1}\right)$ and $\delta\left(\delta=\frac{E_2}{E_1}\right)$ for $\frac{k_2}{k_1}$=2 50

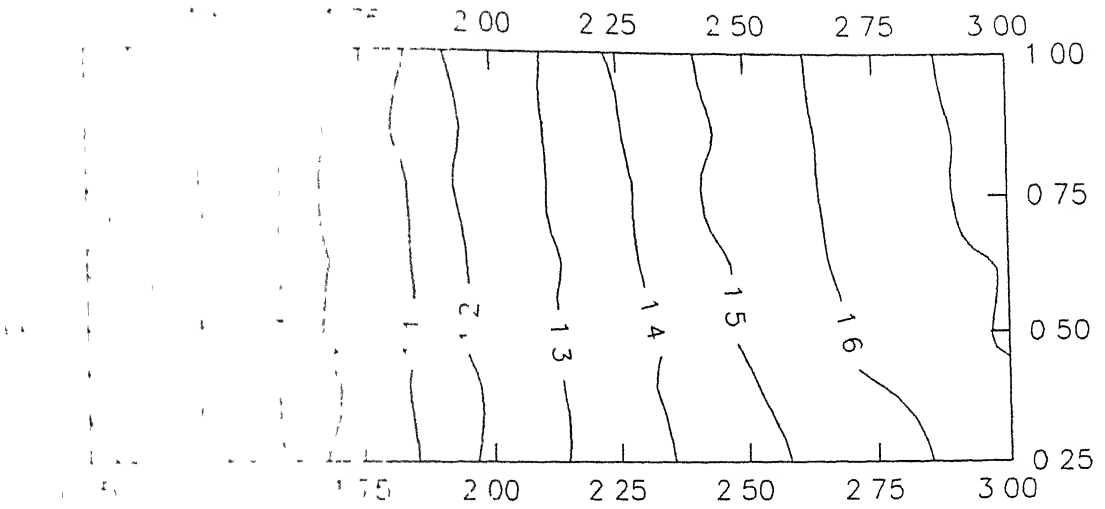

Fig 4 17 Surface view of variation of n^* as a function of $\gamma\left(\gamma=\frac{\alpha_2}{\alpha_1}\right)$ and $\delta\left(\delta=\frac{E_2}{E_1}\right)$ for $\frac{k_2}{k_1}$=2 75.

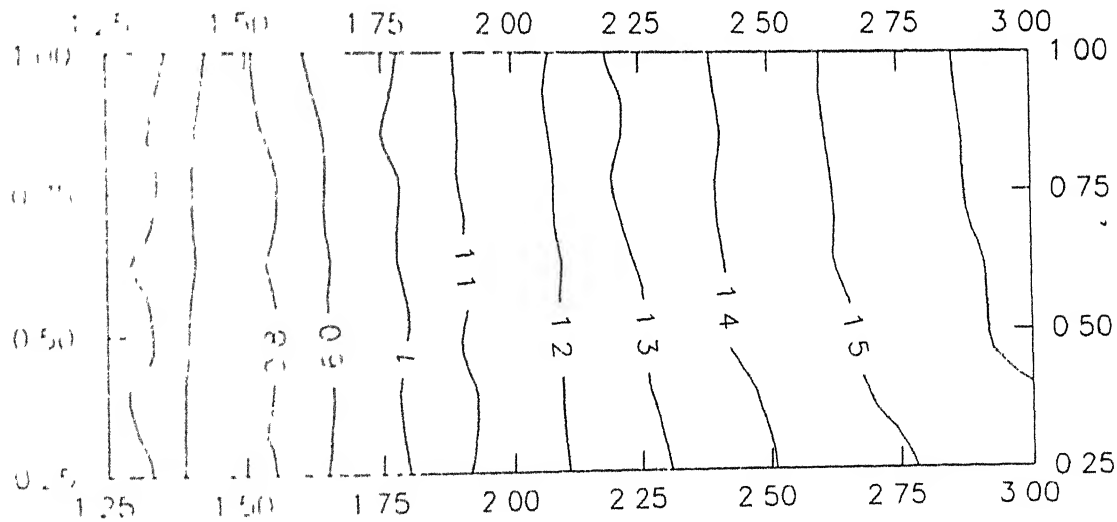

Fig 4 18. Surface view of variation of n^* as a function of $\gamma\left(\gamma=\frac{\alpha_2}{\alpha_1}\right)$ and $\delta\left(\delta=\frac{E_2}{E_1}\right)$ for $\frac{k_2}{k_1}$=3.00.

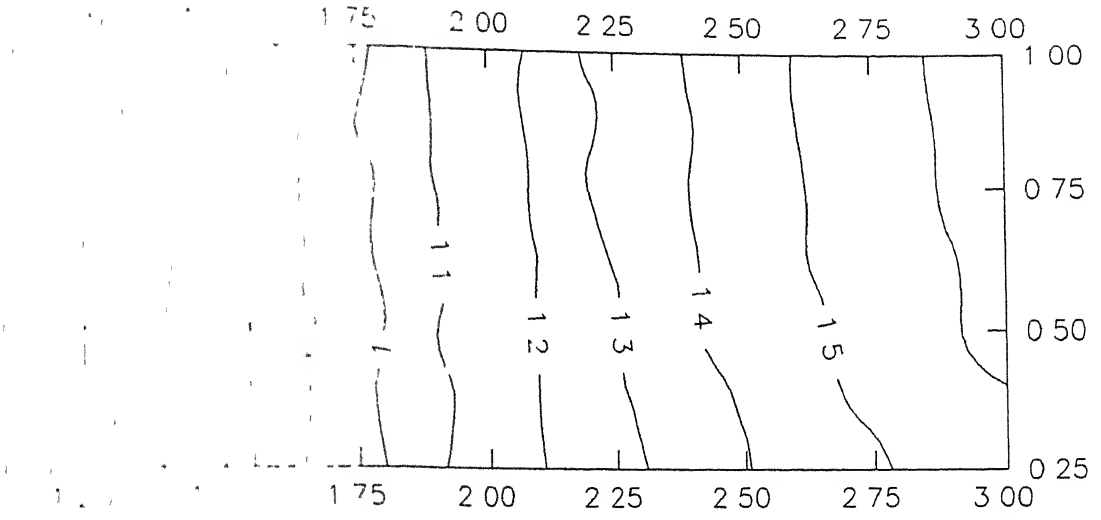

Fig 4 19 Surface view of variation of n^* as a function of $\gamma\left(\gamma=\frac{\alpha_2}{\alpha_1}\right)$ and $\delta\left(\delta=\frac{E_2}{E_1}\right)$ for $\frac{k_2}{k_1}$=3 25

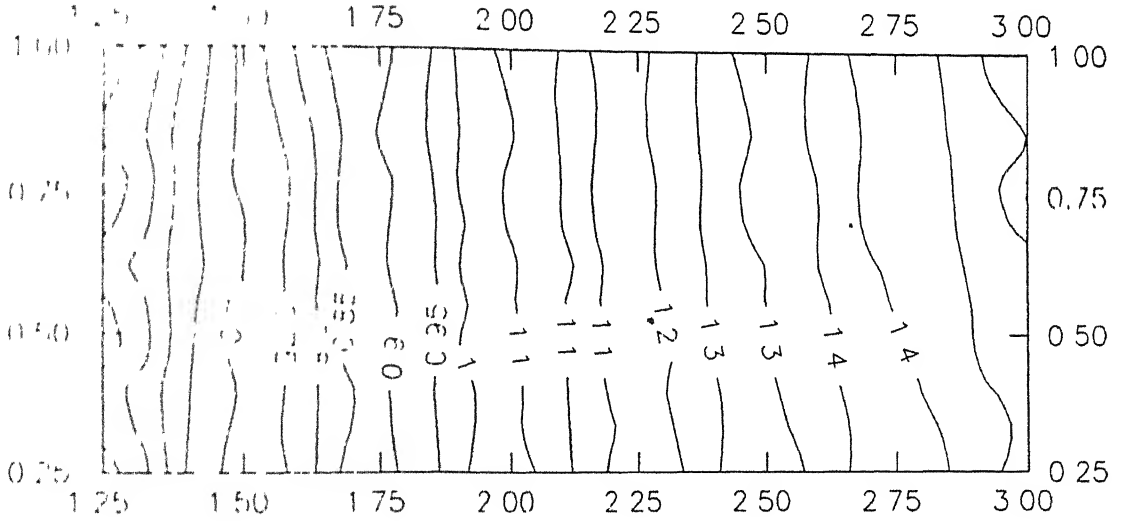

Fig 4 20 Surface view of variation of n^* as a function of $\gamma\left(\gamma=\frac{\alpha_2}{\alpha_1}\right)$ and $\delta\left(\delta=\frac{E_2}{E_1}\right)$ for $\frac{k_2}{k_1}$=3 50.

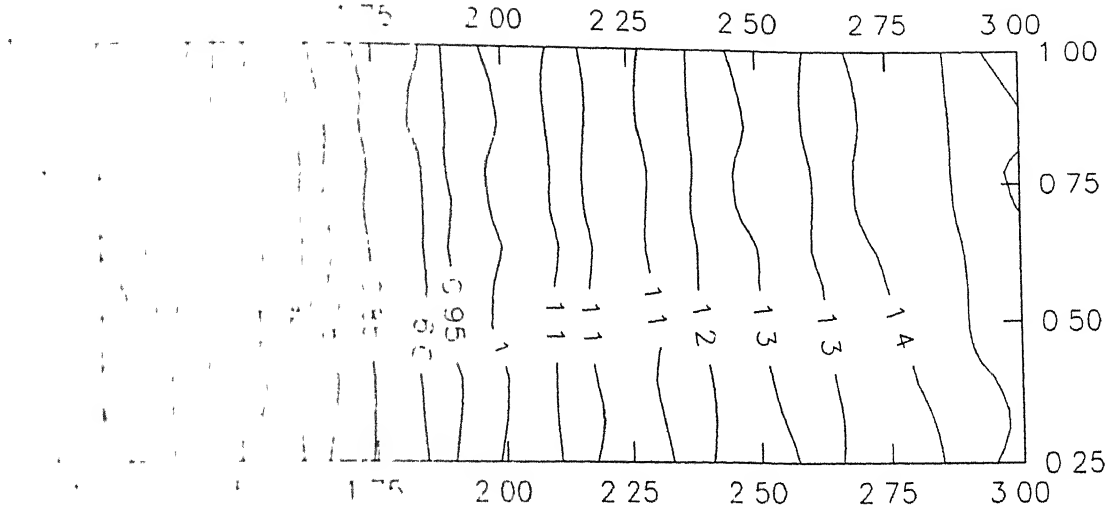

Fig 4 21 Surface view of variation of n* as a function of $\gamma\left(\gamma=\frac{\alpha_2}{\alpha_1}\right)$ and $\delta\left(\delta=\frac{E_2}{E_1}\right)$ for $\frac{k_2}{k_1}$=3 75

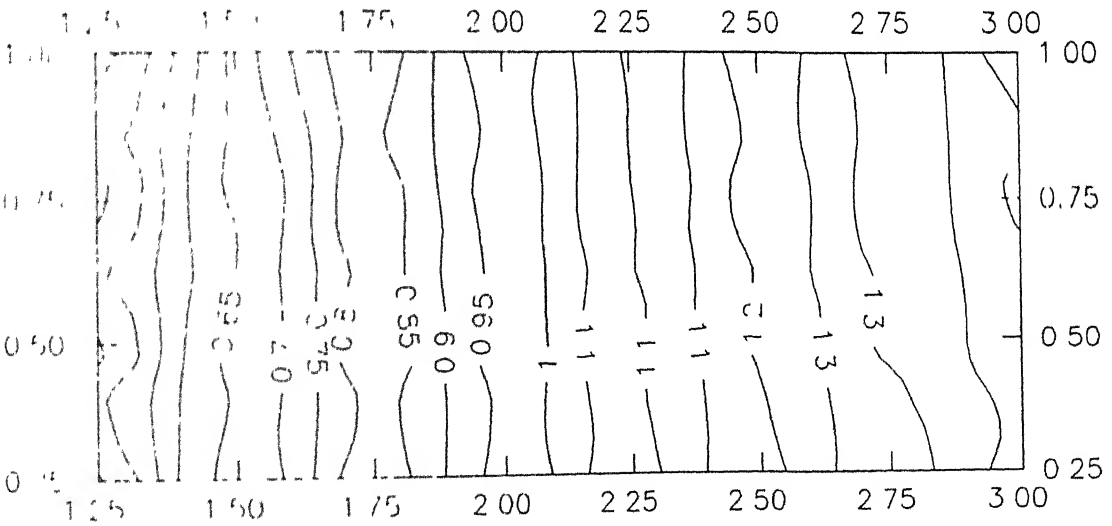

Fig. 4 22· Surface view of variation of n* as a function of $\gamma\left(\gamma=\frac{\alpha_2}{\alpha_1}\right)$ and $\delta\left(\delta=\frac{E_2}{E_1}\right)$ for $\frac{k_2}{k_1}$=4 00.

CHAPTER 5

Effect of Microstructure

5.1 Thermophysical properties of heterogeneous materials

As already has been noted, effective Thermophysical properties of heterogeneous materials are intimately related to the microstructure of the material Along these lines Nan (1993) has identified three basic type of geometric morphologies associated with the distribution of phases within a two-phase material

(1) *Dispersed grain structure* This is characteristic of a material for which the volume fraction of one phase is low, and is discretely and randomly distributed within the host phase [Fig. 5 1a]. It is also characteristic of a material for which the volume fraction of the dispersed phase is somewhat higher, but the phase remains discretely and uniformly dispersed [Fig. 5.1b].

(2) Aggregated grain structure. This morphology characterizes the case for which the volume fraction of the minor phase is increased to the point that it is no longer discrete, but is aggregated in the form of clusters of definite size [Fig. 5.1c].

(3) Percolation-like cluster structure As the volume fraction of the minor phase is increased still further, it reaches a critical value, called the percolation threshold, at which it is interconnected to such an extent that there exists a continuous random cluster, as well as smaller aggregated clusters [Fig. 5.1d].

A great deal of effort has been devoted, over the years, to the development of thermophysical-property models for a dilute, discrete dispersion of one phase within the other. However, the case of intertwined networks of two phases as illustrated in Fig. 5.1d present particularly interesting behavior. If, for examples, the electrical conductivity of one phase is significantly higher than that of other, then a sharp increase in the effective thermal conductivity

of the mixture would take place at the composition for which the relative amount of the higher conductivity component reaches its percolation threshold value A schematic illustration of this behavior is given in Fig.5.2. Indeed, a variety of topological features of the microstructure need to be considered in order to develop physically realistic property models These include directionality, connectivity, and irregularity of the phases that are present [Markworth et al , 1995]

A question that must also be addressed is that of how much information regarding microstructure must be included in order to describe adequately material properties and behavior. Becker and Richmond treated this particular issue, as it relates to effects of grains, pores, and second-phase particles in numerical simulations of the mechanical response of ductile materials. Their models were limited to two dimensions, although the need for inclusion of micro-structural features, in order to be physically realistic, was demonstrated

The description of these complex microstructures can involve some unusual difficulties, one example being the case of percolation. Chernikov and Rogalsky (1994) have pointed out that studies in two dimensional percolation theories, have, over the past decade, borne considerable fruit. However, the three-dimensional problem presents greater difficulties, there still being no exact analytical treatments for lattice percolation and random continuum percolation, although numerical studies have been carried out.

5.2 Percolation Theory

Percolation theory has been studied for various physical (transport) properties by a number of workers over the last two decades and thecurrent approaches are described in various texts such as Efros (1986) and Staufer and Aharony (1992).

The phenomena best described by percolation theory are critical phenomena. They are characterized by a critical point at which some of the properties of the system undergo abrupt changes. Critical phenomena include second-order phase transitions (e.g. the transition of a metal from its normal to its superconducting phase when its temperature is lowered). The physics of all critical phenomena si very unusual, but there are some common features, the most important of which is that in the neighborhood of the critical point, the system appears to break into blockks which differ in their properties, with the

size of the individual blocks growing until the system approaches the critical point The blocks are quite randomly shaped In some phenomena the whole configuration changes chaotically because of thermal motion, while in other phenomena the configuration may be frozen in time but changes from specimen to specimen. The blocks are in complete disorder, so that no regularity is discernible from an instantaneous photograph However, this geometry, which can be called the geometry of disorder, has quite definite properties "on the average". Actually, geometry is inseparable from physical properties For instance, the physical properties of a crystal are determined by the geometry of its lattice Likewise, the "geometry of disorder" determine a number of properties of a system in the vicinity of a critical point The most interesting feature is that owing to the large size of the blocks the geometry is virtually independent of the atomic structure of the material and thus possess properties common to a number of quite dissimilar systems; hence, the universality of the physical properties that we find in the neighborhood of critical points This type of relation between physics and geometry can be traced in percolation theory

5.3 Percolation in heterogeneous materials

As the volume fraction of the minor phase is increased in heterogeneous materials, it reaches a critical value, called the percolation threshold, at which it is interconnected to such an extent that there exists a continuous random cluster, as well as smaller aggregated clusters.

As soon as the volume fraction of the minor phase reaches its percolation threshold, there is a steep change in transport properties of heterogeneous mixture This change is proportional to $(v-v_c)^p$, where v_c is the percolation threshold and p is a constant (Staufer, 1992).

If thermal conductivity of one phase is significantly higher than that of the other, then a sharp increase in the effective thermal conductivity of the mixture would take place at the composition for which the relative amount of the higher-conductivity component reaches its percolation threshold value. This can be demonstrated through a simple numerical exercise where a two phase microstructure is created numerically. A grid consisting of specified number of cell is chosen. The number of cells corresponding to a given volume fraction is determined and specific cells corresponding to the second phase are chosen using random number generation. The range of random numbers is chosen so

as to cover the total numbers of the cells The results of such an exercise are described in section 5 5

5.4 Percolation in FGM

The importance of percolation in heterogeneous materials has been discussed in the preceding section. It had implicitly been assumed that the heterogeneity is spread uniformly through the material

In the case of a FGM we are dealing with a material, which is heterogeneous yet there, is a bias in the distribution of the second phase. Percolation in such materials may be analyzed in a similar manner (as in section 5.3) except that the effect of bias (concentration profile) must be accounted for. A numerical study of the same was carried out as follow:

A grid comprising of 45*20 cells was generated The continuous variation of concentration was assumed equivalent to step-like variation through a layer (20*5 cells each). The volume fraction for each layer was determined so as to give equivalent linear variation over the entire thickness The corresponding number of cells representing the 2^{nd} phase was identified in each layer and their sequence determined through a random number routine. The results of such an exercise are shown in section 5.5.

In terms of incorporating such effect in calculation of temperature field and thermal stress, Surersh et al., have considered micromechanical approach where they simulate such microstructure and model heat transfer and stress in each grain We suggest an alternative approach where the overall microstructure effect of formation of percolation cluster on the transport properties is considered in terms of variation of the said property with concentration (and therefore, spatial position in FGM) and these expressions are directly used in conjunction with the equations derived earlier (chapter 3 and 4). The variation of a property with volume fraction (incorporating the percolation effect) is adequately described by an expression having the following form. For thermal conductivity for example:

I

$$k_x = k_1 + (k_2 - k_1)\left[1 - e^{-\left(\frac{v}{v_c}\right)^p}\right] \qquad (4.22)$$

Define a nondimensional parameter k as follow

$$k = \frac{k_1 - k_1}{k_2 - k_1} \tag{4.23}$$

then

$$k = 1 - e^{} \tag{4.24}$$

where the symbols used has following meaning

k_1 = Effective thermal conductivity of FGM at an arbitrary location.

k_1 = Thermal conductivity of ceramic in ceramic-metal FGM

k_2 = Thermal conductivity of metal in ceramic-metal FGM.

v = Metal volume fraction at an arbitrary location in FGM.

v_c = Percolation threshold of metal volume fraction.

p = An arbitrary index

Values of these parameter taken in this study are as follow:

k_1=30 W/m K

k_2=300 W/m K

v_c = .20, .25, 40

p = 5

Now temperature distribution in FGM is given by the following expression:

$$\theta = 1 - \frac{\int_0^{\beta_1} \frac{d\beta_1}{30 + 270\left[1 - e^{-\left(\frac{\beta_1}{v_c}\right)^p}\right]}}{\int_0^{1} \frac{d\beta_1}{30 + 270\left[1 - e^{\left(\frac{\beta_1}{v_c}\right)^p}\right]}} \tag{4.25}$$

Assuming liner variation of metal volume fraction in FGM, then $v = \beta_1$. Hence above expression become as follow:

$$\theta = \frac{\int_0^{\beta_1} \frac{d\beta_1}{30 + 270\left[1 - e^{-\left(\frac{\beta_1}{\beta_c}\right)^n}\right]}}{\int_0^{\beta_1} \frac{d\beta_1}{30 + 270\left[1 - e^{-\left(\frac{\beta_1}{\beta_c}\right)^n}\right]}} \qquad (4\ 26)$$

Similarly the expression for H ($H = \frac{q_x X}{(T_1 - T_2)k_1}$) is given as follow.

$$H = \frac{\int_0^{\beta_1} \frac{1}{d\beta_1}}{\int_0^{\beta_1} \frac{1}{1 + m\left[1 - e^{-\left(\frac{\beta_1}{\beta_c}\right)^n}\right]}}$$

Expression for thermal stress distribution remain same as eq. 4.9, with change in the values of a, b and variation of θ.

5.5 Results and discussion

Fig. 5.3 depicts microstructures of heterogeneous material for different volume fractions of individual constituent

Initially there is no intertwined structure, but as soon as the volume fraction of phase 2 is about 30% the percolation effect appears

Similarly Fig. 5.4 shows microstructure of an FGM of two phases 1 and 2. Phase 2 is represented by black box It is observed that at about 25-30% volume fraction of phase 2, percolation effect starts in the FGM, hence a steep change in the transport properties of the material is expected.

Based on equation 4.24, Figs. 5.5- 5.7 shows effect of percolation on thermal conductivity variation in FGM for different values of percolation threshold.

Figs. 5.8- 5.9 shows the corresponding variation of temperature along the thickness direction in the FGM.

The temperature variation in FGM with percolation effect (for $v_c = 25$) is compared with corresponding FGM without percolation in Fig. 5.10. The main observation is that with percolation results in sharp decrease in temperature in FGM for $\eta < 25$ whereas, the slope of the θ/η curve is almost constant for FGM without percolation

The significance of this result can be seen in Fig 5.12, where thermal stresses are compared for a linear variation of composition of metal. It is observed that with percolation effect, there is sharp decrease in temperature on ceramic-rich region, which results in compressive stresses on ceramic-side. This is beneficial from design point of view since ceramics are brittle and fails easily under tensile stresses.

The effect of the value of percolation threshold on the ceramic surface is examined in Fig. 5.11, where it is observed that a lower v_c gives higher compressive stresses. It is speculated that the percolation threshold may be lowered by altering the relative grain sizes of the constituent materials.

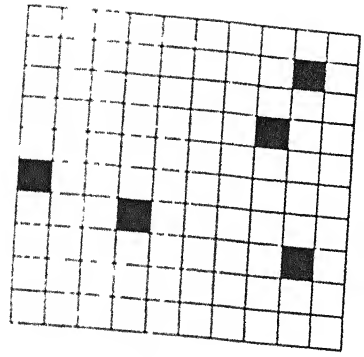

(a) 5 %

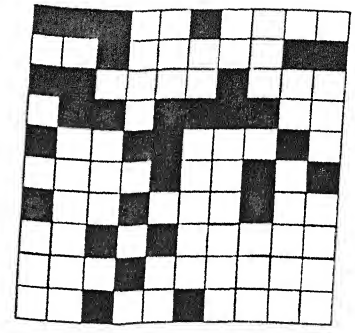

(c) 30 %

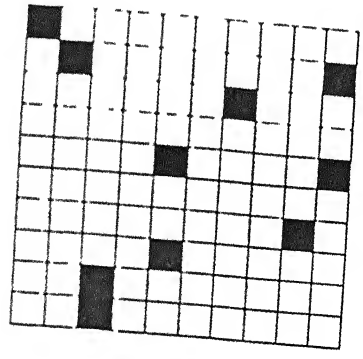

(b) 10 %

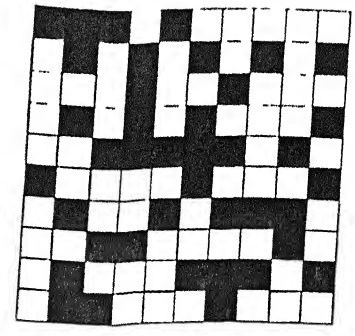

(f) 40 %

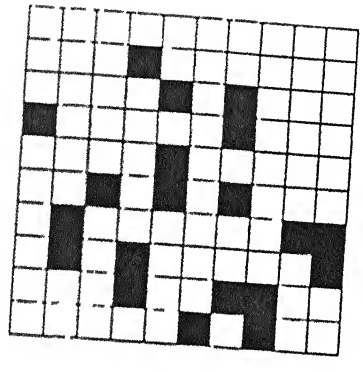

(c) 20%

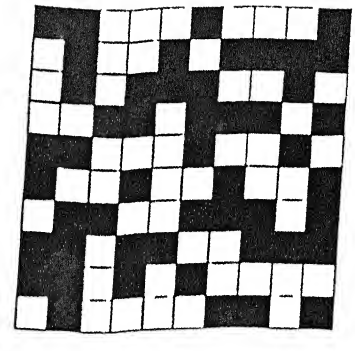

(g) 50 %

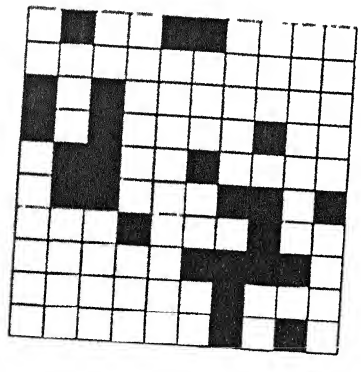

(d) 25 %

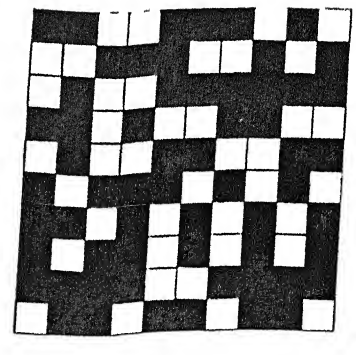

(h) 60 %

Fig 5 3 Illustration of percolation behavior in heterogeneous material as a function of volume fraction

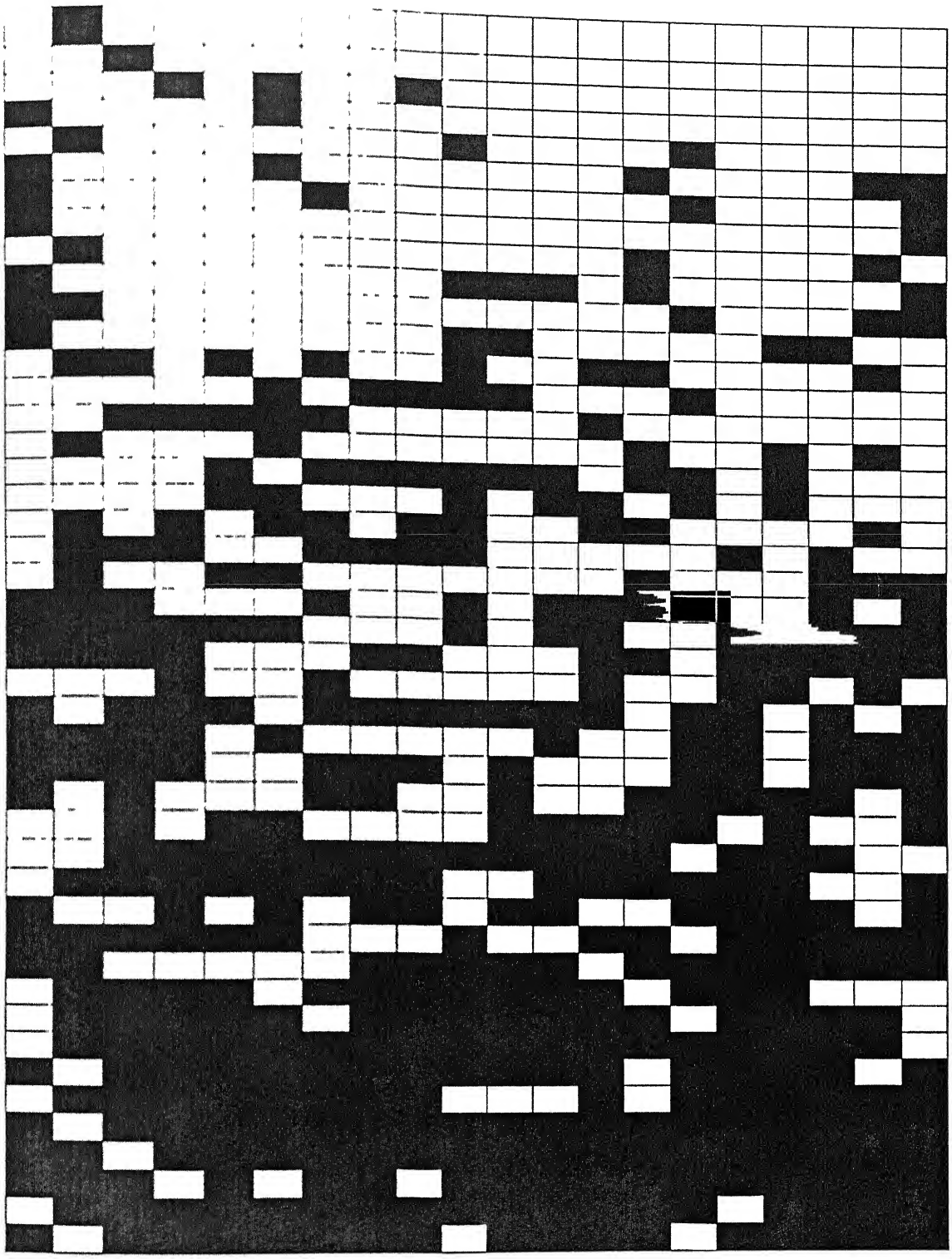

Fig 5.4. Microstructure of a FGM depicting the intertwined network of black box at 25-30% volume fraction (black box represent the metal grain)

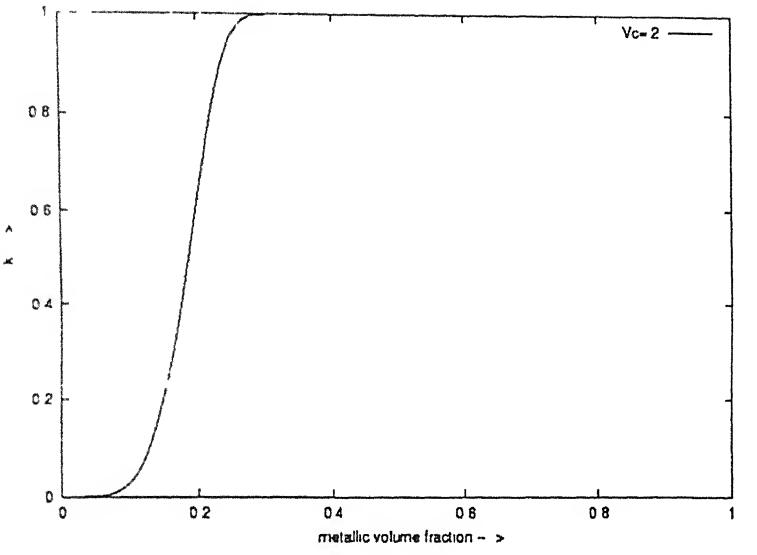

Fig.5 5 Schematic illustration of the variation composition of the thermal conductivity of a two- phases mixture, one being good conductor, the other a poor conductor Percolation threshold is .20

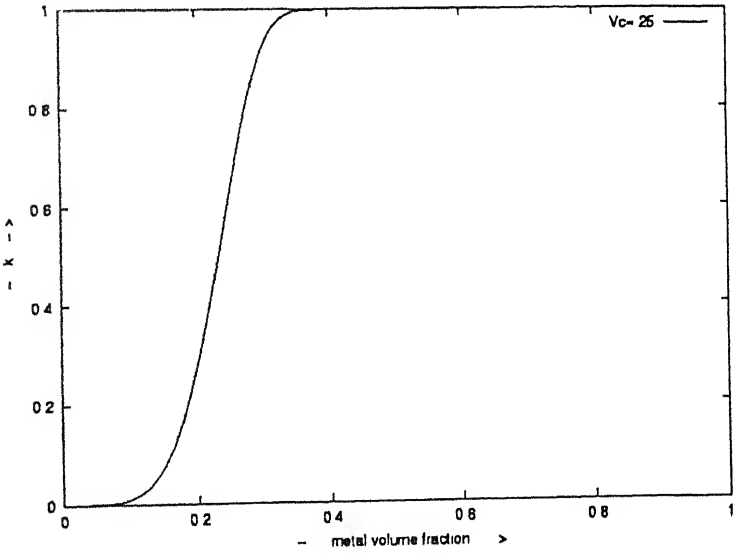

Fig. 5.6: Schematic illustration of the variation composition of the thermal conductivity of a two-phase mixture, one phase being a good conductor, the other a poor conductor. Percolation threshold is .25.

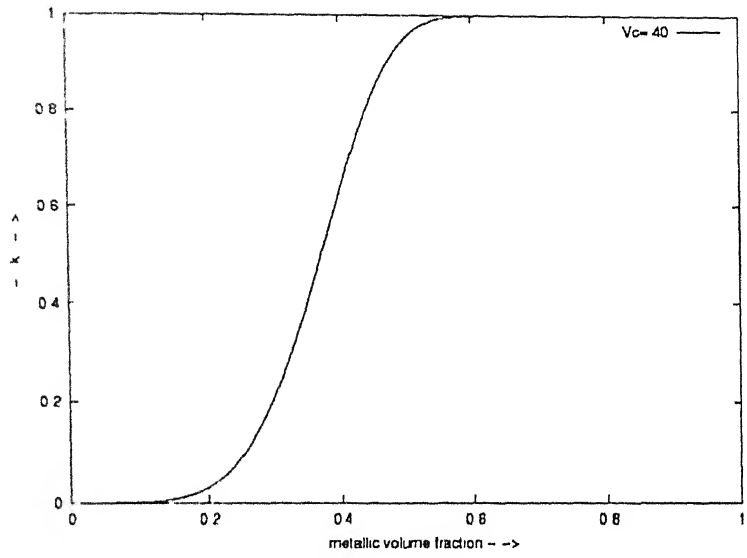

Fig 5 7 Schematic illustration of the variation composition of the thermal conductivity of a two-phase mixture, one phase being a good conductor, the other a poor conductor Percolation threshold is 0 40

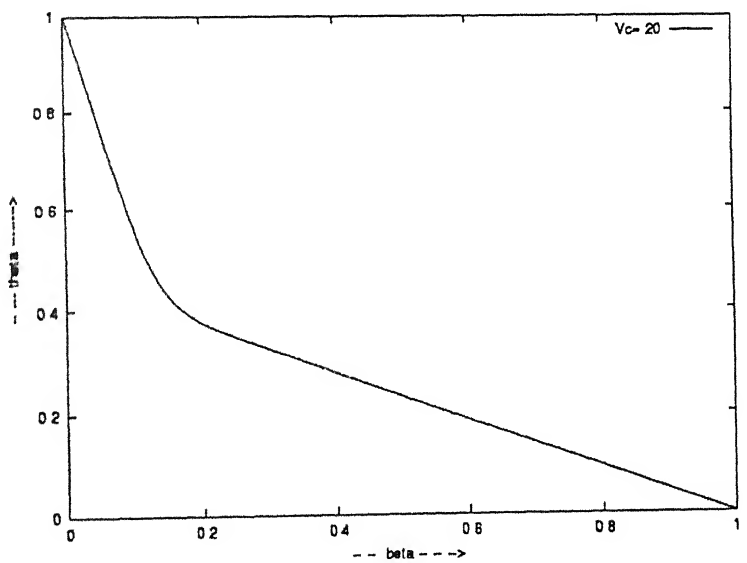

Fig 5 8 Prediction of temperature distribution in FGM with percolation effect (percolation threshold is 0 20)

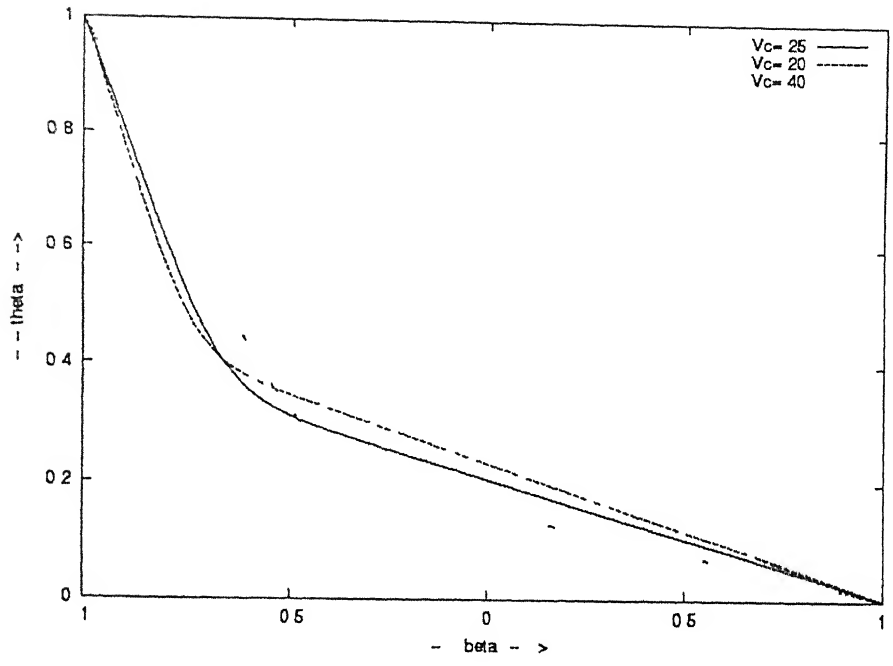

Fig 5 9 Prediction of temperature distribution in FGM with percolation effect for various values of percolation threshold

Fig. 5 10 Comparison of temperature distribution in FGM wit and without percolation effect Percolation threshold is 0 25

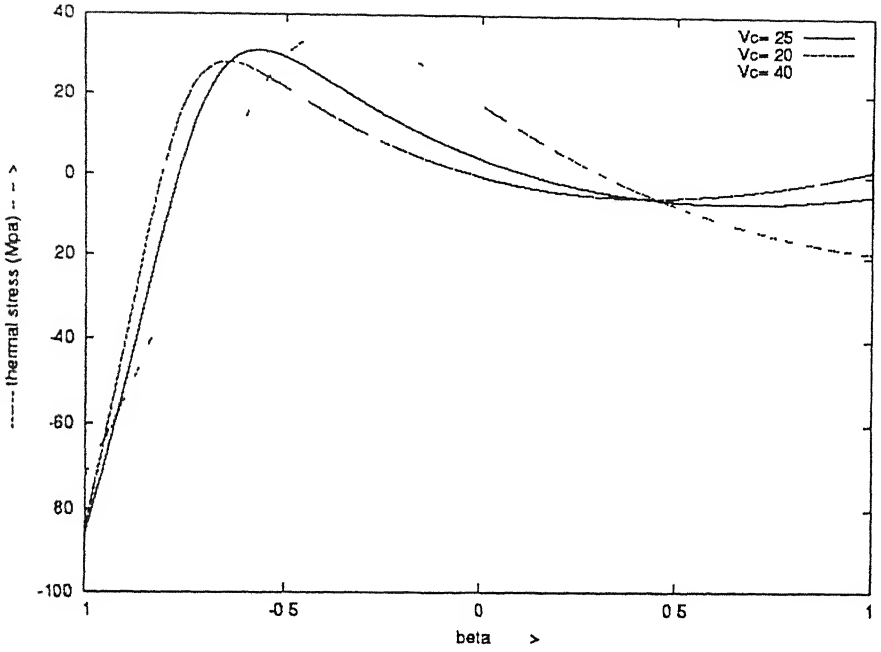

Fig 5 11 Prediction of thermal stress distribution in FGM with percolation effect for various values of percolation threshold

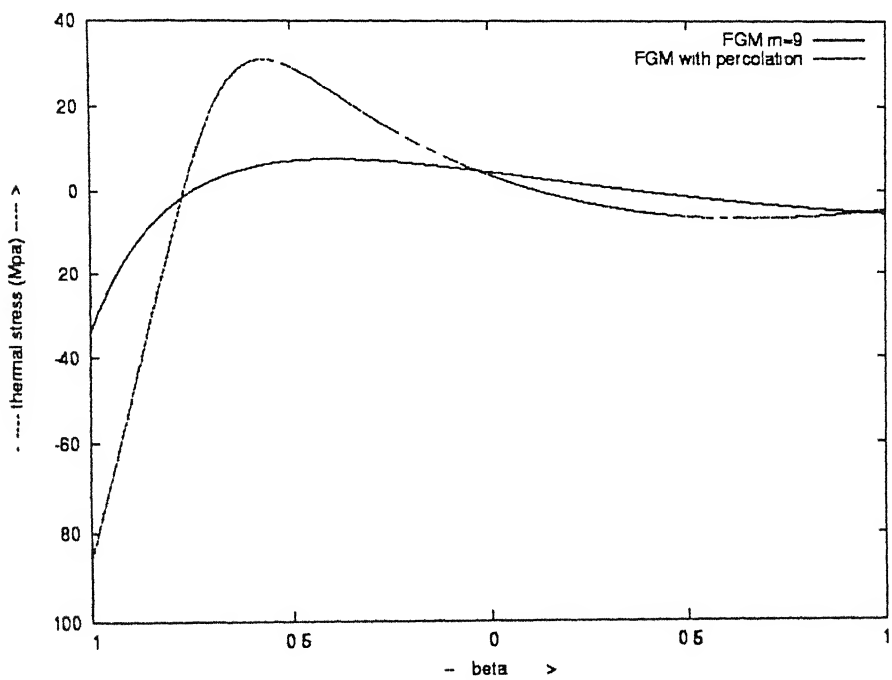

Fig 5 12 Comparison of thermal stress distribution in FGM with and without percolation effect Corresponding percolation threshold is 0 25

CHAPTER 6

Conclusions and Suggestions for Future work

6.1 Conclusions

This work has dealt with the thermomechanical response of functionally graded materials. A plate like structure subjected to sharp temperature gradient in the thickness direction is considered. Theoretical models and numerical results for temperature field, heat flux, thermal residual stress, and thermal stress have been presented both for functionally graded material and equivalent bi-layered materials Significant trends and design guidelines to select appropriate composition profile for specific material pairs have been identified and presented The role of microstructure, especially in regards to percolation phenomenon in transport properties and its significance for FGM are discussed and a novel approach to incorporate such effects in design calculation is presented

The major findings are·

1. The steady state temperature field in a FGM subjected to temperature gradient along thickness direction varies in a continuous manner unlike in bi-layered material
2 By proper choice of composition profile, stresses in FGM can be optimized to suit specific requirements For example, It is possible to have zero stress on ceramic or metal surface in FGM, by adjusting the composition profile.
3. There is no sharp decrease in stress profile across the plate thickness unlike as in bi-layered material. Hence there are lesser chances of material failure by crack propagation.
4. The discontinuity in stress profile in ceramic-FGM-metal tri-layered structure can be avoided by proper choice of composition profile.
5. Percolation effect become dominating, at a particular volume fraction and at this volume fraction, and steep change in the transport properties is expected.

6 Temperature distribution in FGM with percolation effect is continuous, but there is steep change in temperature for $v < v_c$ It is advantageous in a way to have more compressive stresses on ceramic surface in FGM

6.2 Suggestions for Future work:

1 Heat flow rate through FGM with percolation effect and without percolation effect should be calculated Basic equations have been developed in the preceding chapters
2 Behavior of FGM, in plastic region should be investigated
3. Nucleation of crack and failure of FGM by crack propagation should be investigated
4. There is a need to investigate Creep behavior of FGM since FGM are used in high temperature applications
5. A thought can be given to FGM having 2-dimensional and 3-dimensional composition gradient.

References:

1. Agullo J. M , Maury F., Jonın F., J. de Phys 4, Colloq. C3, pp. 549-555,1993

2 Argyrıs J , Computer Meth appl. Mech. Eng. III, p. 203, 1994.

3 Atarashıya K , "Joınıng Metals to Ceramıcs Usıng FGMs", Mater. And Proc. Rept , Hokkaıdo Unıv., Elssevıer Sc. Publishıng Co. Inc., pp.5-6, 1992

4. Atarashıya K , Ishıda Y., Nagaı T., Uda M , Ceramıc Transactıon , Vol 34-Functıonally graded materıals, pp. 141-148, 1993

5. Baker-Jarvıs J., Inguva R., J. Heat Transfer (Trans. ASME) 107, p. 39, 1985.

6. Ben-Amoz M , J. Appl. Math. Phys. 27, p. 335, 1976.

7. Bennett C.E G., McKınnon N.A , Wılliams L.S., Natuıe 217, pp. 1287-1288, 1968.

8. Chernıkov A A , Rogalsky A V., chaos4, p 35, 1994.

9. Dao M , Gu P , Mahewal A , Asaro R J., Acta mater , Vol 45, No.8, pp. 3265-3276, 1997.

10. Efros A.L., Physıcs and Geometry of percolatıon theory, 1986.

11. Erdogan F., Ozturk M., Int. J Engng. Scı., Vol. 33, No 15, pp. 2179-2195.

12. Eroglu S., Bırla N C., Demırcı M., Baykara T., J. Mater. Scı. 12, pp. 1099-1102, 1993.

13 Finot M , Suresh S , Bull C , Sampath S , J Mat Sc Eng , A205, pp. 59-71, 1996

14. Fiister k , Bunk W , "Proc 1st Int Symp On FGM", Tokyo FGM forum and the society of Non-traditional Technology), pp 91-96, 1990

15. Hirano T , Yamada T , Teraki J , Niino M , Kumakawa A., "Proceedings of the 16th International Symposium on Space Technology and Science", Sapporo, Japan, p 375, 1988.

16. Holman J P., Heat Transfer, 1997.

17. Hirari T , "Functionally Graded Materials", Vol XX, No. 1, 1995.

18. "Improved shuttle tile", Aerospace Engr , p 29, 1994.

19. Ishihara S , Getto H , Sumida A , in All division 5 Conference "Forest Products", p 423, 1992

20. Jin Z -H , Noda N , Int J. solids struct 31, p 203, 1994.

21. Kawasaki A , Watanabe R , J. Jpn Soc. Powder Powder Metall 37, pp 287-291, 1990.

22. Kawakami S., Nishizawa J., Proc. IEEE 53, pp. 2148-2149, 1965.

23. Kawai T., Miyazaki S., J. Ceram Soc. Jpn. Int. Ed. 98, 168-172, 1990.

24. Koike Y., Tanio N , Nihei E., Ohtsaka Y., Polym. Eng. Sci. 29, pp. 1200-1204, 1989.

25. Koike Y., Polymer 32, pp. 1737-1745, 1991.

26. Kesler O., Finot M., Suresh S., Sampath S., Acta Mater., Vol 45, No. 8, pp. 3123-3134, 1997.

27. Kuwahara O , Wang N., Ueha S , Jpn. J. Appl Phys. 31, p. 102, 1992.

28. Levit M., Grimberg I , Weiss B. –Z , J Mat. Sc & Tech , A206, pp. 30-38, 1996

29. MRS Bulletin " Functionally Graded Materials" Vol. XX, No. 1, Jan. 1995.

30. Markworth A J , Ramesh K. S , Parks W. P , J Mat Sci. 30, pp. 2183-2193, 1995.

31. Matsuzaki Y., Fujioka J., Ueda S , Wakamatsu Y , "Thermal barrier Design of FGM for Scramjet Engine Applications" Akashi Technical Institute, Kawasaki Heavy Industries Ltd , Japan, 1992.

32 Nan C -W Progr. Mater Sci 37, pp 1-4, 1993

33. Osaka T , Matsubara H , Homma T , Mitamura S., Noda K., Jpn. J. Appl Phys 29, pp. 1939-1943. 1990

34. Oonishi H , Noda T., Ito S , J Appl. Biomater. 5, pp 23-37, 1994.

35. Ostoja-Starzewski M , Jasiuk I., Wang W , Alzebdeh K., Acta mater., Vol. 44, No. 5, pp 2057-2066, 1996.

36. Omori M., Sakai H., Ohkubo A., Kawahara M., Hirai T., J. Jpn. Soc. Powder Powder Metall. 41, pp. 649-652, 1994.

37. Rabin B.H , Heap R J , "Ceramic Transaction", Vol. 34, pp. 173-180, 1993.

38. Sata N., Ceramic Transaction, Vol 34-Functionally graded materials, pp. 109-116, 1993.

39. Srinath L S., "Advanced Mechanics of Solids", 1993.

40. Stauffer D., Aharony A , Introduction to percolation Theory, 1992.

41. Suresh S., Giannakopolous A.E , Alcala J., Acta mater , Vol. 45, No. 4, pp. 1307-1321, 1997.

42. Suemitsu I , Matsuzaki Y., Fujioka J., Uchida M , Sohda Y., "Ceramic transaction" Vol. 34, pp. 315-322, 1993.

43. Stewart D.A., Leiser D B, kolodziez P , Smith M., J. spacecraft 23, pp 420, 1986.

44. Tani J., Liu G.-R., JSME Int. J. Ser. A36, pp. 152-155, 1993.

45. Teraki J., Hirano T., Wakashima K., "An Elastic-Plastic Analysis of Thermal stresses in FGM plate under cyclic thermal load", MEC Laboratory, Daikin Industries, Tsukuba, Japan, 1994.

46. Taya M , Lee J E., Mori T , Acta mater., Vol. 45, No. 6, pp. 2349-2356, 1996.

47 Torquato S , Appl Mech Rev 44, p 37, 1991

48. Tanaka K , Tanaka Y , Enomoto K , Poterasu V.F , Sugano Y., Computer Meth Appl Mech Eng. 106, p. 271, 1993

49. Watanabe Y , Nakamura Y., Fukui Y., Nakanishi K., J. Mater. Sci. Lett. 12, pp. 326-328, 1993.

50. Watari F., Bull. Ceramic Soc. Jpn. 29, pp. 191-193, 1994.

51. Weissenbek E., Pettermann H. E., Suresh S., Acta mater., Vol. 45, No. 8, pp. 3401-3417, 1997.

52. Watanabe R., Kawasaki A , "Proceedings of the 1st International Symposium on FGM", Sendai, Japan, p 107, 1990.

53. Watanabe R., Kawasaki A., Takahashi H , "Mechanics and Mechanisms of Damage in composites and Multi-Materials".Baptiste, D (Ed), London: Mechanical Eng. Publishers, pp. 285-289, 1991

54. Zhang Q. –J , Zhang L. M., Yuan R. Z , "A coupled Thermoelastic Model of FGMs under sudden high heating" submitted for publication.